UNIVERSITÉ DE GRENOBLE

THESE

Pour obtenir le grade de

DOCTEUR DE L'UNIVERSITE DE GRENOBLE

Spécialité : Physique

Arrêté ministériel : 7 août 2006

Présentée et soutenue publiquement par

Köster, Robert

le **28/06/2010**

Croissance auto-assemblée de fils de GaN sans catalyseur par épitaxie en phase vapeur d'organo-métalliques

---

Thèse dirigée par **Eymery, Joël**

JURY

M. Renevier, Hubert	**Prof./INP Grenoble**	**Président**
M. Ougazzaden, Abdallah	**Prof./Georgia Tech/Metz**	**Rapporteur**
M. Zúñiga-Pérez, Jesus	**Chercheur /CRHEA/Valbonne**	**Rapporteur**
M. Harmand, Jean-Christophe	**Dir. de Rech./LPN/Paris**	**Examinateur**
M. Gendry, Michel	**Dir. de Rech./INL/Lyon**	**Examinateur**
M. Durand, Christophe	**Maître de Conf./Univ. Grenoble**	**Co-directeur**
M. Eymery, Joël	**Chercheur/CEA Grenoble**	**Directeur**

Thèse préparée au sein du **CEA Grenoble, Equipe mixte CEA/CNRS/Université Joseph Fourier « Nanophysique et Semiconducteurs »,** dans **l'Ecole Doctorale de Physique**

Acknowledgements

I would like to express my gratitude to my supervisor Dr. Joël Eymery. His vast knowledge and encouragement have been of great value for me. His understanding and personal guidance have provided a very good basis for this thesis.

I'm very grateful to Dr. Christophe Durand. His detailed and constructive comments in all kind of topics related to this work were an indispensable help.

My warm and sincere thanks go to Dr. Henri Mariette, Director of the group "Nanophysics and semiconductors" (NPSC) and to Dr. Jean-Michel Gérard, Director of INAC's division of Physics of Materials and Microstructures (SP2M), for their able leadership that has created a warm and familiar atmosphere in the lab.

I owe my most sincere gratitude to Dr. Mohamed Azize, postdoc during the first two years of my thesis, for his encouragement. With his broad knowledge he directed this thesis into the right direction.

I'm deeply indebted to Xiaojun Chen for fruitful discussions and insight in his ideas. He was a real cornerstone during the last year of this work. For his own thesis I wish him only the best.

I convey my thanks to the members of the jury: the president Prof. Dr. Hubert Renevier (INP, Grenoble), the referees Prof. Dr. Abdallah Ougazzaden (Georgia Tech, Metz) and Dr. Jesus Zúñiga-Pérez (CRHEA, Valbonne) and the examinators Dr. Jean-Christophe Harmand (CNRS/LPN, Paris) and Dr. Michel Gendry (CNRS/INL, Lyon) for accepting to serve in the jury, despite of their busy schedule.

I wish to direct sincere thanks to Dr. Fabrice Donatini, Jun-Seok Hwank, Dr. Ho-Sang Kwack and Prof. Dr. Daniel Le Si Dang (Institute Néel, CNRS) for cathodoluminescence measurements which make up for an essential part of this thesis. With their wide knowledge and their honesty they gave me important impulses during my work.

I'm grateful to Dr. Eva Monroy for RHEED measurements and her excellent advices during many interesting discussions. I would like to thank Diane Sam-Giao, Dr. Julien Renard and Dr. Bruno Gayral for photoluminescence measurements. In fruitful discussions they have contributed to the success of this thesis. I'm grateful to Dr. Joel Bleuse for PL mapping and discussions with scientific and non-scientific background. I thank Guillaume Perillat-Merceroz for STEM and CBED measurements. I thank Violaine Salvador for her technical support on SEM observations. I thank Lucien Notin for his technical support on AFM measurements.

I also wish to thank Jean Dussaud and Matthieu Lafossas for supporting us with their technical expertise regarding the MOCVD system.

I'm grateful to Dr. Isabelle Schuster for her encouragement regarding the necessary administration tasks related to this thesis.

Special thanks go to Dr. Matt Charles, Stefan Engels and Ian Tanwiar of Aixtron for their support and help regarding the MOCVD system.

Individual acknowledgements go to my friends and colleagues in the lab: Alex, Dayane, Ervin, Jun-Seok, Karthik, Miryam, Megan, Mohamed, Nitin, Oliver, Prem, Rudeesun, Sandeep, Sudarshan, Veeresh, Vincent and Xiaojun. The friendship with you helped me through all these years. I will never forget the times we had together. For your future I wish you all the best.

Finally, I have to thank my family. Your support made all this possible. Thank you!

Robert Köster

Table of contents

Résumé en Français de la thèse

Chapitre I : **Fils de nitrures III-V**

Les études concernant les nanofils de semi-conducteurs se sont considérablement développées ces dernières années à la fois du point de vue fondamental: optique, nanoélectronique, spintronique, mécanique… qu'appliqué avec l'amélioration ou la miniaturisation de dispositifs.

Le premier chapitre de cette thèse s'intéresse à faire une synthèse rapide des avantages généraux intrinsèques de la géométrie fils, ainsi que des différentes méthodes utilisées dans la littérature pour faire croître et utiliser les fils de nitrures de gallium (GaN) et leurs hétérostructures. Ces systèmes se sont avérés très intéressants en opto- et nanoelectronique avec par exemple la réalisation de diodes électroluminescentes [Kim04, Qian05], de nanolasers pompés optiquement [Qian08] et de transistors de haute mobilité électronique [Li06].

Il est rappelé que des approches très différentes ont été mises en place pour effectuer la croissance de ces matériaux: sans et avec l'utilisation de catalyseurs (principalement de Ni et parfois d'Au), et avec différentes techniques de dépôt telles que la MBE, la HVPE ou la MOCVD[1]. Il est rappelé quelques points importants.

Du point de vue chimique, la voie non-catalysée permet de s'affranchir de l'incorporation des éléments contenus dans les catalyseurs qui peuvent dégrader les propriétés physiques des fils. Du point de vue de la morphologie, la croissance sélective des nanofils qui permet de contrôler indépendamment la taille, la position et la densité a été reportée à la fois en MOCVD et en MBE, mais souffre d'une complexité de réalisation pour structurer les surfaces. Enfin, la croissance de fils en MBE sur Si (111), spontanée et sans catalyseur (nous dirons par la suite « auto-organisée »), a été obtenue par de nombreux groupes dans le monde. Ces fils sont en général petits en diamètre (20-50 nm) et permettent la réalisation d'hétérostructures longitudinales (*i.e.* le long de l'axe de croissance).

Cette analyse bibliographique a ainsi permis de définir et de justifier l'originalité des deux objectifs principaux de cette thèse.

- Le premier sera de démontrer la *croissance épitaxiale* de fils de GaN par la technique *MOCVD* avec une approche *auto-organisée sans catalyseur*, chose qui n'était pas reportée dans

[1] Voir le glossaire dans cette thèse.

la littérature. On s'intéressera à prouver que cette technique, facile d'utilisation et privilégiée dans l'industrie, est compatible avec la réalisation de fils de bonne qualité structurale et optique.

- Le second consistera à explorer les potentialités de ces fils en tant que gabarits pour faire croître des *hétérostructures,* en particulier des modulations de *dopages* n et p et des *puits quantiques InGaN/GaN* intéressants pour leurs propriétés optiques d'émission de couleur bleu. Ces deux point n'ont pas été étudiés dans la littérature et sont des briques indispensables pour réaliser des composants. On verra par la suite que les puits que l'on fait croître avec cette méthode sont très différents de ceux que l'on obtient en MBE.

Chapitre II: **Croissance bidimensionnelle de GaN par MOVPE**

Ce travail de doctorat a commencé par l'installation du premier bâti MOCVD dans le laboratoire de Physique des Matériaux et Microstructures (CEA/INAC/SP2M). Aussi avant de commencer la croissance de fils, il a fallu valider l'installation de notre équipement en réalisant des croissances standards bidimensionnelles de couches de GaN.

Après une courte introduction concernant les nombreux mécanismes impliqués dans la technique MOCVD et une description de l'équipement (réacteur de type «douchette », Aixtron), ce chapitre s'intéresse à la caractérisation de couches minces bidimensionnelles de GaN et du contrôle de leurs dopages n et p. La croissance de couches AlGaN et d'InGaN (< 20 % en Al et In) sera aussi détaillée. Une structure complète de diode électroluminescente bleue a été réalisée en combinant toute ces briques élémentaires. Le composant une fois contacté a démontré une forte électroluminescence bleue, ce qui a validé par conséquent nos capacités à croître ce type de matériaux avec cet équipement.

D'autres points importants concernant la reproductibilité et l'homogénéité des dépôts sur des substrats de saphir 3x2" d'orientation c ont aussi pu être vérifiés lors de ces expériences. On peut citer quelques résultats importants :

- Le dépôt de films de GaN a été obtenu en utilisant un régime de nucléation à basse température, utilisé classiquement dans la littérature. Des études de microscopie électronique à balayage et de microscopie à force atomique ont montré l'homogénéité morphologique de ces couches peu rugueuses (RMS[2] de 0.42 nm sur 64 μm^2). La densité de dislocation est estimée à environ 2 x 10^{8} cm^{-2}. La bonne qualité optique des couches a pu

[2] Racine carrée de la moyenne du carré de la hauteur.

être testée en photo-luminescence, avec notamment très peu de bande de défauts et une largeur de l'émission du bord de bande en accord avec les données de la littérature. Des couches d'alliages AlGaN avec une concentration maximale d'environ 20% ont aussi été obtenues avec cette technique.

- Le contrôle de niveaux de dopage compatibles avec la réalisation de composants (par exemple des LEDs) a pu être démontré, à la fois pour le type n ($5\ 10^{18}$ cm^{-3}) et pour le type p ($4\ 10^{17}$ cm^{-3}) beaucoup plus difficile à atteindre. Des mobilités respectives d'environ 320 et 9-12 cm^2/Vs ont pu être mesurées.
- La croissance de multi-puits quantiques InGaN/GaN a été réalisée et mesurée en photoluminescence. La longueur d'onde d'émission à température ambiante est comprise entre 442 et 447 nm avec une largeur à mi-hauteur d'environ 35 nm. Cette fluctuation des longueurs d'onde pourrait par exemple s'expliquer par une variation de température de seulement ± 1.5 K sur toute la surface du substrat de saphir 2".
- La combinaison de ces différentes briques de bases: croissance planaire du GaN, contrôle du dopage, réalisation de puits quantiques a permis de réaliser une diode luminescente bleue (contact électriques élaborés par le CEA/LETI/DOPT).

Le système MOVPE a par conséquent été validé par rapport aux points délicats de la technologie des composes de nitrures. Ces différents aspects vont être transposés dans les chapitres suivants au cas des fils de GaN (intentionnellement dopées ou non) et des hétérostructures de puits InGaN/GaN.

Chapitre III: **Croissance des fils de GaN par MOVPE**

Dans la littérature, les fils de GaN obtenus en MOCVD et MOVPE utilisent en général des catalyseurs d'Au et de Ni, ou des nanostructurations de surface. Ce chapitre décrit une méthode alternative originale qui n'utilise pas de catalyseur « ajouté » ni de préparation de surface extérieure au réacteur. Le procédé a lieu entièrement *in situ* dans le réacteur et on utilisera un effet d'auto-organisation des croissances de fils. Il en résulte une méthode facile à réaliser, reproductible et rapide qui s'est avérée intéressante pour étudier les mécanismes physiques mis en jeu.

La croissance des fils a été optimisée sur la surface de saphir d'orientation c déjà utilisée pour les croissances bidimensionnelles. Préalablement à la croissance des fils et après un nettoyage à haute température du substrat, on dépose *in situ* dans le réacteur une

fine couche de SiN_x d'environ 2 nm[3] en faisant réagir le silane et l'ammoniac sur la surface. Cette couche est suffisamment fine pour permettre une épitaxie des fils d'axe c sur le substrat. Les diamètres des fils sont dans la gamme 200 – 1500 nm avec une assez forte distribution et le rapport longueur/diamètre peut être supérieur à 100 pour des durées de croissance suffisamment longues. Les fils sont positionnés d'une façon quasi aléatoire sur la surface sans un contrôle direct de la position des sites de nucléation initiaux.

Une étude détaillée des mécanismes physiques mis en jeu dans la croissance est donnée dans le chapitre. Plusieurs paramètres clés nécessaire à la croissance verticale des fils sont identifiés et étudiés indépendamment les uns des autres. La méthode MOCVD est réputée pour être complexe car elle met en jeu de nombreux paramètres. La méthode auto-organisée a permis d'explorer une grande partie de ces paramètres en faisant un grand nombre de croissances et ensuite de faire une synthèse.

Il faut schématiquement contrôler trois étapes importantes pour l'obtention de fils de bonne qualité structurale et optique. Les point importants ont été publiés dans la référence [Köster2010] et peuvent être résumés ainsi:

- La préparation initiale de la surface, avant la croissance des fils, doit être contrôlée en détail par des recuits spécifiques et par l'utilisation de silane.

Pendant le recuit, nous avons observé la formation d'une fine couche d'AlN sur le saphir par plusieurs techniques (RHEED après un transfert dans un bâti MBE et réflectivité de rayons X) en accord avec la bibliographie existante. Une couche, dite de masquage[4], de SiN_x est obtenue directement en faisant réagir l'ammoniac et le silane. Un temps de dépôt d'environ 100 s et d'un recuit sous ammoniac correspond à des conditions optimales pour la formation de centres de nucléation hexagonaux plats qui sont apparus comme essentiels à la croissance de fils de bonne qualité. Pour des temps de dépôts plus longs ou en omettant le recuit sous ammoniac, la forme du germe de nucléation devient pyramidale ce qui conduit par la suite à des croissances parasites de multipodes et à des fils ayant beaucoup de défauts.

---

[3] La stœchiométrie exacte de cette couche n'a pas été déterminée. Des expériences d'XPS pourrait par exemple donner des informations quantitatives à condition que la surface soit « protégée » de la MOCVD jusqu'au bâti d'analyse.

[4] La croissance de GaN est très sélective vis-à-vis du nitrure de silicium. Plusieurs techniques de croissance sélective l'utilisent comme masque à la croissance.

- Le temps d'injection du triméthylgallium pendant la phase de nucléation détermine la taille du germe de nucléation. Des expériences de microscopie électronique à balayage et de force atomique ont expliquées la formation de défauts structuraux par la coalescence des germes et par l'accrochage latéral des germes sur des inhomogénéités de surface. Ces défauts ne peuvent pas être guéris lors de la croissance cristalline du fil. Lors des croissances développées dans cette étude, nous avons trouvé un temps optimal de nucléation d'environ 10 s, suffisamment petit pour éviter les coalescences de fils et l'augmentation du nombre de défauts.

- Un faible rapport d'élément V/III envoyé dans le réacteur est essentiel pour avoir une bonne croissance de fils. Une valeur de 16 environ conduit à une croissance optimale du point de vue structural (et optique comme on le verra par la suite) alors que des croissances avec un rapport de plusieurs centaines donnent une forte croissance latérale. Pour des fabrications de composants, cet effet est parfois utilisé pour faire coalescer des assemblées de fils à leurs sommets.

- La croissance des fils est réalisée avec le même rapport V/III que pour l'étape de nucléation, mais avec une injection simultanée de silane. Dans nos conditions, l'apport de silane est fondamental pour favoriser la croissance verticale le long de l'axe c. Des expériences de croissance à différents flux de silane donnent une valeur optimale de flux de silane de quelques centaines de nmol/min. Cette observation expérimentale n'a pas encore été confrontée à des modèles, bien que l'on puisse supposer une modification des énergies de surface du sommet et des facettes des fils par rapport au matériau non dopé.

- Les étapes de nucléation et de croissance des fils sont réalisées à 1000 °C. Une diminution de la température se traduit par une augmentation de densité mais aussi par une diminution de la qualité structurale. Une augmentation de cette température conduit à une forte évaporation du matériau et à une croissance plus difficile des fils.
Dans des conditions normales de température, on a montré que l'on avait une vitesse de croissance constante directement influencée pas les flux de gaz porteur. Cette vitesse augmente avec une diminution des gaz porteurs.

Les fils obtenus dans des conditions standards ont été étudiés en diffraction de rayons X en incidence rasante. La croissance le long de l'axe c a été confirmée ainsi que les relations

d'épitaxie dans le plan avec la rotation classique de 30° du réseau GaN par rapport au saphir sous-jacent. La largeur à mi-hauteur de la distribution angulaire des fils dans le plan est d'environ 0.61 ° et hors du plan 0.34 °. Des expériences de microscopie électronique à balayage en transmission (STEM) et de diffraction en faisceau convergent (CBED) ont montré que les deux types de polarités (Ga et N) pouvaient coexister dans le même fil séparés par une paroi d'antiphase dont le plan est perpendiculaire à l'axe c. Les fils ayant la polarité Ga montrent une instabilité du sommet du fil qui passe de l'orientation c à des plans inclinés qui peuvent induire un fort ralentissement (ou même un arrêt) de la croissance.

Enfin, les observations de microscopie électronique à balayage sur les surfaces non recuites de SiN_x ont permis de proposer un mécanisme de formation des multipodes mettant en jeu la forme et l'épitaxie du germe de nucléation.

Chapitre IV: **Propriétés optiques des fils de GaN et d'hétérostructures obtenus par MOVPE.**

La première partie du chapitre discute de la réalisation d'hétérostructures dopées. Le passage de fils dopés n (de part l'adjonction de silicium) à des fils non intentionnellement dopés (appelé par la suite structure « n-u ») est obtenue en arrêtant le flux de silane dans le réacteur après qu'une certaine longueur du fil ait été atteinte. L'incorporation de Mg en injectant du Cp_2Mg pendant la croissance des fils permet en principe d'obtenir un dopage p. L'influence de la température sur cette incorporation a été étudiée du point de vue des propriétés structurales et optiques.

- La mesure en cathodo-luminescence des structures n-u permet de localiser la signature optique des différents niveaux de dopages le long du fil. Au bas du fil, l'émission du bord de bande de GaN est située à 350 nm (3.55 eV) avec une largeur de 120 meV ce qui indique un niveau de dopage d'environ $10^{20}/cm^3$. La poursuite de la croissance sans silane ne donne pas de changement significatif de la forme du fil (pour une température maintenue à 1000 °C). L'émission du bord de bande est plus intense et se déplace à 355 nm (3.496 eV) ; elle a une largeur d'environ 70 meV compatible avec une concentration de porteur d'environ $10^{19}/cm^3$. Cette valeur est donc beaucoup plus importante que la valeur d'une couche de GaN non intentionnellement dopée qui a été mesurée à $3\ 10^{16}\ cm^{-3}$ dans

notre système. Cet « d'effet mémoire » lors de la croissance des fils restera à quantifier dans des études ultérieures[5].

- Les mesures de cathodo-luminescence effectuées sur des structures de fils commençant par une partie n et se poursuivant par une injection de Cp_2Mg montre à côté du pic de bord de bande à 355 nm, un second pic d'intensité plus faible à 370 nm (3.55 eV). A cette température (1000 °C) et comme dans le cas des hétérostructures n-u, les fils continuent à croître verticalement sous injection de Cp_2Mg. A plus basse température (850 °C), la morphologie prend une forme "d'esquimau glacé", et la cathodo-luminescence indique le même pic caractéristique d'émission que précédemment (croissance à 1000 °C) mais avec une intensité beaucoup plus importante. Corrélativement, on observe une forte émission de la bande jaune due à la croissance à basse température.
Les mesures électriques ont bien confirmé le caractère n des fils que l'on a fait croître. Pour le type p et la réalisation de diodes, les études sont en cours.

La seconde partie de ce chapitre s'intéresse au dépôt d'une structure à base de puits quantiques InGaN/GaN sur les gabarits formé par les fils en utilisant des recettes similaires à celles présentées dans le chapitre 2. Les émissions spatiales et spectrales de ces structures ont été étudiées par cathodo-luminescence en fonction de la concentration en indium (variée en changeant la température) et de la largeur du puits quantique d'InGaN.

- La microscopie électronique révèle une forte croissance radiale des multipuits quantiques autour des fils de GaN. La mesure de cathodo-luminescence montre que l'émission caractéristique du puits est localisée sur les facettes du fil et non pas seulement au sommet. Nous avons une géométrie de type cœur/coquille avec une croissance le long des plans m et non pas le long de l'axe c, et donc une contribution très différente du champ piézo-électrique.

- Des expériences de micro-photoluminescence sur des fils uniques ayant des multi-puits quantiques ont montré un déplacement vers les hautes énergies lorsque l'on augmente la température. Cela a été attribué à une baisse de la quantité d'indium incorporé.

[5] Cet « effet mémoire » n'est pas observé en croissance 2D dans le cas du silicium et dans ce type de bâti.

- La décroissance de la durée de croissance des puits, à largeur de barrière fixe, induit un déplacement vers le bleu du pic d'émission que l'on attribue à un confinement quantique dans le puits. Le comportement asymptotique de l'énergie de transition du puits en fonction du temps de croissance pour des puits de plus en plus petits, ainsi que l'absence de déplacement vers le bleu lorsque l'on excite fortement l'échantillon en cathodo-luminescence exclu la présence d'un champ piézo-électrique notable dans ces puits. Ces mesures sont donc en accord avec une croissance sur des plans m.

Chapitre V: **Conclusions et perspectives**

Ce chapitre résume rapidement les points importants et originaux obtenus durant ce travail et met en avant quelques perspectives.

L'avantage essentiel de la croissance auto-organisée aura été de fournir une méthode rapide et reproductible pour réaliser des fils et d'apporter les premiers éléments pour étudier leurs mécanismes de croissance. Le contrôle de la position, de la densité et de la taille des objets n'a toutefois pas pu être étudié en détail de part les limitations intrinsèques de cette méthode. Une perspective intéressante, déjà en cours d'étude dans le laboratoire (sujet de thèse de M. Xiajun Chen), est de développer la croissance sélective des fils sur des motifs de géométries et de tailles contrôlées. Elle devrait permettre de mieux comprendre, pour les croissances sans catalyseur, comment la matière est incorporée au sommet des fils et notamment le rôle des énergies de surface, de la morphologie et de la diffusion de surface.

Les gabarits constitués par les fils ont été ensuite utilisés pour moduler les dopages et pour émettre de la lumière avec des puits InGaN/GaN. D'autres utilisations des fils peuvent être envisagées par exemple pour faire croître des puit GaAlN/GaN en MOCVD ou des boîtes quantiques sur les facettes m en utilisant des recroissances MBE.

Pour ce qui concerne le contrôle du dopage, plusieurs études doivent être envisagées pour quantifier l'incorporation du silicium et du magnésium, ainsi que les profils de dopages accessibles : valeurs limites, raideur des interfaces... Les mesures électriques doivent être poursuivies, notamment pour évaluer les phénomènes d'activation thermique du dopage p. La taille suffisamment grande de nos objets permet d'envisager des mesures originales sur des objets uniques à la fois en spectroscopie de masse d'ions (SIMS) et en microscopie de fluorescence X. Ces deux voies sont en train d'être explorées par notre équipe en collaboration avec la PFNC du CEA Grenoble et l'ESRF. Ces résultats

pourraient également être confrontés à des mesures d'holographie électronique ou de tomographie à effet de champs qui sont ou seront accessibles localement.

Dans le cas des puits InGaN/GaN, le mécanisme de croissance cœur/coquille des hétérostructures[6] doit être mieux maîtrisé pour obtenir une couverture plus uniforme du fil. Les paramètres de croissance qui guident le recouvrement à partir du sommet des fils devront être optimisés pour en améliorer la qualité structurale et optique. L'incorporation maximale d'In dans les puits devra être comparée à ce qui est obtenu en croissance bidimensionnelle et l'apparition des dislocations devrait pouvoir être mise en évidence[7]. Une hétérogénéité du dépôt sur les arrêtes des fils pourrait être intéressante à mettre en évidence. Ces expériences devront être couplées à des mesures de microscopie électronique en transmission pour estimer l'épaisseur (et les compositions des puits en perte d'énergie) qui ne sont pas faciles à mettre en œuvre, compte tenu de la nécessité d'amincir les fils. Le diamètre est en effet trop grand pour une observation directe des fils (comme en MBE) et leur relativement faible densité rend difficile les préparations conventionnelles avec un amincissement ionique. Des mesures de sélection/positionnement et amincissement avec des faisceaux d'ions focalisés (FIB sont en cours pour essayer de répondre à ce problème.

[6] Contrairement à la croissance en épitaxie par jets moléculaires qui présente en général des croissances longitudinales.

[7] Au regard de la taille des fils, on s'attend à voir assez peu d'effet de relaxation des contraintes par rapport à une croissance bidimensionnelle.

Introduction

A *nanowire* is a nanostructure with the diameter of the order of nanometers and an aspect ratio of the length to the diameter typically larger than 10. Alternatively, nanowires can be defined as structures that have a thickness or diameter constrained to tens of nanometers or less and an unconstrained length. At these scales, quantum-mechanical effects may become important. By extension, the term *wire* and *rod* have been used for typical diameters up to micrometers. From the past ten years the research on wires and nanowires has been of increasing interest. Today nanowires have a huge impact on research, both in fundamental understanding and in technological development. Their geometry opens new possibilities in device fabrication and manipulation that stimulate their use to get a deeper insight into fundamental processes on the nanometer scale. Perhaps the most obvious use for nanowires is in electronics. Some nanowires are very good conductors or semiconductors and their miniscule size means that manufacturers could fit millions of transistors or functions on a single microprocessor. Nanowire heterostructures allow also longitudinal as well as lateral quantum confinement. A better control of the size and position of the quantum dots compared to 2D layers may be achieved, which represents a promising system for the future development of single electron transistors. But nanowires also may play an important role in many other fields like sensors, neuronal connections, thermoelectricity or electricity generation, quantum computers and optoelectronics with their inclusion in solar cells or in light emitting diodes (LEDs) including single photon emitters. All these works are still in the phase of fundamental research but guide a path to future technological innovations.

This thesis focuses on gallium nitride (GaN) based wires. Polycrystalline GaN was first synthesised in 1932 [Johnston32]. With the beginning of the 1970s, the growth of the first epitaxial GaN layers was reported in literature [Maruska71, Manasevit71, Yoshida75]. At this point in time, the scientific community became aware of the huge potential of GaN, InN, AlN and their alloys. The final breakthrough came in 1989 with the successful p-doping of GaN with Mg followed by activation with low-energy electron beam irritation (LEEBI) [Amano89] and later by a thermal annealing under nitrogen [Nakamura92a]. GaN and its alloys became the preferred materials for the production of blue and white light LEDs and the blue laser diode first fabricated by the Nichia Corporation. GaN exhibits remarkable emission properties in the UV range and by applying InGaN, the emission range can be extended up to green. Recently, an InGaN-based green emitting laser diode,

grown on semi-polar GaN, was demonstrated by Osram AG [Avramescu09]. This recent achievement shows the persistent interest in these materials not only in basic research but also in industrial device fabrication.

The great success of bi-dimensional (2D) GaN-based devices has inspired the research on GaN-based nanowires. Optoelectronic devices as semiconductor nanowire based LEDs [Kim04, Qian05], optically pumped lasers [Qian08] and photovoltaic devices [Kempa08, Dong09] have been demonstrated in the past years. Furthermore, semiconductor nanowires are used as building blocks in nanoscale electronics, as high electron mobility transistors (HEMTs) [Li06b] and neuronal connections [Patolsky06]. Both, molecular beam epitaxy (MBE) and metal-organic chemical vapour-phase deposition (MOCVD) are today the two most important growth techniques for GaN-based nanowires. In MBE, nanowires are grown by a catalyst-free, self-assembled approach [Calleja00, Tchernycheva07, Songmuang07, Landré08, Ristic08, Aschenbrenner09] as well as by a catalyst-assisted approach [Duan00, Lee04, Geelhaar07]. For MOCVD, the growth techniques can be divided into two approaches, a catalyst-assisted approach [Kuykendall03] comparable to the catalyst-assisted approach in MBE and a catalyst-free approach using pre-patterned substrates [Deb05, Hersee06]. The MOCVD growth of catalyst-free self-assembled nanowires, equivalent to the MBE catalyst-free self-assembled approach, is not yet reported in literature and will be the main goal of this thesis. Surface preparation and the wire growth will be carried out in the same process run, making this approach time efficient compared to other techniques using metal catalysts and pre-patterned substrates.

All the experiments described in this work were carried out in a Thomas Swan (Aixtron AG since 2008) 3x2" close coupled showerhead (CCS) MOCVD setup, the first one of this type in the laboratory. The installation began in January 2007 with the positioning of the system in the laboratory followed by the installation of the technical infrastructure i.e. the electricity- and gas-line system as well as the security system by external contractors. The system itself was installed from May 2007 and tested by Aixtron engineers. This procedure included the connection of the system to the external gas-line system and the verification of absence of leaks in the gas-line system, the preparation of the scrubber, the installation of the material sources and the mounting of the heater in the reactor chamber followed by a temperature calibration. At the end of June 2007, the system was ready for the validation period. During this time, the process was adjusted to fulfil the expected specifications of high quality growth of bi-dimensional GaN and the ternary alloys InGaN and AlGaN.

After the successful validation of the system, the first attempts in the direction of wire growth were started in September 2007. Several months were necessary to gain the first promising results. Afterwards, the growth parameters were optimised step by step. In parallel, the impact of the different growth parameters was studied, allowing a deeper understanding of the involved processes. The optimisation of the *in situ* surface treatment, as well as the actual growth parameters resulted in wires suitable as templates for the growth of longitudinal heterostructures with doping variation and the deposition of a core-shell InGaN/GaN multi quantum well (MQW) structure. The optical properties of the grown structures were measured by micro-photoluminescence (μPL) and cathodo-luminescence on single wires respectively.

The thesis manuscript is subdivided into five chapters.

- **Chapter 1** will first give a short historical overview and a description of the (nano)wire geometry advantage and will then present the fundamental properties of the III-nitride compounds. The rest of the chapter will resume the state of the art in III-nitride wire growth and their applications.

- **Chapter 2** will deal with the general description of the MOCVD setup and its experimental validation procedure. The standard growth and properties of GaN bi-dimensional films, doping control and growth and properties of AlGaN films and InGaN/GaN MQWs will be discussed, finally allowing the fabrication of a blue light emitting diode.

- **Chapter 3** will describe the self-assembled growth of GaN wires by MOCVD, starting with the *in situ* surface preparation and the deposition of a thin dielectric SiN_x layer followed by the deposition of GaN. The importance of experimental key parameters as the SiN_x deposition time and annealing, the reactor temperature, pressure, V/III ratio and the injection of silane during growth will be studied. In parallel the importance of the nucleation process will be stressed as well as the structural quality and epitaxial relationships of the wires.

- **Chapter 4** will address the growth and optical properties of longitudinally doped heterostructures and radial InGaN/GaN multi quantum-wells using the GaN wires

as templates. The optical features, for example the spatial and spectral emission, will be quantitatively studied and compared with the literature results.

- **Chapter 5** will finally summarize the most important results of this thesis and will propose a few perspectives of this work.

Chapter 1

III-nitride wires

1.1. Introduction of nanowire growth and properties

1.1.1. Historic overview of nanowire growth

Nanowire-like structures were first mentioned in literature in 1964 with respect to the growth of silicon whiskers by a catalyst-driven mechanism [Wagner64] called VLS (vapour liquid solid) growth. A small piece of gold is placed on a silicon substrate, which is then heated up. The gold forms small droplets and under injection of $SiCl_4$ and H_2 they catalyse the growth of Si whiskers. Figure 1.1 a) shows the principle of this catalyst-driven growth. Wagner and Ellis explain this phenomenon through the fact that the liquid droplet is a preferred site for deposition from the vapour, which causes the liquid to become supersaturated with Si. The whisker grows by precipitation of Si from the droplet with the same crystalline orientation as the silicon substrate (<111>-direction).

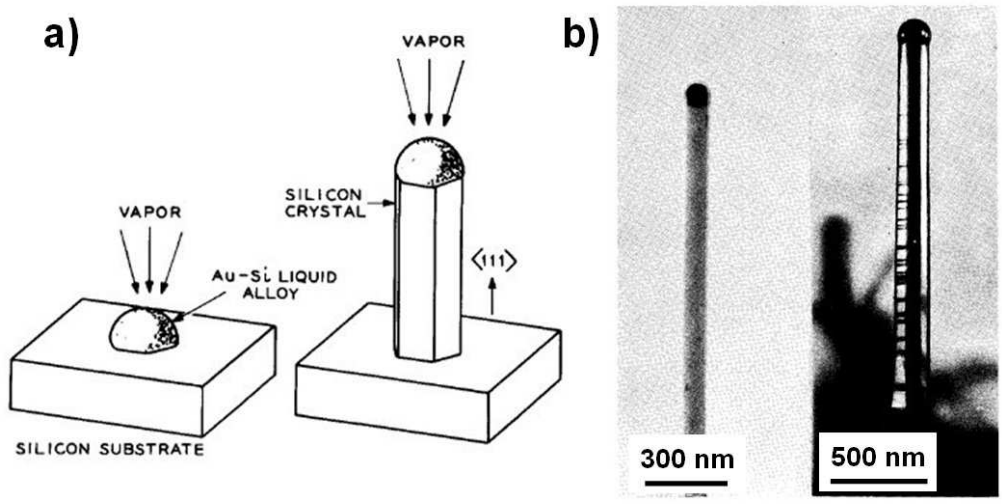

Figure 1.1 a) Schematic view of catalyst-driven growth of silicon wires, b) TEM images of silicon wires with a gold catalyst on top [Wagner64]

The silicon leaving the catalyst is replaced by material from the gas phase[8]. In Figure 1.1 b) two TEM images of the resulting whiskers are shown. The whisker diameter is comparable to the catalyst size (black dot on top). This kinetics and the mechanisms of the VLS growth were then modelled by Givargizov in 1975 [Givargizov75].

These results increased the interest to develop new fabrication techniques for this kind of nanostructures. In the following years other approaches, both top-down and bottom-up techniques, were developed by taking advantage of the improvement of growth methods (molecular beam epitaxy, metal-organic chemical vapour deposition…).

For example, Reed *et al.* [Reed88] studied electronic transport through three-dimensionally confined GaAs/GaAlAs quantum-wells in a wire geometry using a top-down approach (electron-beam lithography to define metallic dot mask and reactive ion etching with BCl_3). Petroff *et al.* [Petroff84] used a molecular beam epitaxy (MBE) step flow technique to get wire heterostructures and Kapon *et al.* [Kapon89] developed the "V-groove approach" to arrange quantum wells in wire geometry. The VLS or catalyst-assisted growth was then reintroduced in the mid-nineties corresponding to the beginning of modern nanowire research.

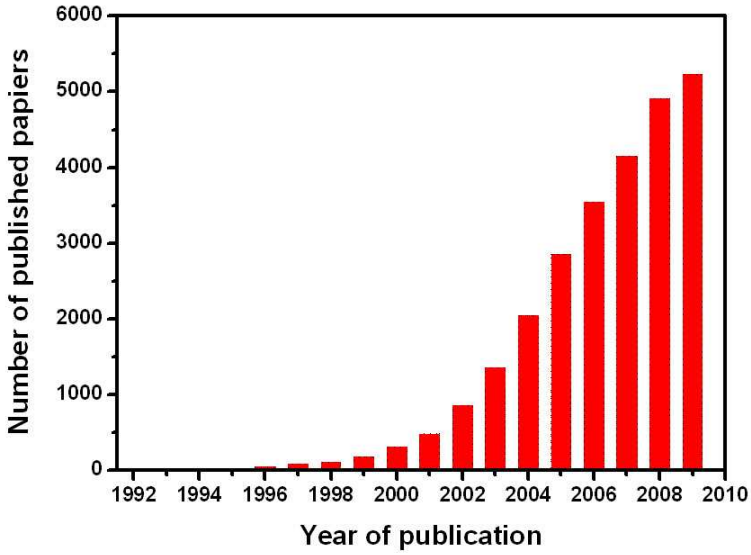

Figure 1.2: Number of publications per year dealing with the growth or the application of nanowires from 1992 to 2009 Source: ISI Web of Knowledge – number of publications found for the topic keyword "nanowires" for the respective year

[8] Surface diffusion along the wire edges, which is also an important point to explain the growth mechanisms [Givargizov75], was not explicitely mentioned in this pionneer paper.

Hiruma *et al.* demonstrated the first nanowire heterostructure (GaAs/InAs) in 1996 [Hiruma96] with the catalyst-assisted approach. This method has later been applied to many materials such as GaAs, GaP, InP, InAs, ZnS, CdS, ZnSe, CdSe, Si and SiGe [Duan00a] with some leading groups in Europe (Lund) and the United States of America (Harvard, Berkeley).

The growth of GaN nanowires actually started in the 2000s by use of catalysts [Duan00b] and by a catalyst-free approach [Calleja00]. In the following years, first devices as GaN nanowire based LEDs [Kim04, Qian05], high electron mobility transistor (HEMT) structures [Li06b], single wire photovoltaic devices [Dong09] and optically pumped single nanowire lasers [Qian08] were demonstrated.

The growth of GaN nanowires and the realisation of GaN nanowire-based devices are still in an experimental stage. Deeper understanding of the fundamental processes during the growth as well as fabrication techniques for industrial applications still have to be developed in order to demonstrate that they can be used as building blocks for future technological innovations.

1.2. Advantages of the wire geometry

Nanowires are longitudinal nanostructures with diameters of some ten nanometers with an aspect ratio (Length/Diameter) larger than 10. The small diameter allows lateral confinement of carriers that can be used to get electrical and optical properties different from the bulk properties.

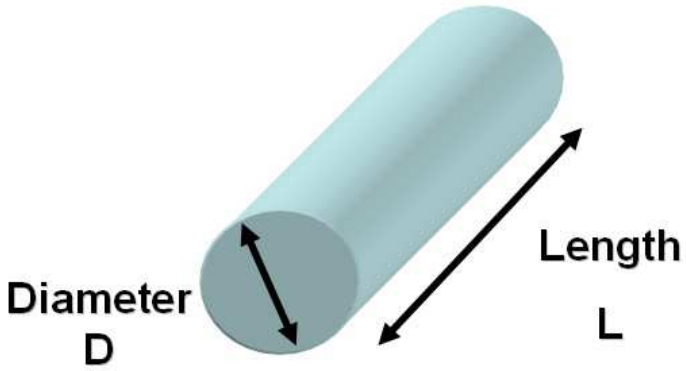

Figure 1.3: Schematic illustration of the nanowire geometry

The 1D nanowire geometry exhibits some advantages compared to 2D structures:

- Due to their small lateral dimensions, nanowires may exhibit surface-strain relaxation without the formation of extended defects usually observed in highly mismatched materials. Therefore nanowires are usually mono-crystalline and exhibit a high structural quality.

- The surface/volume ratio is large compared to 2D layers or bulk materials; this is why they are a promising building block for future application in sensors [Zheng05] and photovoltaic devices [Kempa08].

- Their geometry enables wave-guiding as demonstrated in CdS nanowires by Barrelet *et al.* [Barrelet04], which makes them an interesting building block for nanoscale photonic devices.

- Nanowires allow the control of the longitudinal and lateral carrier confinement of quantum dots (QDs) heterostructures and also an extremely easy manipulation and electrical contacting. This explains why these structures have motivated a large number of studies in spintronics [Fert99, Allwood05, vanDam06], nanoelectronics [Thelander05, Thelander06]) and optics [Pauzauskie06, Li06a].

- The use of catalysts allows the control of the nanowire diameter as well as the density of the nanowire assembly. Pre-patterned substrates additionally allow the control of the position of the nanowires on the substrate [Hersee06, Kishino08].

Surface strain relaxation may enable the growth of defect-free longitudinal heterostructures even for materials with several percent of lattice mismatch [Eterkin05, Glas06a]. The growth of III-nitride heterostructures is especially difficult in 2D layers because of the lattice mismatch of 2.4 % between GaN and AlN and 11 % between GaN and InN. For sufficiently small diameters (*i.e.* when the surface relaxation will play an important role), the nanowire geometry opens the way to grow high quality heterostructures without any defects. Figure 1.4 depicts the calculation of the critical thickness for 60 ° misfit dislocation nucleation as a function nanowire radius for longitudinal heterostructures. In core/shell

nanowire systems, the core radius and the shell thickness both play an important role as was shown by Raychaudhuri and Yu [Raychaudhuri06]. Figure 1.5 a) shows the GaN core radius as a function of the InGaN critical shell thickness for different indium concentrations[9]. Below the respective lines, the formation of dislocations is not expected and therefore the heterostructure should be defect free.

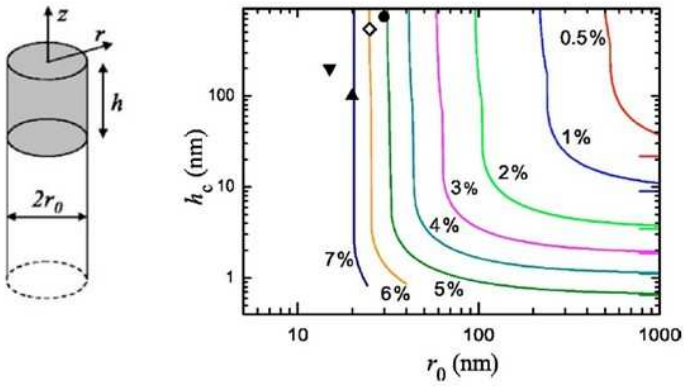

Figure 1.4: Variations of the critical thickness of a misfitting layer growing on top of a nanowhisker as a function of the whisker radius, for various values of the misfit given in percent near each curve and a Poisson's ratio of 1/3. [Glas06a]

Figure 1.5 b) provides the critical core radius for different core/shell systems as a function of the alloy composition. Below the critical radius, defect formation is not expected whatever the shell thickness.

[9] In this case, a pure edge dislocation along the [0001] direction with Burgers vector in the <11-20> plane is expected to be stable and to relieve strain in the cross section of the nanowire. The occurrence of relaxation by a dislocation loop is also discussed in this paper

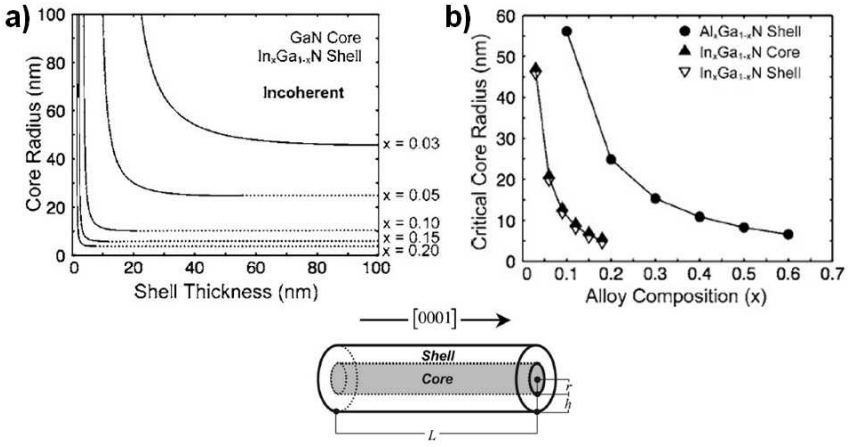

Figure 1.5: a) Limit between coherent and incoherent core/shell heterostructure. The GaN core radius is given as a function of the InGaN shell thickness for different indium concentrations. b) Critical core radius as function of the alloy composition for different core shell systems (black dots: GaN core – AlGaN shell, black triangles: InGaN core – GaN shell, white triangles: GaN core – InGaN shell)

1.3. Properties and application of III – nitride wires

1.3.1. III-nitride properties

III-nitrides (GaN, AlN, and InN) and their alloys are nowadays widely used in light emitting devices for example blue and white LEDs and blue laser diodes. Research on III-nitrides started in the 1970s, when the first epitaxial GaN layers where grown by hydride vapour phase epitaxy (HVPE) in 1969 [Maruska71], then in 1971 by metal organic vapour phase epitaxy (MOVPE) [Manasevit71] and later in 1975 by MBE [Yoshida75].

Crystalline structure

III-nitrides crystallise in two crystallographic configurations: the hexagonal wurtzite phase and the cubic zinc-blende phase. Figure 1.6 shows the stacking periodicity of the wurtzite phase a) and the zinc-blende phase b). This section will be focussed on the wurtzite phase, the thermodynamically most stable configuration for the III-nitrides under standard conditions [Yeh92].

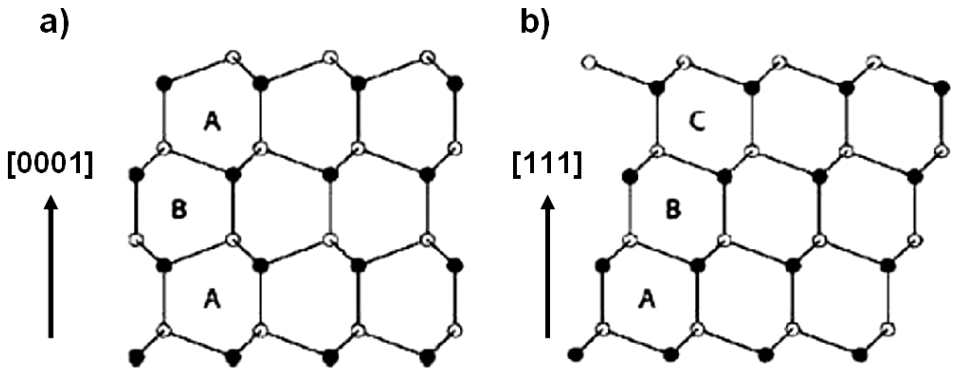

Figure 1.6: a) Wurtzite ABABA… planes along the [0001] axis and b) Zinc-blende ABCABCA… stacking along the [111] axis. Structures are viewed respectively along the [1 1 -2 0] and [1 -1 0] directions

The wurtzite structure consists of two hexagonal-closed-packed (HCP) lattices of metal- and nitrogen atoms. The unit cell is represented by two interconnected hexagonal close-packed (HCP) sublattices shifted 5/8 of lattice parameter c along the c-axis ([0001]-direction). Figure 1.7 shows the atomic positions in the wurtzite structure and a schematic view of the most stable crystallographic planes. The hexagonal unit cell is defined by the length of the hexagon's side (a) and the height (c) of the hexahedron. Table 1.1 gives the lattice parameters for GaN, InN and AlN at room temperature.

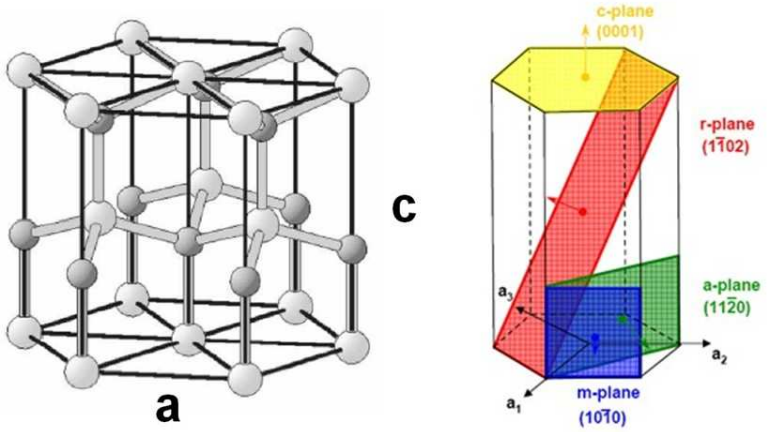

Figure 1.7: a) Left: Wurtzite structure consisting of two HCP lattices, metal atoms – light grey, nitrogen atoms – dark grey. Right: Usual planes in the hexagonal lattice

Lattice parameter [Å]	GaN	InN	AlN
a	3.189	3.540	3.112
c	5.185	4.982	5.705

Table 1.1 : Lattice parameters for GaN, InN and AlN at RT [Morko94]

For alloys as $In_xGa_{1-x}N$ and $Al_xGa_{1-x}N$, the lattice parameters are usually approximated by Vegard's law [Vegard21].

$$a_{A_xB_{1-x}N} = xa_A + (1-x)a_B$$
$$c_{A_xB_{1-x}N} = xc_A + (1-x)c_B \qquad \text{(eq. 1)}$$

Ga – and N-polarity

The Wurtzite structure is not central-symmetric and the $[0001]$ and $[000\bar{1}]$ directions are not equivalent. The (0001)-face exhibits different properties than the $(000\bar{1})$-face in terms of surface morphology, chemical reactivity and growth conditions. Figure 1.8 shows a schematic view of the two possible orientations of the GaN stacking.

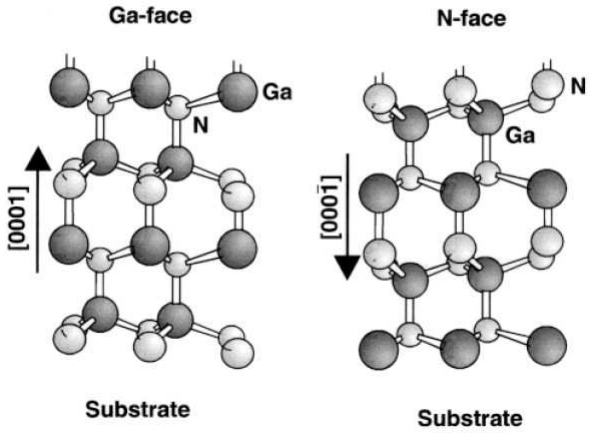

Figure 1.8: The two polarities of GaN with Ga-face and N-face orientations [Ambacher98]

Spontaneous and piezoelectric polarisation

Nitrogen atoms exhibit a larger electro-negativity than metal atoms and therefore the bond has an electric dipole. Along the [0001] direction, this charge distribution cannot be compensated, and leads to a macroscopic spontaneous polarisation in nitride materials reported in Table 1.2 for GaN, InN and AlN. The resulting electric fields can reach up to several MV/cm in (0001) orientated quantum wells [Bernardini97].

	GaN	**InN**	**AlN**
P_{sp} [C/cm^2]	-0.029	-0.032	-0.081

Table 1.2 : Calculated spontaneous polarisation for GaN, InN and AlN [Bernardini97]

Strain can modify the atomic position and the charge distribution in the crystalline lattice and can also lead to a piezoelectric polarisation. The piezoelectric polarisation in wurtzite III-nitrides can be calculated with the following equation [Romanov06]:

$$\vec{P}_{pz} = \begin{pmatrix} 0 & 0 & 0 & 0 & e_{15} & 0 \\ 0 & 0 & 0 & e_{15} & 0 & 0 \\ e_{31} & e_{31} & e_{33} & 0 & 0 & 0 \end{pmatrix} \times \begin{pmatrix} \varepsilon_1 \\ \varepsilon_2 \\ \varepsilon_3 \\ \varepsilon_4 \\ \varepsilon_5 \\ \varepsilon_6 \end{pmatrix} \qquad \text{(eq. 2)}$$

e_{ij} are the piezoelectric coefficients of the material and $(\varepsilon_1, \varepsilon_2, \ldots \varepsilon_6)^T$ the stress tensor.

	GaN	**InN**	**AlN**	**Ref.**
e_{15} [C/m^2]	-0.30	-	-0.48	[Ambacher00]
e_{31} [C/m^2]	-0.49	-0.57	-0.60	[Bernardini97]
e_{33} [C/m^2]	0.73	0.97	1.46	[Bernardini97]

Table 1.3 Calculated piezo electric constants e_{15}, e_{31} and e_{33} for GaN, InN and AlN

For a growth direction along c, $P_{pz} = 2\left(e_{31} - \frac{C_{13}}{C_{33}} e_{33}\right)\varepsilon$ where $\varepsilon = (a - a_0)/a_0$ (a_0 and a are the in-plane lattice constants of the unstrained and strained crystals).

The vector sum of the spontaneous and the piezoelectric polarisation gives the overall polarisation in the crystal.

Discontinuities of the polarisation vector at interfaces lead to charge accumulation, which in turn generates internal electrical fields. Such large fields have huge influence on the optical properties of the structure. The most obvious one is the Quantum Confined Stark Effect (QCSE) which will be discussed later since it introduces a red shift in the emission energy of quantum wells.

Dislocations

Dislocations in nitrides are generated via plastic relaxation of the material. They are extended linear defects propagating along specific directions and defined by their Burgers and line vectors[10]. They are known to decrease the performance of optoelectronic devices by creating non-radiative recombination centres [Sugahara98]. The lattice mismatch between the substrate and the overgrowth can create "misfit dislocations". When they propagate to the surface, they are called threading dislocations (TDs) [Kapolnek95, Chien96, Ponce96]. Three types of dislocations are usually distinguished: edge, screw and mixed.

In edge-type dislocations, the Burgers vector is perpendicular to the dislocation line. A half-plane perpendicular to $\vec{b}$ is inserted into the crystal as illustrated in Figure 1.9.

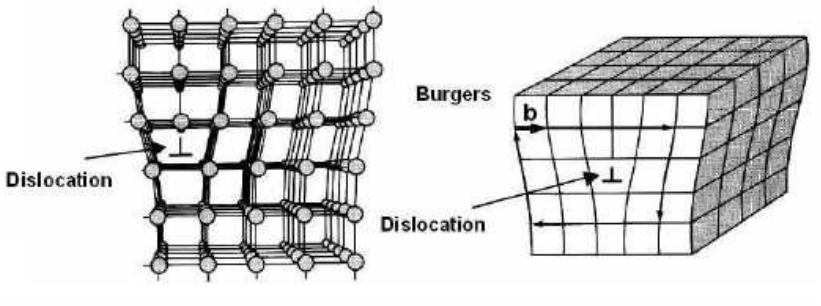

Figure 1.9: Edge-type dislocation with $\vec{b}$ perpendicular to the dislocation line

[10] The dislocation line separates the unaffected part of the crystal from the shifted region. It represents the line of propagation of the dislocation. The Burgers vector is defined as the vectorial difference between two closed lattice circuits: one in the deformed crystal that surrounds the dislocation line and a similar one in the crystal without deformation. It is invariable around all points of a given dislocation and independent on the chosen closed circuit. Its module carries information about the shift magnitude and the strain energy released by the formation of the dislocation.

In the case of wurtzite nitrides they lie in the $(1\bar{1}00)$ planes and their line is along the [0001] direction. The Burgers vector is typically $1/3 <1\bar{2}10>$. They mainly occur at the first stage of the growth when the material coalesces to a 2D layer [Hiramatsu91, Heying96].

Screw-type dislocations present dislocation lines parallel to the Burgers vector <0001>. Two regions are shifted with respect to each other separated by the dislocation line (Figure 1.10). Like the edge-type dislocation, the screw-type dislocation lies in the $(1\bar{1}00)$ planes. The Burgers vector is along the $[0001]$ direction.

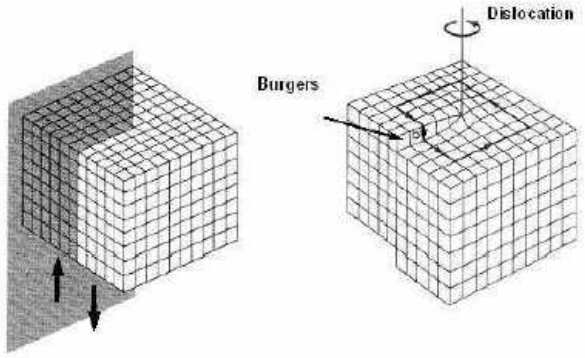

Figure 1.10: Screw-type dislocation with $\vec{b}$ parallel to the dislocation line

A combination of these two dislocation types is called a mixed dislocation. An example of a mixed dislocation is given in Figure 1.11. The dislocation is of the screw-type when it enters the crystal in A and leaves the crystal as an edge-type dislocation in B. In GaN, the Burgers vector is usually $1/3 <11\bar{2}3>$.

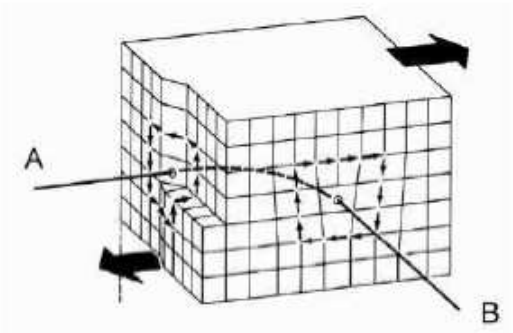

Figure 1.11: Mixed dislocation: a combination of Screw-type and edge-type dislocation

Electronic properties

III-nitride semiconductors exhibit a direct band gap reported at room temperature (RT) in Table 1.4. Figure 1.12 shows the position of the band gap as a function of the lattice parameter for several usual semiconductor compounds. The illustration reveals that the Ga/In/Al-N alloys cover the whole spectrum from the deep ultra violet to the near infrared; this explains their interest for optoelectronic applications.

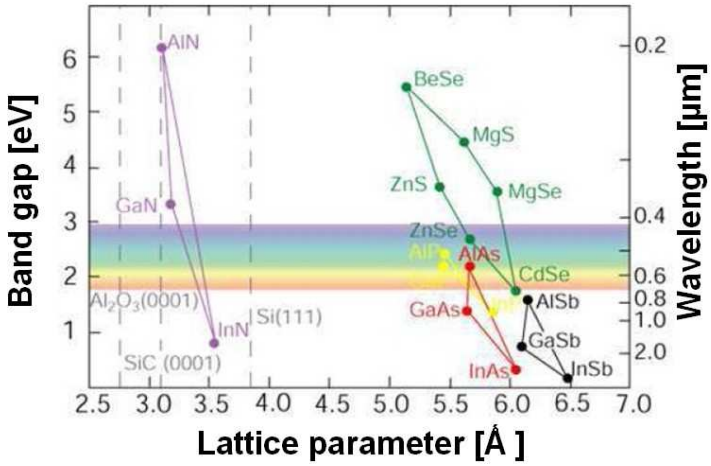

Figure 1.12: Band gap energy/emission wavelength as a function of the lattice parameter for several semiconductor families

	GaN	InN	AlN	Ref
E_g at 300 K [eV]	3.51	0.65	-	[Pugh99]
	-	-	6.24	[Wang04a]

Table 1.4 : Band gap of GaN, InN and AlN at RT

Figure 1.13 illustrates the Brillouin zone of wurtzite GaN and the corresponding band structure showing the direct band gap along Γ.

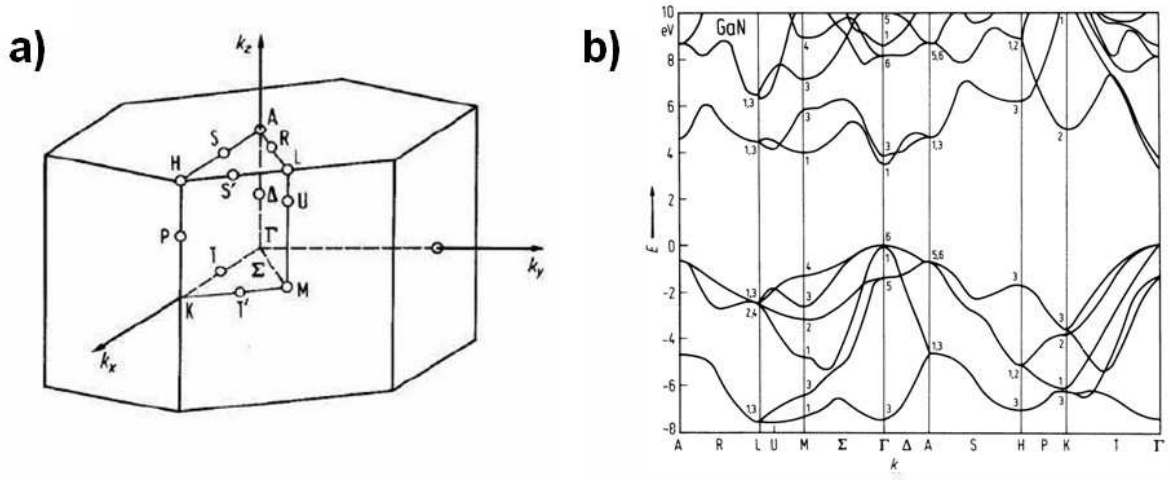

Figure 1.13: a) Brillouin zone of wurtzite GaN [www.ioffe.ru/SVA/NSM/] and b) its band structure [Bloom74]

The variation of the band gap with temperature is given by Varshni's law [Varshni67].

$$E_g(T) = E_g(0) - \frac{\alpha T^2}{\beta + T} \qquad \text{(eq. 3)}$$

$E_g(0)$ is the band gap energy at 0 K. The parameters α and β are tabulated, taking into account the electron-phonon interaction. As shown in Table 1.5, the red shift between 0 K and 300 K is about -68, -66, -96 meV for GaN, InN and AlN respectively.

	$E_g(0)$ [eV]	**α [meV/K]**	**β [K]**	**E_g (300 K) [eV]**	**Ref.**
GaN	3.489 3.492	0.887 0.531 0.909	874 432 830	3.421 3.426	[Leroux99] [Tripathy99] [Vurgaftman03]
InN	0.69	0.414	454	0.641	[Walukievicz04]
AlN	6.126	1.799 1.999	1462 1429	6.03	[Guo94] [Vurgaftman03]

Table 1.5 : Calculated values for $E_g(0)$ and Varshni's parameters (α and β) specifying the calculated band gap at RT

The band gap of ternary alloys $A_xB_{1-x}N$ is usually calculated by the following formula:

$$E_g^{A_xB_{1-x}N}(x) = (1-x)E_g^{AN} + xE_g^{BN} - x(1-x)b^{ABN} \qquad \text{(eq. 4)}$$

b denotes the bowing parameter [Wu03].

	b(eV)	Ref.
$In_xGa_{1-x}N$	1.782 ± 0.076	[Liou05]
	1.916 ± 0.068	[Liou05]
	1.440 ± 0.000	[Caetano07]
$Al_xGa_{1-x}N$	0.353 ± 0.024	[Kuo02]
	0.341 ± 0.035	[Liou05]
	0.351 ± 0.043	[Liou05]

Table 1.6: Values of the bowing parameters for InGaN and AlGaN alloys

1.3.2. Properties and applications of III-nitride nanowires

The application of III-nitride nanowires, especially GaN nanowires, range from the fabrication of optical devices as nanowire-based LEDs [Kim04, Qian05] and optically pumped nanowire-based lasers [Qian08] to high electron mobility transistors [Li06b]. Sensor fabrications based on III-nitride nanowires, as Au [Dobrokhotov06] or DNA [Simpkins07] functionalised GaN nanowires have not been developed as far by now.

1.3.2.1. GaN wires

GaN (nano)wires have been fabricated by MBE and MOCVD with both catalyst and non-catalyst methods. Their diameter ranges from tens of nanometers up to more than a micrometer. They exhibit wurtzite structure with hexagonal cross section, *i.e.* for a growth along the c-direction, but nanowires grown by the catalyst-assisted MOCVD preferentially grow along the a-axis with a triangular cross-section [Kuykendall03]. The wires are generally strain-free due to surface relaxation and exhibit good optical quality. For MBE

catalyst-free wires, a near band edge (NBE) FWHM of 1.26 meV at low temperature has been reported [VanNostrand06].

The coalescence of GaN wires has been used to grow free standing c-plane GaN layers [Bougrioua07]. This technique overcomes the lattice-mismatch occurring at the interface between the 2D layer and the substrate. A similar approach, using catalyst assisted MOCVD growth has been used to grow free standing a-plane GaN [Li09].

The covering of the full 0.2 – 2 μm emission range with III-nitride compounds (shown in Figure 1.12) can be obtained by controlling the growth of ternary InGaN and AlGaN alloys. In contrast to the huge amount of publications concerning the growth of GaN wires, InN/InGaN and AlN/AlGaN wires are rarely reported.

1.3.2.2. InN alloy based nanowires

Pure InN/InGaN-based nanowires

Kuykendall *et al.* [Kuykendall07] demonstrated the growth of InGaN nanowires with an indium concentration of up to 90 % by CVD. Chloride precursors has been used allowing a growth temperature between 600 – 650 °C suitable for the incorporation of high indium concentrations. Figure 1.14 shows SEM images of the resulting nanowire growth. For low indium concentrations, the wires exhibit a diameter of several tens of nm and a needle-like shape. For high indium concentrations (75% - 90%), the nanowires become thicker and reach a diameter of about 100 nm with a hexagonal cross section. No phase separation has been observed and optical measurements revealed the full tunability of the band gap from 3.4 to 1.25 eV (see the plot in Figure 1.14).

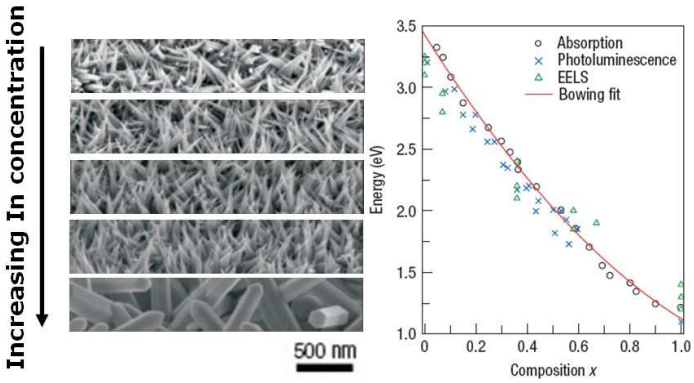

Figure 1.14: Growth of InGaN alloy wires by CVD (left). Band edge energy as function of the alloy composition (right) [Kuykendall07]

With increasing indium molar fraction a broadening of the emission peak is observed (not displayed here). These results have been interpreted as promising for the development of nanowire-based light emitting devices covering the full visible spectrum up to the near infrared.

1.3.2.3. InGaN/GaN-based nanowire heterostructures

Like in 2D materials, InGaN/GaN heterostructures are the main building block for nanowire-based LEDs, lasers and photovoltaic devices. The experimental realisations are still at the beginning of their development but they already shows a trend for potential commercial applications. In this section, a short overview on the basic properties of these devices will be given.

LED

Kim *et al.* [Kim04] demonstrated the fabrication of a longitudinal InGaN/GaN nanowire LED assembly. The wires are grown directly on a 2D GaN template by metal organic hydride vapour phase epitaxy (MO-HVPE) without the use of catalysts or pre-patterned substrates. The nanowires consist in stacking n-type GaN at the bottom followed by $In_{0.25}Ga_{0.75}N$/GaN superlattice and by p-type GaN on top. The whole array is buried in spin-on glass (SOG) after the growth in order to electrically isolate the individual wires. The top of the resulting 2D structure is covered with a transparent Ni/Au electrode (see Figure 1.15 a)). A thick Ni/Au electrode (p-pad) is deposited on the surface and the n-contact, consisting of Ti/Al electrodes, is deposited on n-type GaN after etching. This vertical design leads to an efficient flow of the injected carriers confined inside the wires. Figure 1.15 b) shows the light-output power as a function of the applied current.

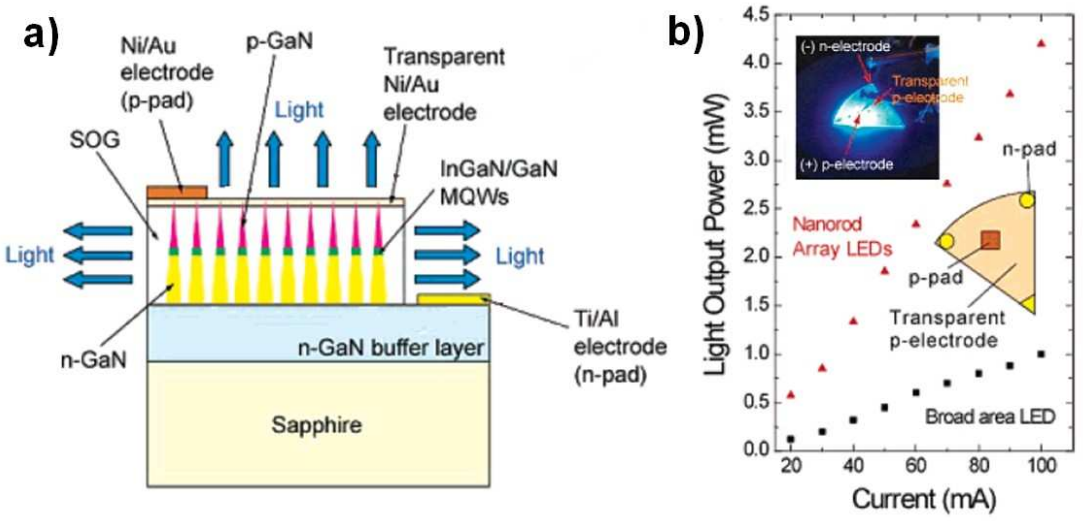

Figure 1.15: a) Schematic view of the longitudinal InGaN/GaN MQW LED b) Light-output power as the function of the applied current. The inset shows the light emission of the device under electrical injection [Kim04]

Another important result based on single GaN nanowires has been obtained by Qian *et al.* [Qian05]. Triangular shaped n-doped GaN nanowires grown by the catalyst-assisted MOCVD method have been used as a template for the deposition of an InGaN/GaN/p-AlGaN/p-GaN shell structure (see Figure 1.16 a)). The emission wavelength of the InGaN shell is controlled by changing the indium concentration in the InGaN active layer. The inset in Figure 1.16 b) shows a SEM image of a single contacted nanowire with the n- and p-pads. The current versus voltage plot demonstrates the rectification behaviour expected for the n-p-junction. Figure 1.16 c) shows the normalised electroluminescence (EL) emission for wires having different indium concentrations. The wavelength ranges from 367 nm for an In-concentration of about 1 % to 577 nm for an In-concentration of 35 % in the active layer. Figure 1.16 d) shows optical microscopy images of the structure under a forward bias of 9 and 11 V respectively. The emission is mainly observed at the top of the wire, giving evidence of light guiding inside the nanowire.

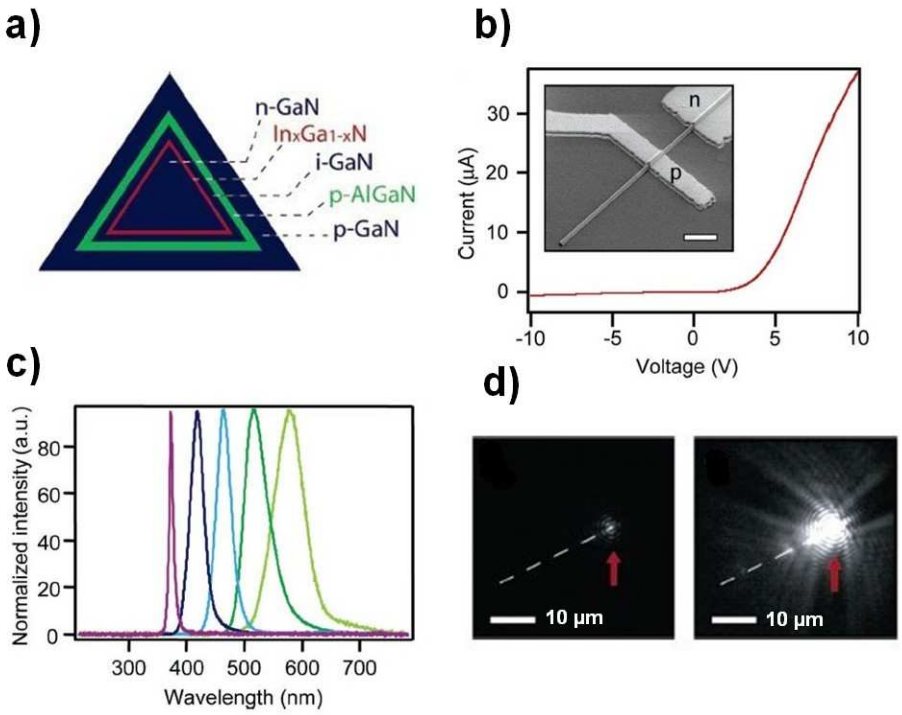

Figure 1.16: a) Schematic view of single nanowire LED structures based on an n-GaN core wire with InGaN/i-GaN/p-AlGaN/p-GaN shells, b) Connected wire with n- and p-pads and corresponding I-V curve, c) Normalised EL spectra for different In-concentrations, d) Optical microscopy images for 9 and 11 V forward bias [Qian05]

Laser

Qian *et al.* [Qian08] also demonstrated lasing on single GaN nanowires with an InGaN/GaN MQW core-shell heterostructure. As before [Qian05], the GaN core wire was grown by catalyst-assisted MOVPE growth resulting in a triangular cross section. This step is immediately followed by the InGaN/GaN MQW (x 26) shell deposition. A schematic view of the structure is given in Figure 1.17 a). Dark-field cross-section STEM revealed the MQW structure growing along the $(1\bar{1}01)$ facets, but not along the third facet of the triangle, i.e. the (0001) facet in which the growth rate is very small. The nanowire is optically pumped and shows lasing for power densities larger than 700 kW/cm^2. Figure 1.17 c) shows the PL spectra of four nanowires with different In-concentrations in the QWs. The emission lines span from 381.1 nm for the lowest indium concentration (5%) up to 477.9 nm for the highest concentration (23 %). An electrically pumped nitride nanowire based laser is not yet reported in the literature.

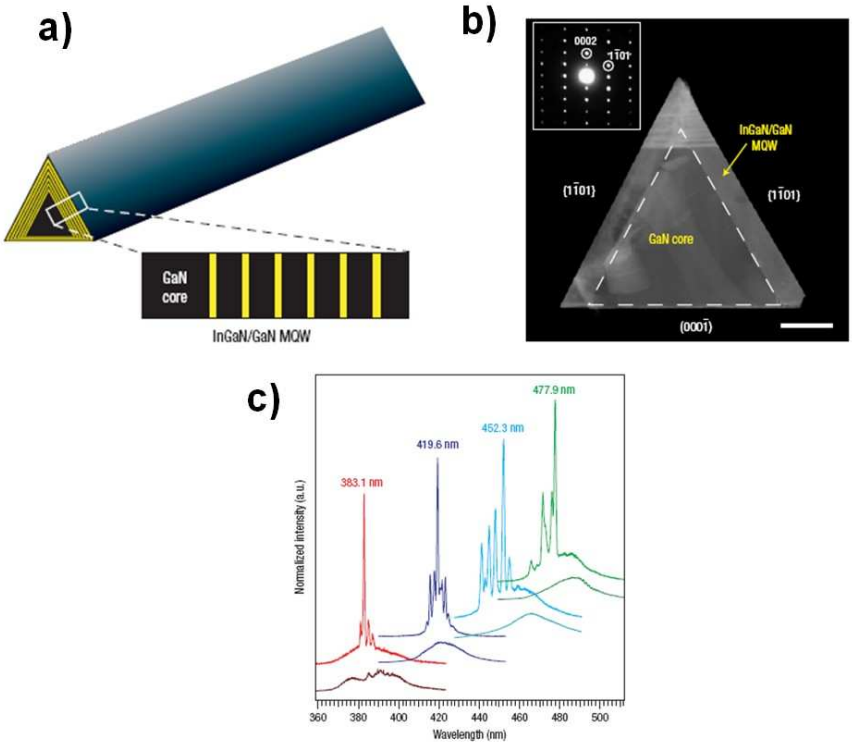

Figure 1.17: a) Schematic view of a GaN/InGaN MQW (x 26) heterostructure grown around a GaN wire template. b) TEM cross-section and diffraction pattern. c) PL emission for wires with different indium concentrations in the MWQs [Qian08].

Photovoltaic device

Core/shell n-GaN/InGaN/p-GaN heterostructures also offer potential applications in photovoltaics as demonstrated by Dong *et al.* [Dong09]. The n-GaN core wire grown by the catalyst-assisted technique described by Qian *et al.* [Qian05, Qian08] is followed by the deposition of an InGaN shell and is finished with p-GaN (see Figure 1.18 a)). For the electrical measurements, the wire is etched down to the n-GaN core on one side and then contacted in the horizontal configuration (see Figure 1.18 b)).

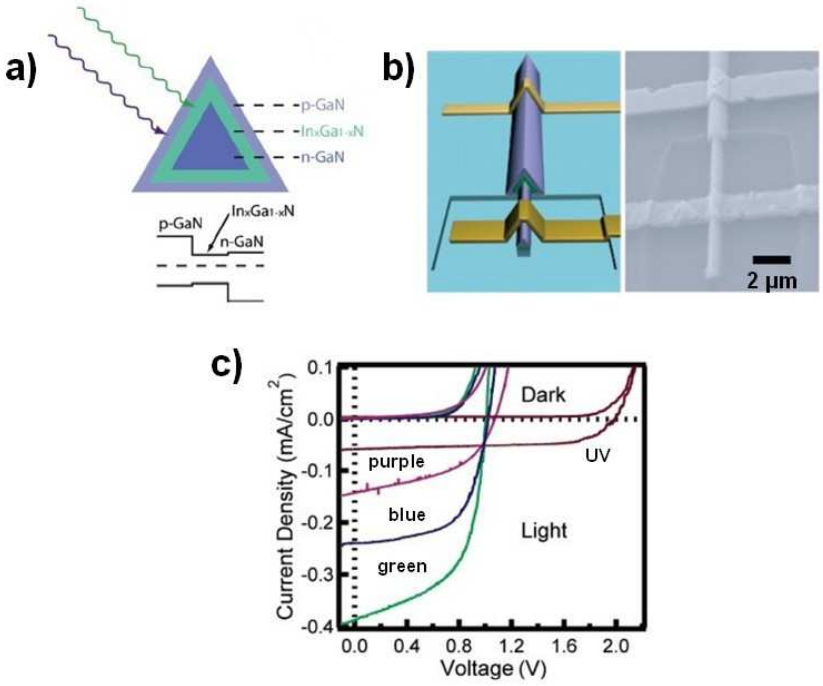

Figure 1.18: a) Schematic cross-section of n-GaN/InGaN/p-GaN core/shell nanowires and corresponding band diagram. b) Electrical contact schematic and corresponding SEM image. c) I-V curve for nanowires with different indium concentrations with and without illumination [Dong09].

I-V measurements were carried out under illumination with 1-sun AM 1.5G light source[11], imitating the solar spectrum after passing the atmosphere – the standard conditions for solar cell testing. Figure 1.18 c) shows the I-V curves for nanowires with different In-concentrations in the InGaN shell. The absorption correspond to UV (371 nm), purple (396 nm), blue (457 nm) and green (556 nm) wavelengths. The threshold voltage increases with decreasing In-concentration due to the InGaN band-gap increase. Under illumination, the open circuit voltage V_{oc} is increased from 1 V to 2 V with decreasing In-concentration. The short circuit current density ranges from 0.059 to 0.39 mA/cm^2. This change is not attributed to the change of the indium concentration, but to the anisotropic spectrum of the light source.

The resulting yield is small compared to 2D devices and a lot of efforts have still to be made to optimise these devices.

[11] 1 sun AM 1.5 G is defined as the solar irradiance reaching the ground after passing the earth's atmosphere at an angle of 48.2 ° with respect to the zenith.

1.3.2.4. AlN alloy-based nanowires

AlN based nanowires

The growth of AlN nanowires has been achieved by Yazdi *et al.* [Yazdi09] by a MBE self-assembled VS approach on SiC without catalysts. Figure 1.19 a) shows two SEM images at different magnifications. The wires grow along the [0001] direction and are mono-crystalline. Diameters between 40 nm and 500 nm were observed depending on the growth conditions. The nanowires can reach a length of more than 100 µm. The nanowires grow on hexagonal shaped islands and exhibit a hexagonal shape and show no tendency to grow laterally after having emerged from the pyramids. CL measurements on single wires revealed their optical properties (Figure 1.19 b)). The spectrum exhibits the AlN near band edge emission at 209 nm (5.93 eV) (indicated by the black arrow) and a broad defect band centred at 374 nm (3.3 eV) attributed to oxygen impurity vacancy complexes. The optical properties clearly need to be improved.

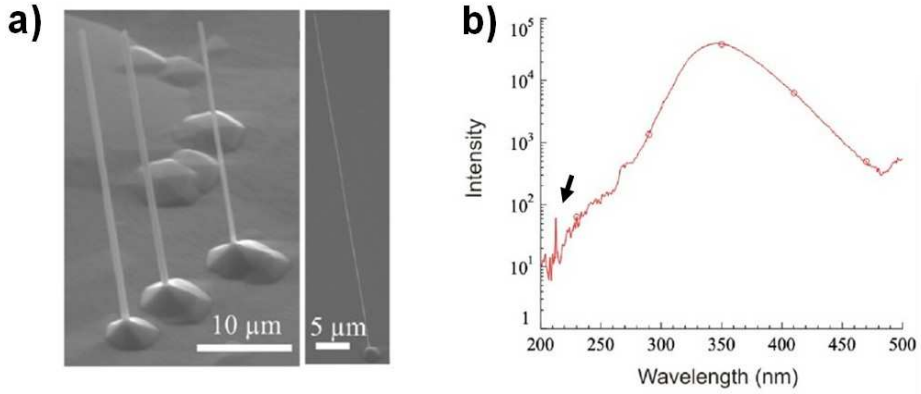

Figure 1.19: a) MBE grown catalyst-free AlN wires, b) CL spectra of an AlN wire with band-edge emission (black arrow) and a strong defect band [Yazdi09]

More recently, the growth of catalyst-free AlN nanowires has been achieved by plasma-assisted MBE on SiO_2/Si (100) by taking advantage of the Volmer–Weber growth mode of AlN on amorphous SiO_2 [Landré2010]. Using a combination of high resolution transmission electron microscopy (HRTEM) and Raman spectroscopy, it becomes evident that AlN nanowires are completely relaxed. Elastic strain relaxation of AlN nanowires has

been further confirmed by photoluminescence experiments showing in addition that spectra are dominated by near-band-edge emission (a defect band is not discussed).

With the MOCVD technique, Su *et al.* [Su05] reported the growth of AlGaN nanowires by catalyst-assisted growth on a poly-crystalline alumina sample coated with a several Á thick Ni layer. The wires grow along the a-direction and exhibit a triangular shape with a diameter around several tens of nanometers. A change of the alloy composition along the cross-section of the wires with a strong Al content in the shell and a high Ga content in the core was observed.

1.3.2.5. AlGaN/GaN-based nanowire heterostructures

GaN/AlN quantum dots

The growth of GaN/AlN quantum dots (QDs) on top of GaN nanowires (about 20 nm in diameter) was demonstrated by MBE by Songmuang *et al.* The general idea is to grow GaN dots in between AlN barriers as shown in Figure 1.20 (see experimental details in [Renard08]). The nanowire geometry allows the detailed study of the photoluminescence of single QDs [Renard08, Renard09] with a low background level compared to usual QDs embedded in 2D structures.

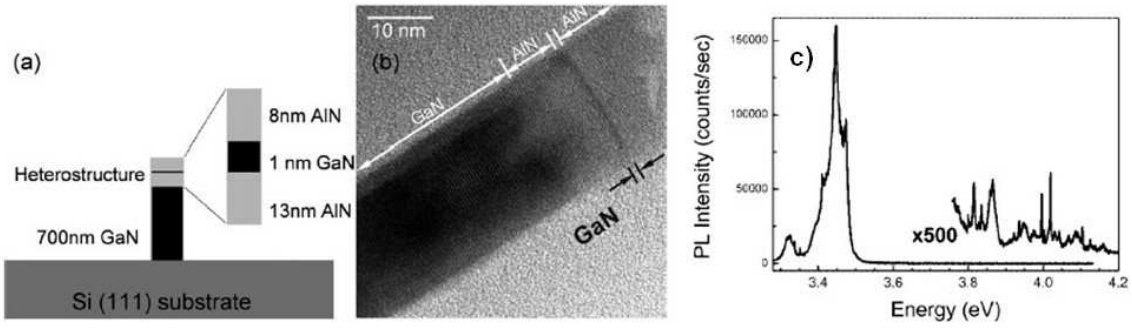

Figure 1.20: a) Schematic view of a GaN nanowire with an AlN/GaN/AlN heterostructure on top of a c-oriented GaN nanowire, b) TEM image of the top region containing the QD heterostructure, c) corresponding μPL spectra of the heterostructure [Renard08]

Microcavity

Ristic *et al.* [Ristic05] demonstrated the catalyst-free MBE growth of longitudinal AlGaN/GaN nanocavities in GaN nanowires. The structures were grown by a self-assembled approach on Si(111) starting with the growth of GaN nanowires. The active region consisting of GaN multiple quantum disks (3 nm thick GaN) embedded in longitudinal AlGaN layers (28 % Al) is trapped between two AlN/GaN distributed Bragg reflectors (DBR) (see Figure 1.21 a,b)). The emission wavelength of the GaN quantum disks was measured to be 345.4 nm (3.591 eV). The thickness of the overall cavity, including the DBR, was chosen to be 172.7 nm, i.e. half of the GaN quantum disk emission wavelength.

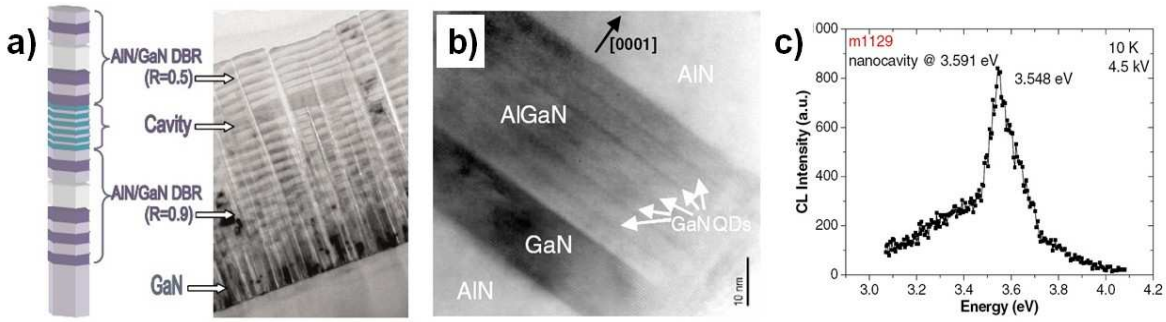

Figure 1.21: a) TEM viewgraph of GaN/AlGaN MQW inside distributed Bragg reflectors inside a nanowire template, b) High-resolution TEM of the AlGaN/GaN cavity, c) CL spectra for a cavity with 3 nm thick GaN quantum disks

CL measurements show an emission peak centred at 349.8 nm (3.548 eV) (see Figure 1.21 c)). The broadening of the peak is attributed to an inhomogeneous strain distribution inside the GaN quantum disks. These kinds of structures can be considered as promising for applications in nanowire-based nanolasers, but homogeneity and reproducibility requirements still have to be improved.

High electron mobility transistor (HEMT)

Li *et al.* [Li06b] demonstrated high electron mobility transistor (HEMT) heterostructures based on GaN/AlN/AlGaN core/shell nanowires. The GaN wire core was grown by a catalyst-assisted MOVPE method followed by the deposition of an AlN (1.8 nm thick) and

AlGaN shell. These wires are grown along the a-direction and have a triangular cross-section with non-equivalent facet planes (see indexation in Figure 1.22 a)).

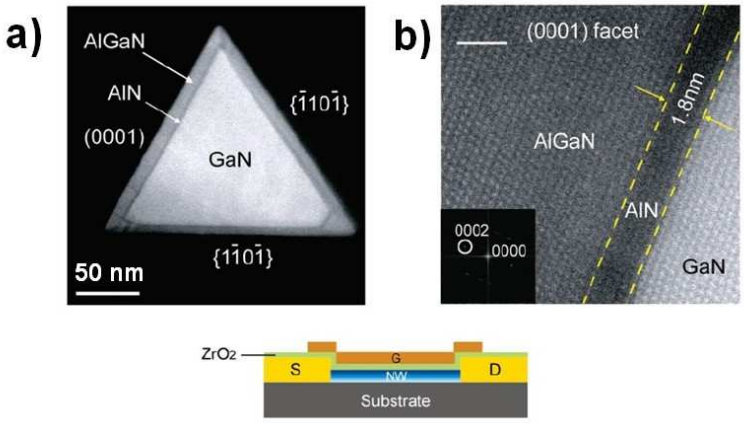

Figure 1.22: a) Cross section TEM of a triangular nanowire with the GaN core and the AlN/AlGaN shells, b) High resolution TEM showing the 1.8 nm thick AlN layer between the GaN core and the AlGaN outer shell

This nanowire geometry was used to fabricate horizontal field effect transistors (FETs) (see the schematic at the bottom of Figure 1.22). Transport measurements showed the formation of a 2D electron gas with a very high electron mobility of 3100 up to 21 000 V/ for 300 K and 5 K respectively. Moreover a large on/off current ratio of 10^7 was reported in this structure (compared to 2500 V/cm^2 and 10^6 for an electron mobility and an on/off current ratio respectively in current HEMT transistors).

1.4. Growth of gallium nitride wires

1.4.1. MBE growth

As illustrated by the previously presented applications, two main approaches have been developed in MBE for the growth of gallium nitride nanowires: the catalytic way using metal catalysts as Ni and Au to promote the vertical growth [Duan00, Lee04, Geelhaar07] and the catalyst-free way [Calleja00, Tchernycheva07, Songmuang07, Landré08, Ristic08, Aschenbrenner09].

1.4.1.1. Catalyst induced growth of GaN nanowires

The growth of GaN nanowires with metal catalysts is generally explained by the VLS mechanism. One example of this catalyst-assisted approach is the growth of GaN nanowires on c-plane sapphire reported by Geelhaar *et al.* [Geelhaar07]. The substrate is covered *ex situ* by a thin (several Å thick) layer of Ni and is then *in situ* annealed at 750 °C for 15 min. Atomic force microscopy (AFM) measurements on a reference sample revealed the formation of Ni islands on the substrate surface (dewetting phenomena).

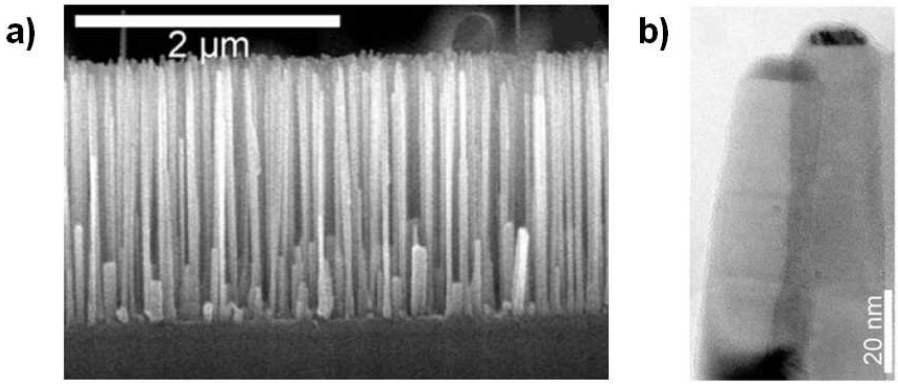

Figure 1.23: GaN nanowire growth by MBE on a c-plane sapphire using a Ni catalyst: a) SEM cross-section, b) TEM image with the Ni catalyst on top of the wire. [Geelhaar07]

The annealing is immediately followed by the GaN deposition at 730 °C leading to the growth of perpendicularly oriented GaN nanowires with a length of about 2 µm and a diameter between 50 and 70 nm (see Figure 1.23 a)). TEM images reveal the Ni catalyst on top of the wire (see Figure 1.23 b)). The V/III ratio was found to be the key parameter for the formation of wires. The nanowire growth (c-plane direction) is observed for nitrogen-rich conditions (high nitrogen flow). Under Ga-rich conditions, the formation of a 2D layer is observed. The growth rate is larger compared to the growth of 2D GaN.

The modelling of the VLS growth mechanism has been quite extensively developed in the literature [Dubrovskii08 and forthcoming papers]. The growth starts with the formation of a liquid metal droplet in which the semiconductor material is incorporated directly from the gas phase. The material nucleates at the interface between the droplet and the nanowire. In parallel, the material already deposited on the surface diffuses along the wire's side facets into the droplet and contributes to the wire growth (see Figure 1.24). During the VLS growth, the catalyst droplet and the semiconductor form a liquid alloy [Harmand07], whereas in some specific systems the catalyst may remain solid (it is named

vapour solid solid (VSS) mechanism). The direct flow of material into the catalyst droplet combined with the additional material diffusion along the wire sides may explain the higher growth rate of GaN nanowires compared to the 2D growth [Geelhaar07].

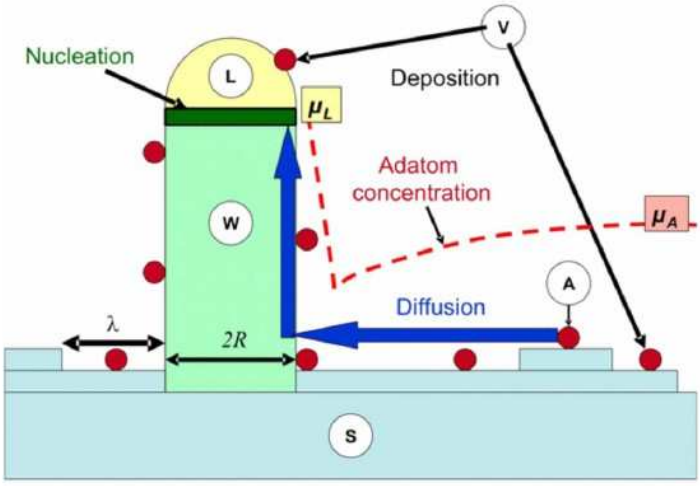

Figure 1.24 : Schematic illustration of the VLS growth mechanism in MBE [Dubrovskii08]

1.4.1.2. Catalyst free growth of GaN nanowires

An example of the catalyst free growth of GaN nanowires on Si(111) can be found in the work of Tchernycheva *et al.* [Tchernycheva07]. Prior to the GaN nanowire growth, a 1 - 4 nm thick aluminium layer is deposited at 650 °C leading to aluminium droplets on the silicon. These droplets are annealed under NH_3 to form AlN islands. SEM measurements revealed island diameters between 20 and 50 nm. The substrate temperature was raised to 800 °C to grow the nanowires, which have similar diameters to the AlN islands. The nanowires grow along the [0001] direction with wurtzite structure and exhibit a hexagonal cross-section (see Figure 1.25 a), keeping a constant diameter along the growth direction. The growth rate of about 150 nm/h is rather slow. These nanowires exhibit good optical properties as confirmed by PL measurements on nanowire assemblies with a NBE emission at 3.433 eV (85 meV FWHM) at RT and 3.478 eV (9 meV FWHM) at 4 K. μPL measurements on single nanowires led to similar results demonstrating the excellent homogeneity of the assembly.

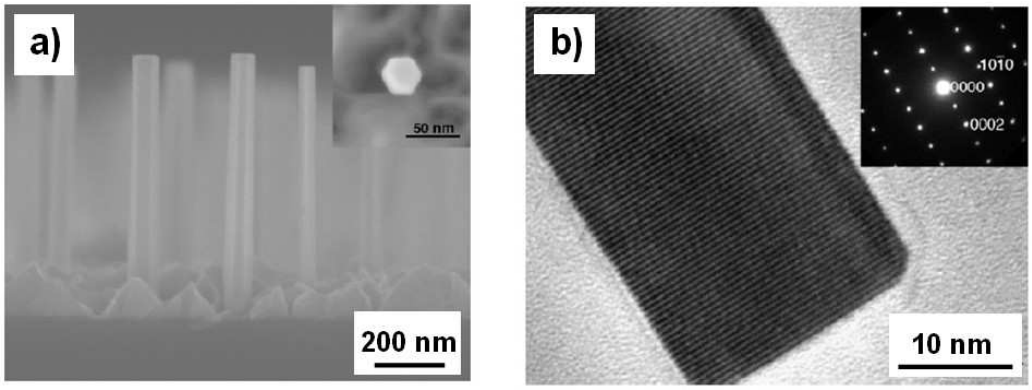

Figure 1.25: a) SEM cross-section image of a nanowire ensemble. b) HRTEM image along the $\langle 1\bar{2}10 \rangle$ direction [Tchernycheva07]

The growth of catalyst-free nanowires was demonstrated by Songmuang *et al.* in a similar way [Songmuang07]. A 2 nm thick AlN layer was first grown on Si(111) (see also [Calleja00]). The following GaN deposition led to the formation of GaN islands, which were expected to be nucleation sites for further GaN nanowire growth. Nitrogen-rich conditions at a temperature around 765°C were used. The growth rate was in the 0.1 to 0.66 Å/s range depending on the Ga cell temperature being significantly higher than the 2D growth rate. Recently, Aschenbrenner *et al.* [Aschenbrenner09] have also shown the catalyst-free growth of GaN nanowires on r-plane sapphire. AlN islands were grown by sapphire nitridation in a MOCVD reactor before introducing the sample into a MBE setup for GaN deposition. The nanowires grew in c-plane direction with a diameter of several hundred nanometers and were surrounded with by a compact a-plane GaN layer.

1.4.1.3. Selective area growth

GaN has been grown by selective area growth (SAG) in MBE on patterned substrates [Seon00, Tang06, Cordier09]. Figure 1.26 illustrates the approach of Cordier *et al.* [Cordier09]. A 30 nm thick Si_3N_4 mask deposited on GaN grown on silicon is patterned with circular holes being 250 nm in diameter (see Figure 1.26 a)). GaN is then deposited at 800 °C to grow isolated structures with vertical edges (see Figure 1.26 b)).

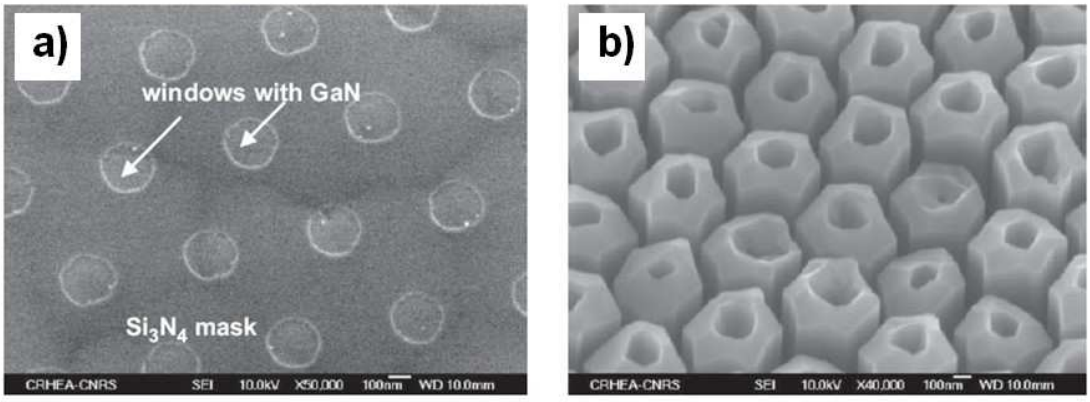

Figure 1.26: a) Patterned Si_3N_4 mask on GaN, b) GaN grown on the patterned Si_3N_4 layer [Cordier09]

Kishino *et al.* [Kishino08] and Sekiguchi *et al.* [Sekiguchi08] demonstrated the growth of GaN nanocolumns on titanium-mask-patterned Si (111) by MBE. SAG occurs at temperatures above 900 °C and the columns grow in the Ti mask openings.

1.4.2. MOCVD growth

Contrary to the self-assembled MBE approach, MOCVD growth of GaN nanowires is not simple to achieve and usually requires an *ex situ* sample surface treatment before nanowire growth. The MOCVD synthesis of GaN nanowires is currently achieved using catalysts involving a poor control of spatial orientation of the wires as well as their epitaxial relationship with the substrate. Novel approaches without catalysts have been reported using SAG on patterned GaN templates that allow growing well-controlled arrays of GaN nanowires.

1.4.2.1. Catalyst growth

The MOCVD growth of GaN nanowires commonly requires metal nanoparticles (Au, Ni or Fe), which act as catalysts following the VLS growth mode. The catalyst-assisted growth of GaN nanowires by MOCVD was first reported by Kuykendall *et al.* in 2003 [Kuykendall03]. Many groups have successfully grown GaN nanowires using Ni catalysts obtained either by dewetting a thin Ni layer or by dripping a Ni-nitrate solution on the substrate surface. Nanowire growth usually occurs at temperatures between 800 and

1000 °C. Trimethylgallium (TMG) and ammonia are used as precursors. Figure 1.27 a) shows nanowires grown on an *ex situ* gold-coated c-plane sapphire substrate. The nanowires exhibit a triangular shape (see inset) indicating a growth direction along the non-polar [210] direction and more rarely along the [100] direction.

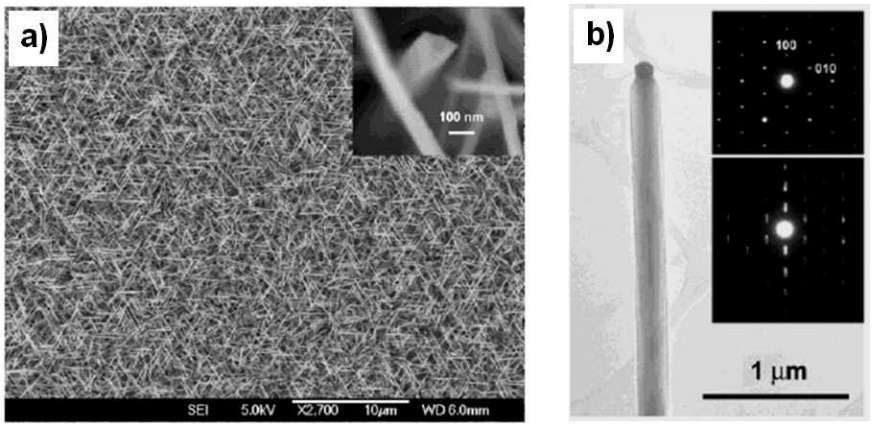

Figure 1.27: a) Gold catalysed GaN nanowires, b) TEM viewgraph and diffraction patterns of a single nanowire with a gold catalyst on top

PL measurements show a broad emission peak between 360 and 385 nm centred at 370 nm (3.35 eV) at 5 K and 380 nm (3.26 eV) at 285 K. No yellow band could be observed, which indicates good optical properties of the nanowires. Electrical measurements done on single wires gave a carrier mobility of 65 cm^2/Vs and a carrier concentration of 4 x 10^{18} cm^{-3}.

A control of the crystalline direction of the nanowires was reported as a function of the substrate nature. Catalyst growth on γ-$LiAlO_2$ (100) and MgO (111) substrates resulted in the growth of nanowires in the orthogonal [1-11] and [001] directions respectively [Kuykendall04].

The growth of vertical catalysed nanowires is achieved using r-sapphire substrates [Wang06]. As the vertical nanowires grow along the non-polar [210] direction, the same group has succeeded in the growth of a-plane GaN templates by full coalescence in the upper section of the nanowires [Li09].

The catalyst approach allows only the growth of GaN nanowire-based radial heterostructures since indium and aluminium precursors suppress the catalytic process due to a formation of stable chemical phases in the droplet. The growth of axial nitride heterostructures is thus very difficult to accomplish using the conventional catalyst approaches.

1.4.2.2. Selective area growth

In SAG, pre-patterned substrates are applied for the growth of nanowires in order to control their diameter, position and density independently. The patterning techniques may be time-consuming and expensive, for example when e-beam lithography is required to reach very high resolution.[12] In the literature, interferometric lithography and porous anodic alumina (PAA) templates have been used for the growth of GaN wires.

Hersee *et al.* [Hersee06] demonstrated the catalyst-free growth of GaN wires through a patterned SiN_x layer deposited by low pressure chemical vapour deposition (LPCVD) on a 600 nm thick GaN template. The SiN_x layer was patterned by interferometric lithography and dry etching to obtain holes with diameters of about 220 nm ordered in hexagonal lattice with a 500 nm period.

The GaN wires were grown at 1050 °C and with a reactor pressure of 133 mbar in a mixture of hydrogen and nitrogen carrier gas in a P75 Veeco TurboDisk MOCVD reactor. The V/III ratio was set to 1500 to ensure a proper filling of the holes before switching the system to the "pulsed growth mode" where the precursors are injected alternately. This technique prevents lateral growth of the wires after they emerged from the holes.

The wires exhibit a hexagonal shape with a diameter matching the diameter of the holes (see Figure 1.28 a)). The wires are well ordered in the patterned hexagonal lattice and grow along the [0001] direction. It has been shown that they have a very low density of threading dislocations (see Figure 1.28 b)). In this pioneer study, the optical properties of the wires were not reported.

In the industry, glō AB[13] founded by the Lund University's Nanometer Structure Consortium[14] is a venture-backed, development-stage company focused on the development and commercialisation of entirely new, highly energy efficient and very low cost nanowire light-emitting diodes (nLED). This company is presently developing GaN-based LEDs among several III-V systems, but has not publish their main results up to now for intellectual property reasons.

---

[12] Combined with the nanoimprint technique, molds can be reused to reach volume production.

[13] GLO web site: http://www.glo.se/

[14] Lund University's Nanometer Structure Consortium web site: http://nano.lth.se/

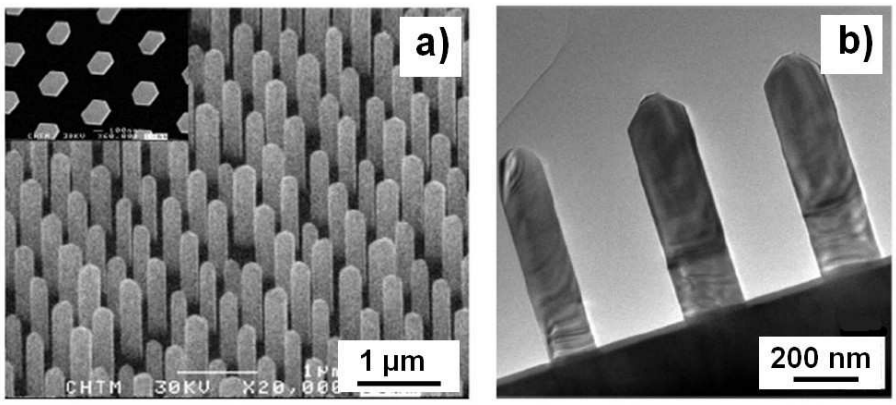

Figure 1.28: a) GaN nanowires grown on a patterned template, b) TEM viewgraph of the nanowires [Hersee06]

Deb *et al.* [Deb05] demonstrated the patterning of SiO_x using intermediate porous anodic alumina (PAA). The process starts with the deposition of a 5 µm thick layer of GaN by HVPE on a c-plane sapphire followed by the deposition of a 60 nm thick layer of SiO_x. A one micrometer thick Al layer is deposited and oxidised by anodisation to form a nanoporous oxide layer with a pore diameter between 10 and 15 nm. The pore diameter is increased to 60 nm by etching in H_3PO_4, and the pattern is then transferred to the SiO_x layer by SF_6/O_2 reactive ion etching (see Figure 1.29 a)).

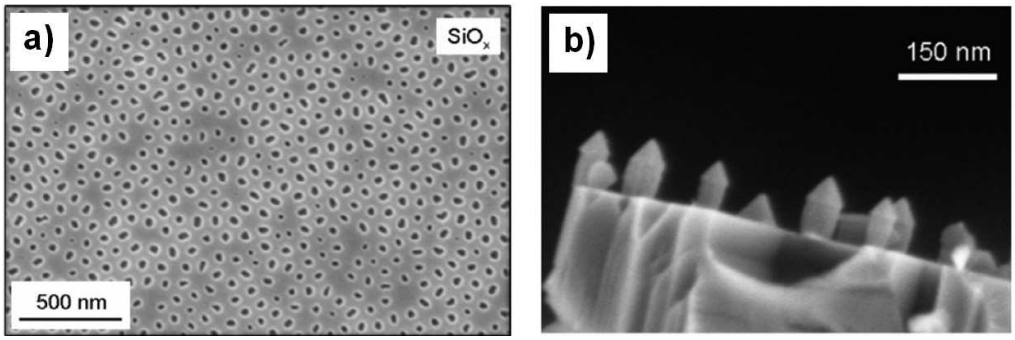

Figure 1.29: a) Transfer of porous alumina patterning to a SiO_x layer by reactive ion etching, b) GaN nanowires grown on a GaN layer by selective area growth with a SiO_x mask (removed in this figure) [Deb05]

The remaining PAA is removed by H_3PO_4. For the GaN nanowire growth, the ammonia and TMG are used with a V/III ratio of 1500. The growth is carried out for 5 minutes corresponding to a film thickness of 100 nm for 2D growth. The resulting nanowire height is in the same order of magnitude. The remaining SiO_x layer is finally removed from the sample by means of hydrofluoric acid (HF). The nanowires (Figure 1.29 b)) are grown

along the c-direction in epitaxial relationship with the underlying GaN template. As in the previous case, the density of threading dislocations is quite low with this method and the optical properties are not described in detail.

1.5. Conclusions

The huge interest in nanowires in the past ten years has been reviewed in this chapter to show their role in fundamental research and potential applications. In this context, the growth of GaN nanowires and GaN nanowire based heterostructures is particularly interesting for opto- and nanoelectronics with the demonstration of nanowire-based LEDs [Kim04, Qian05], optically pumped single nanowire lasers [Qian08] and HEMTs [Li06b] as worked out in this manuscript. Furthermore, these 1D structures are of interest in fundamental research of confinement effects of electron gases as well as single electron transistors.

The growth of GaN nanowires with diameters from some tens up to several hundreds of nanometres is widely reported and has also been achieved by catalyst-assisted growth [Duan00, Kuykendall03, Geelhaar07] by MBE and MOCVD as well as catalyst-free approaches by MBE [Calleja00, Tchernycheva07, Songmuang07, Landré08, Ristic08, Aschenbrenner09]. Catalyst-free approaches by MOCVD could be grown by means of SAG [Deb05, Hersee06]. InGaN wires with an In-concentration up to 90 % [Kuykendall07] and AlN wires [Yazdi09, Landré2010] have been grown by MOCVD and MBE respectively. These results still are outnumbered by the results dealing with the growth of GaN wires.

Very different approaches have been explored to grow these materials with or without the use of catalysts, and with MBE, HVPE and MOCVD growth techniques. From the chemical point of view, the non-catalytic way prevents contamination that may degrade the physical properties of the wires. From the morphological point of view, the selective area growth of nitride-wire heterostructures (independently controlling the size, position and density) has been reported both by MOCVD and MBE but suffers from complexity in the template preparation. In MBE, the very convenient self-organized growth method without catalyst is routinely being developed for nitride nanowires by several groups in the world

mainly on Si substrate to obtain small (20-50 nm) nanowires and longitudinal heterostructures. A similar catalyst-free approach in MOVPE has not yet been reported in the literature.

This work will be focussed on the demonstration of the epitaxial growth of GaN heterostructures by MOCVD with a self-organied approach using no catalyst. The objective will be to demonstrate that this easily applicable (and industrial) technique is compatible with the realisation of good nanowires. This chapter has shown that this approach is original with respect to the literature and this PhD thesis will explore the potentialities to obtain doped nanowires and quantum well heterostructures interesting for optoelectronic devices.

Chapter 2

Bi-dimensional growth of GaN by MOVPE

This PhD project started with the installation of the first metal-organic chemical vapour phase deposition (MOCVD) setup in the laboratory. Before the development of the GaN wire growth, it was mandatory to validate this setup by basic bi-dimensional growth.

After a short introduction of the mechanisms involved in MOVPE and a description of our setup, this chapter will deal with the characterisation of bi-dimensional GaN layers and their n- and p-doping controls as well as the growth of AlGaN single layers and InGaN multi quantum wells (MQWs). A blue LED structure was chosen as a demonstrator combining most of these building blocks. The contacted device shows an electroluminescence emission, demonstrating our capacities to grow this type of materials.

2.1. Introduction to the MOVPE process

MOVPE was developed as a technique for deposition of compound semiconductors in the 1960s and is nowadays widely used to grow many III/V materials (especially III-nitrides) to fabricate semiconductor devices such as LEDs and laser diodes. In contrast to MBE, MOVPE does not require ultra-high vacuum (UHV) conditions and can achieve higher growth rates. The throughput can reach a capacity of more than sixty 2" wafers[15], making this technique interesting for industrial mass production. The homogeneity over large surfaces and short process time are the main advantages compared to other growth techniques.

The MOVPE growth process is highly complex because it is governed by thermodynamics, mass and heat transport, chemical reactions of the precursors and surface adsorption/diffusion. Figure 2.1 a) schematically illustrates the mechanisms involved in a MOVPE reactor chamber. The precursors injected into the reactor are transported in a

[15] Aixtron planetary reactor.

carrier gas flow in the direction of the sample surface and undergo chemical reactions. The products (detailed below in this chapter), are adsorbed on the sample surface and may diffuse over the substrate until they are either finally deposited or desorbed. In this case, they leave the reactor chamber through the exhaust with the carrier-gas flow. The following list shows the important processes involved during MOVPE growth:

- Transport of the precursors
- Thermal decomposition of the precursors in the gas phase
- Gas phase reactions forming intermediate products
- Adsorption of the intermediate products onto the substrate surface
- Diffusion of the products
- Evaporation of the products
- Surface diffusion and lattice incorporation of the intermediate products
- Desorption of incorporated material
- Transport of the products, intermediate products and precursors out of the reactor

The MOVPE process can be divided into three main regimes (see Figure 2.1 b)). At low temperature, the growth rate is kinetically limited and directly depends on the reactor temperature. The speed of chemical reactions and the rate of the product formation determine the growth rate. For higher temperatures, the growth becomes transport limited. In this regime, the growth rate is independent of the temperature and only depends on the amount of materials reaching the surface. In this regime, the growth rate is constant all throughout the temperature range. If the reactor temperature is still increased, the materials start to be evaporated from the surface and the growth rate is decreased.

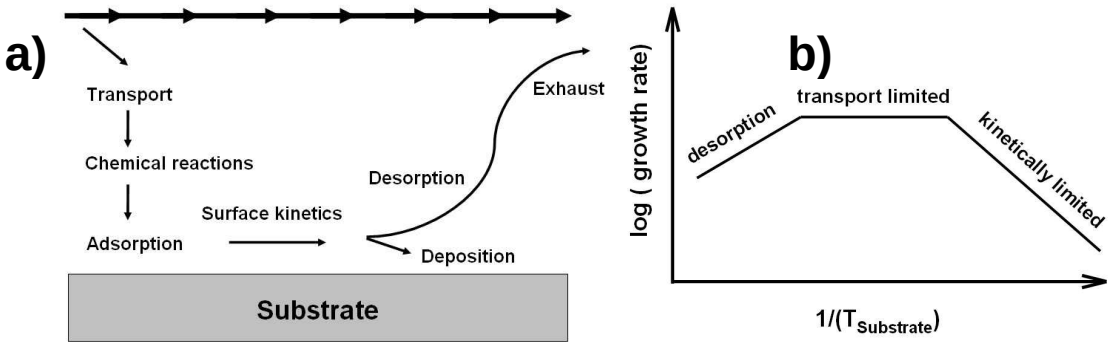

Figure 2.1: a) Schematic of the different mechanisms involved in the MOVPE process, b) Growth rate dependency on substrate temperature

2.2. The GaN MOVPE close coupled showerhead (CCS) setup

A 3x2" Thomas Swan (Aixtron) CCS MOCVD reactor was used for the GaN growth. This commercial system has been specially designed for the growth of high quality 2D film growth with accurate control of thickness, doping and composition.

Figure 2.2 : The Thomas Swan (Aixtron) 3x2" CCS MOVPE reactor (left). View on the susceptor with three 2" substrates (right)

These systems are widely used in industrial production of LEDs (blue and white) and blue laser diodes.

In the industry, most commercial reactors have been using the horizontal geometry. The carrier gas arrives horizontally with respect to the substrate surface. This geometry allows a laminar flow preventing vortices in the reactor chamber. In the planetary reactor

design, the susceptor rotation smoothes concentration and temperature gradients which may induce growth inhomogeneities.

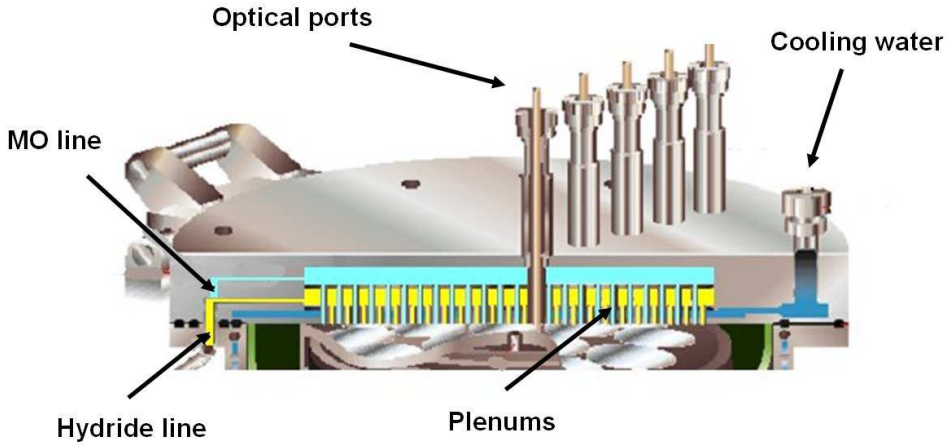

Figure 2.3 : Schematic cross-section view of the reactor lid of a close coupled shower head (CCS) setup

The vortices, which generally occur in standard vertical reactors like quartz tubes are leading to deposition inhomogeneities (especially in the outer parts of the susceptor). They are eliminated in the CCS design by the precursor injection through a showerhead, which is the reactor lid mounted on top of the reactor (see Figure 2.3). The showerhead is close (11 mm) to the substrates and is designed to enable precursors to be separated right up to the point where they are injected into the reactor through a multiplicity of small tubes. The precursors are injected into the reactor chamber through separate orifices in the showerhead in order to create a very uniform distribution of reagent gases (without vortices). This design allows a complete separation of the precursors, avoiding pre-reactions during the gas transport from the precursor sources to the reactor. This advantage compared to other reactor designs allows the growth of heterostructures with sharp interfaces and a good control of thickness, composition and doping. The showerhead is water cooled as are the reactor walls. The temperature is regulated to 50 °C by a flow of warm water distributed by an independent cooling system to avoid reagent adsorption/condensation and pre-reactions of the reagents directly after injection into the reactor.

The susceptor has three rounded 2" wide indentations to position and hold the sapphire substrates (see Figure 2.2). The susceptor is made from graphite covered with about 100 μm of SiC. The high melting points of these two materials allow working temperatures of up to 1200 °C. The heater is based on simple spiral-wound filaments

mounted under the susceptor. Three independent heating zones, adjusted by controlling the current, allow a homogeneous heat distribution all over the susceptor surface[16]. In order to increase the temperature homogeneity and to prevent a cracking of the susceptor due to temperature gradients, the susceptor is rotated during the process with several tens of rotations per minute[17].

During the growth, the showerhead lid is mechanically locked and sealed by a vacuum established between two O-ring seals (< 1 mbar). The reactor working pressure can be varied between atmospheric pressure and a few tens of millibars. The susceptor and the metallic reactor wall are separated by a so called quartz liner, protecting the reactor wall from aggressive reactants.

A vacuum pump installed inside the system controls the reactor pressure and allows the transportation of the gas through the exhaust line. The exhaust line is connected to a scrubber, which cleans the exhaust gases before they leave into the atmosphere (see Figure 2.5).

The setup is equipped with a gas-line system with N_2 and H_2 carrier gases allowing the transport of precursors from the sources into the reactor. Trimethyl-Gallium, -Indium, -Aluminium (TMGa, TMIn, TMAl), Triethyl-Gallium (TEGa), Bis(cyclopentadienyl)magnesium (CP_2Mg), silane (SiH_4) and ammonia (NH_3) are used as precursors. The organometallic precursors are stored in steel containers, so called bubblers installed inside the MOCVD system. The carrier gas (N_2 or H_2) flows into the bubbler, dissolves the metal organics (MO) to form a saturated gas solution, flows out of the bubbler and is pushed into the main carrier line. They are installed in thermal bathes always keeping them at a controlled temperature and guaranteeing a constant vapour pressure. Mass-flow controllers guarantee a constant flow of materials. The system is equipped with gas lines for the metal organics and hydrides, respectively. A gas-detection system closes gas lines and shuts off the reactor as soon as dangerous gases, such as hydrogen or ammonia, are detected inside the setup and independently in the room. Recipes running on the system are defined in a script language. Once started, the system carries out every step automatically. A change of parameters during an operation cycle can be done directly in the

[16] The calibration of the balance between the three zones is very important to minimise the substrate temperature gradient. This may have a significant impact on the material deposition, for example, as will be shown later in the In content in InGaN quantum well.

[17] In practice, a rotation rate of 50 rotations per minute was used for all the samples presented in this manuscript.

control panel implemented in the control software (see Figure 2.5). For the optimisation of a process, single steps, parameters or complete parts of a recipe can be added, removed or changed easily in a text editor in the system control software. This system allows an easy and convenient operation for users.

Precursors

The MOVPE setup is equipped with TMGa, TEGa, TMAl and TMIn as sources for the group III elements Ga, Al and In (see Table 2.1). In TMGa, TMAl and TMIn, three methyl groups are bound covalent to the central metal atom (Figure 2.4). In TEGa, the methyl groups are exchanged by ethyl groups. Due to its lower decomposition temperature, TEGa is manly used for the growth of InGaN, for which a lower growth temperature is required to avoid indium desorption [Stockmann94]. NH_3 is used as a source for nitrogen as a group V element. For security reasons, NH_3 and H_2 are stored outside the building and connected to the system via long gas lines. Silane diluted in H_2 at 100 ppm is the source to n-dope GaN with silicon. The silane bottle is in a special gas cabinet inside the building. Cp_2Mg is the organometallic source to p-dope GaN with Mg, which is also stored inside the system. Details about the system precursors are summarised in Table 2.1 below:

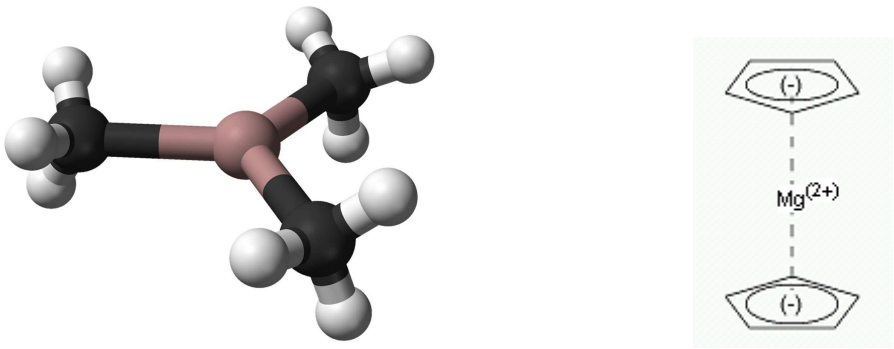

Figure 2.4 : Schematic view of TMGa (left) and Cp_2Mg (right): Left: The central brown atom represents the group III metal. It is bound to three methyl groups (carbon – black, hydrogen – white). Right: the cyclopentadienyl cycle (C_5H_5) is represented schematically to show the charge distribution inside the molecule

Name Function	**Chemical formula**	**P at 298 K (torr)**	**A**	**B**	**Melting point (°C)**
Trimethylgallium (TM-Ga) Metal organic (element-III source)	$Ga(CH_3)_3$	238	1825	8.5	-15.8
Triethylgallium (TE-Ga) Metal organic (element-III source)	$Ga(C_2H_5)_3$	4.79	2530	9.19	-82.5
Trimethylaluminium (TM-Al) Metal organic (element-III source)	$Al(CH_3)_3$	14.2	2780	10.48	15
Trimethylindium (TM-In) Metal organic (element-III source)	$In(CH_3)_3$	1.75	2830	9.74	88
Bis(cyclopentadienyl)magnesium (Cp_2Mg) Metal organic (p-doping)	$Mg(C_5H_5)_2$	0.05	3556	10.56	175
Ammonia Gas (element-V source)	NH_3				
Silane (diluted in H_2 100) Gas (n-doping)	SiH_4				
Hydrogen Carrier gas	H_2				
Nitrogen Carrier gas	N_2				

Table 2.1 : Precursors used in the MOVPE system: Pressure at 298 K, estimation of the vapour pressure P at temperature T: Log(P)=B-A/T and melting points for organometallics

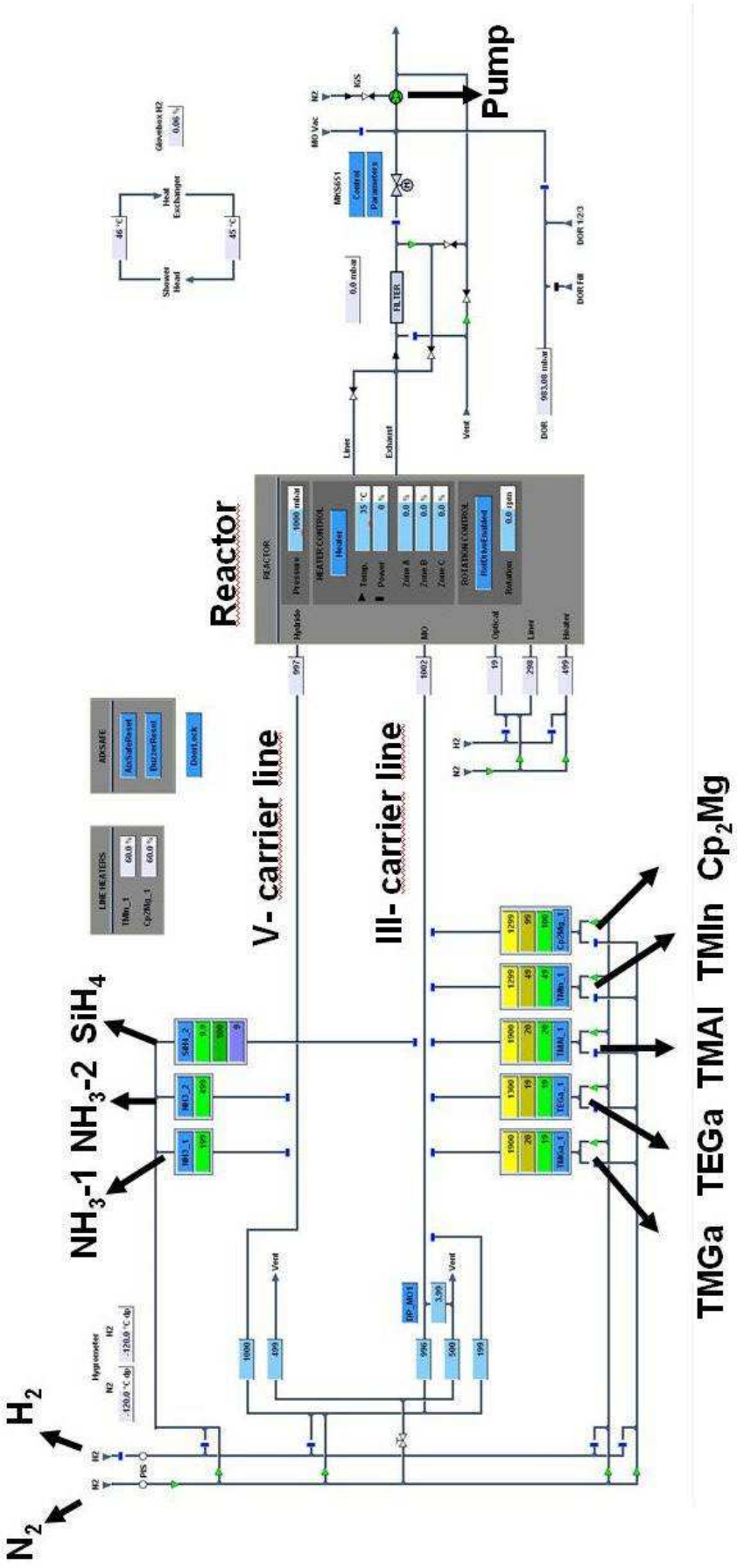

Figure 2.5 : Schematic of the reactor

Chemical reactions inside the reactor

The gas stream is pointed downwards in the direction of the susceptor and is slowed down close to the surface and establishes a boundary layer. The precursors may also react inside this boundary layer before diffusing to the substrate surface and contribute to the growth. Figure 2.6 shows a sketch of the chemical reactions involved in the GaN precursor decomposition [Daulesberg08]. Two main interconnected reaction channels (noted a) and b) in Figure 2.6) can be indentified:

a) TMGa together with NH_3 form the non-stable $Ga(CH_3)_3$:NH_3 reaction product, which can react to form an amide $(CH_3)_2GaNH_2$ by separation of a methane molecule and then an oligomer ($[(CH_3)_2GaNH]_n$) by further methane separation. This oligomer can transform to GaN by separation of 2n methane molecules. This can either happen on the sample surface or in the gas phase and contributes to the growth. In parallel, GaN clusters can be formed with diameters between 10 and 100 nm in the gas phase [Daulesberg08]. This gas phase cluster formation is particularly important at high growth pressure (close to atmospheric pressure). These clusters do not contribute to the growth and leave the reactor through the exhaust line.

b) The TMGa reacts directly to MMGa (monomethygallium) by separation of two methyl groups, which can react in two different ways: (i) MMGa can form molecule the amides already founded in a) with a NH_2 or (ii) MMGa can react with NH_2, CH_3 and H_2 to result GaN in the gas phase.

These complex chemical reactions can be summed up in a simple reaction equation: $Ga(CH_3)_3 + NH_3 \rightarrow GaN_{(sol)} + 3\ CH_4$, but this formulation hides the formation of intermediate compounds that are important in the growth mechanisms like H_2 formation, which can have an etching behaviour on GaN.

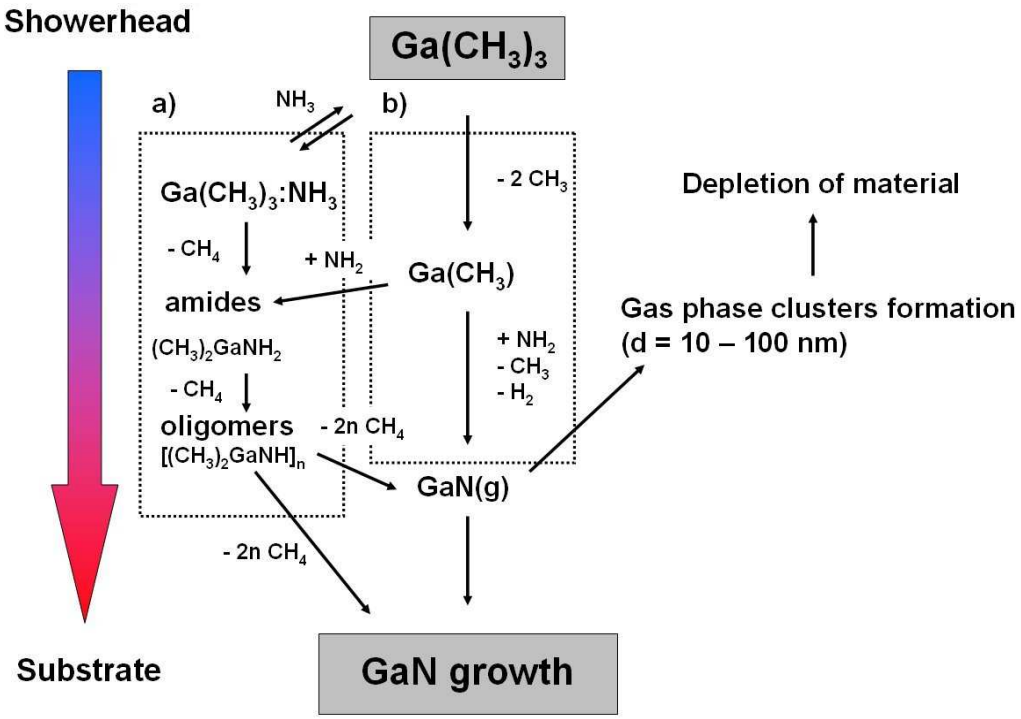

Figure 2.6 : Chemical reactions in the MOVPE reactor (after [Daulesberg08])

The interferometer

The growth process can be monitored *in situ* by a reflectance interferometer and allows the collection of information about thickness and roughness of the layer during growth. The interferometer is mounted on the showerhead. The laser beam passes through a beam splitter reflecting the laser beam perpendicularly on the sample surface. The laser beam with an emission wavelength of 635 nm passes trough one of the optical ports of the reactor and is reflected from the sample surface onto a photodiode recording the intensity signal[18].

[18] An electronic system takes into account the synchronization of the signal acquisition with the sample rotation.

The incident beam undergoes two reflections; one at the air/film interface and one at the film/substrate interface (see Figure 2.8). The reflection from the substrate bottom is

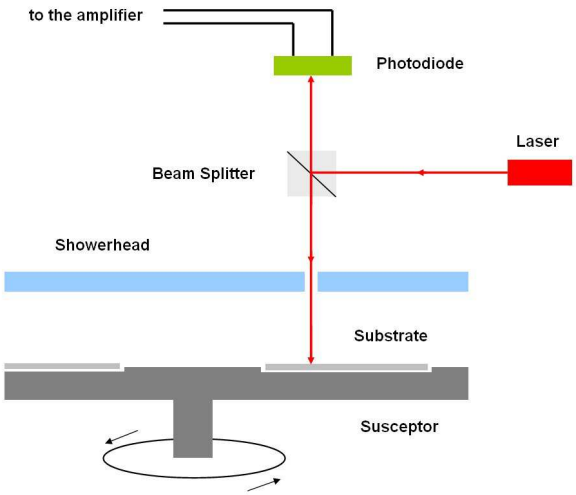

Figure 2.7 : Diagram of the interferometer installed in top of the reactor lid (after [Webb07])

negligible since only one-side polished sapphire substrates were used here. The two reflected beams interfere with each other leading to a total intensity changing as a function of the film thickness and refractive index. During the film growth, the optical path difference between the two reflections is changed leading to a periodic change of intensity of the reflected beam. The distance between the interference maxima also depends on the

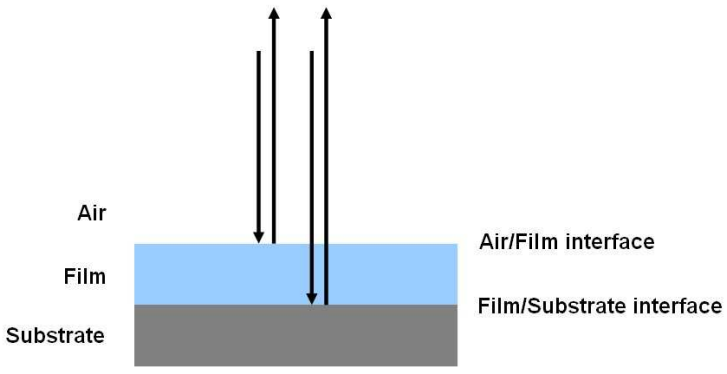

Figure 2.8 : Schematic of the light path inside the layer. The beams reflected at the air/film and film/substrate interfaces interfere with each other; phase shift depends on the thickness of the deposited film

refractive index of the film and the laser wavelength. Considering the difference of optical path between the two beams of Figure 2.8, the grown film thickness between two maxima is directly given by the standard formula:

$$d = \frac{\lambda}{2n} \qquad \text{(eq. 5)}$$

where d is the film thickness, λ the probe wavelength and n the film refractive index. Using a laser diode with 635 nm emission wavelength and a refractive index of 2.3 for GaN, the grown layer thickness between two maxima is calculated to be 138 nm. For 2D growth, the interferometer is absolutely crucial not only for the growth-rate estimation but also for controlling the initial material nucleation and the roughness evolution, as will be discussed in the section 2.3 of this chapter.

The demand of high quality and homogeneity of growth especially in industry has lead to the development of new *in situ* characterisation techniques. *In situ* monitoring techniques using reflectance-anisotropy spectroscopy (RAS) combined with a pyrometer and interferometer (using polychromatic wavelength) allow the *in-situ* measurement of ternary compound composition and dopant concentration in parallel with the growth rate and the substrate-surface temperature.

2.3. Bi-dimensional GaN growth

The control of bi-dimensional III-nitride growth is fundamental to plan the growth of complex heterostructure stackings like GaN-based LEDs and laser diodes but in a more pragmatic way, it is an important point to validate the setup installation. In this section, the steps required to grow high quality GaN films, which have been demonstrated during our MOCVD reception, will be discussed.

2.3.1. Standard process to grow GaN films on sapphire

Standard Kyocera c-plane sapphire substrates 330 μm thick, (0.25 ° misorientated) were used to check the process. The lattice mismatch between GaN and sapphire leads to extended defects in the layer (mainly dislocations) acting as non-radiative recombination centres and lowering the carrier mobility. The objective of the process optimisation was to decrease the amount of dislocations in the GaN layers. Standard recipes can be subdivided into three main parts that will be discussed in the following:

- surface preparation
- low temperature (LT) GaN buffer layer deposition
- high temperature (HT) GaN film growth

The laser interferometry intensity curve during the GaN deposition process given in Figure 2.9 a) – e) is reported in Figure 2.10. Three main steps can be detailed:

- **First step: surface preparation**

The c-plane sapphire sample is first cleaned by an *in situ* bake under H_2 for 20 min at 1200 °C. Surface contaminations as dust, polishing residues and adsorbed gas (and of course water) coming from the transfer procedure are removed during this step. The sapphire substrate is not chemically cleaned *ex situ* to prevent contamination of the reactor by chemicals remaining on the substrate surface.

The sample is then annealed under NH_3. During this step, the first atomic layers of the sapphire surface react with the NH_3 to form a thin AlN layer [Grandjean96 Kim00,

Vennegues99, Dwikusuma03]. This AlN layer enhances the sticking of the GaN and improves the electrical and optical properties of the forthcoming GaN film growth at high temperature[19] [Keller96].

- **Second step: low temperature GaN buffer-layer deposition**

A GaN nucleation buffer layer is grown during 200 s at low temperature (T = 530 °C) and p = 600 mbar with a V/III ratio of 1980 (see Figure 2.9 a)). The enhancement of the sticking coefficient induced by the AlN layer and the low surface mobility (also induced by the low temperature) lead to a complete coverage of the substrate surface by a low quality GaN layer with a high threading-dislocation density of about 10^{10} cm^{-2} [Wu96]. The reflectivity intensity is strongly increased confirming the deposition of a 2D layer.

After this LT nucleation step, the reactor temperature is set to 1040 °C (corresponding to the HT GaN growth temperature). This layer is then annealed under NH_3 and starts to form 3D pyramidal islands (see Figure 2.9 b)), which lead to a decrease of the laser reflected intensity.

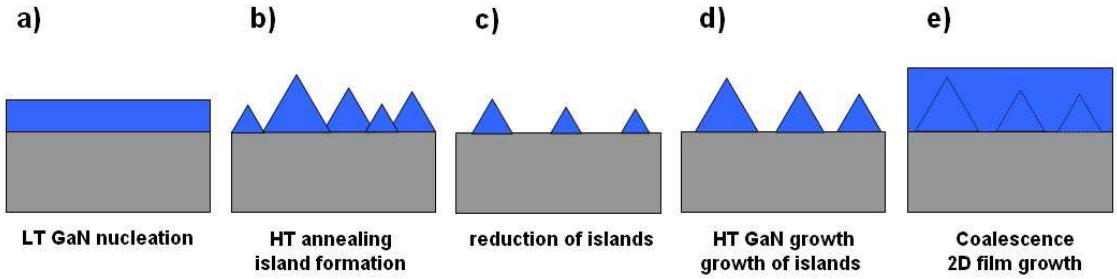

Figure 2.9 : Schematics of the nucleation of GaN. a) LT GaN nucleation, b) HT annealing with island formation, c) reduction of islands by material desorption, d) HT GaN deposition: lateral and longitudinal growth of islands, e) Coalescence of islands and 2D film growth.

During the annealing, the island density is decreased (Figure 2.9 c)) because of a desorption of materials and hydrogen etching at high temperature. The duration of this annealing step is not fixed *a priori*, because it depends on the surface quality, temperature etc. and is adjusted by the operator as a function of the reflectivity spectra evolution.

[19] The importance of this AlN layer will also be stressed for wire growth in the next chapter.

- **Third step: high temperature GaN film growth** (Figure 2.9 d and e)

Spontaneously, the reflected intensity starts to increase again with the decrease of the island density. At this point, the system is switched manually to start the HT GaN growth (T = 1040°C, V/III ratio of 825 and p = 500 mbar). The remaining islands start to grow laterally as well as longitudinally. Reflectivity is again decreased. Finally, the islands become big enough to coalesce to form a 2D continuous GaN film. The reflectivity changes to a periodic pattern whose envelope is stabilised as a function of time. As already mentioned in section 2.2, the growth rate can be directly deduced from the time difference between two maxima.

The 2D GaN layers grown by means of this process allow the production of high-quality films with a threading dislocation density of about 10^8 cm^{-2}, which corresponds to a reduction by a factor of 100 with respect to the LT buffer layer.

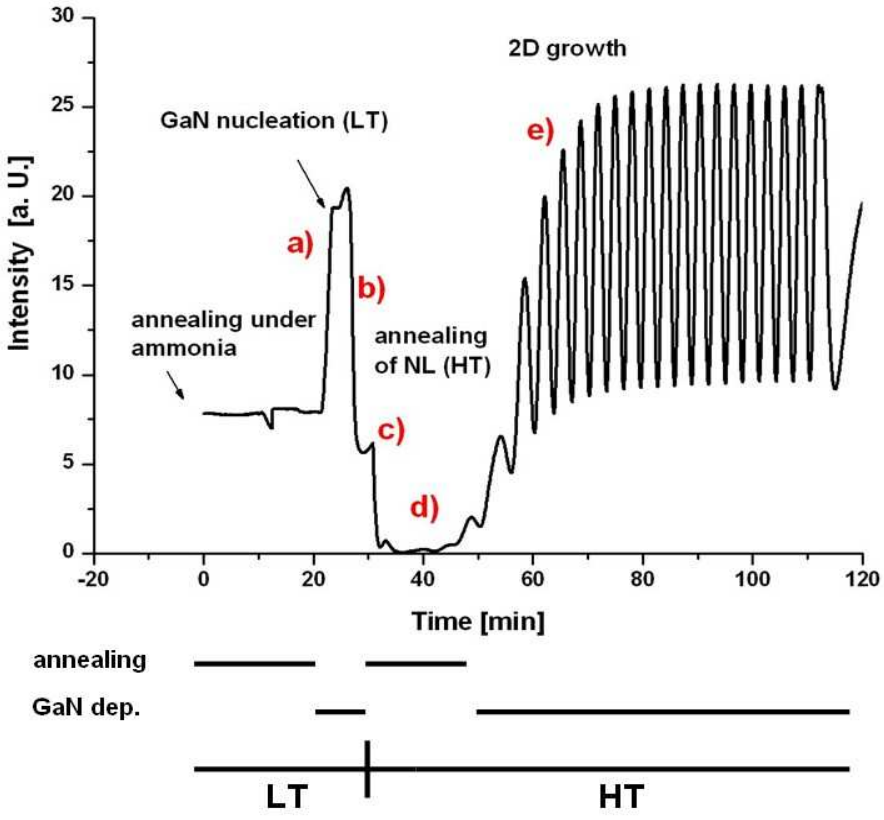

Figure 2.10 : Outline of the laser-reflectivity spectrum during a standard GaN growth. a) LT GaN nucleation, b) HT annealing with island formation, c) reduction of island density by material desorption, d) HT GaN deposition: lateral and longitudinal growth of islands, e) Coalescence of islands and 2D film growth

Morphology of GaN films

Figure 2.11 shows a cross-section scanning electron microscopy (SEM) image of undoped-GaN/n-doped GaN grown on a c-plane sapphire. The three layers' stacking is clearly visible. The LT GaN buffer layer (0.45 μm) followed by a 2.9 μm thick HT u-GaN layer can be seen above the sapphire and the structure is terminated by a 0.83 μm thick n-GaN layer. The rough side edges, which can be seen on the picture, result from the cleaving process.

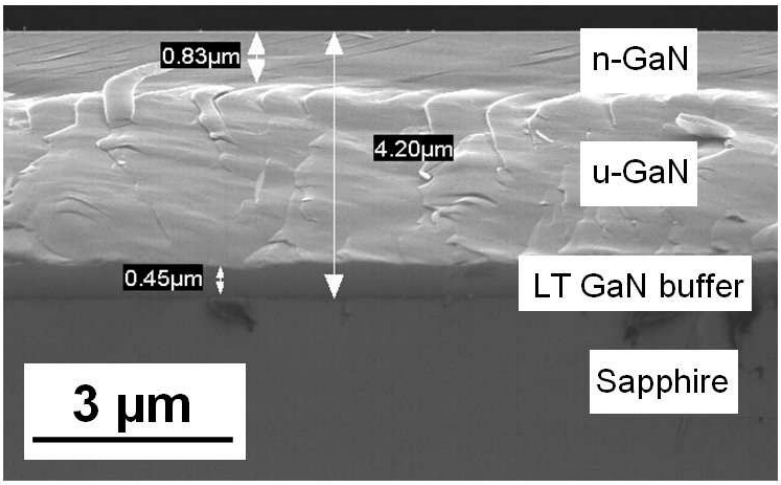

Figure 2.11 : Cross-section SEM view of a GaN stacking (low temperature, undoped and n-doped layers) grown on c-plane sapphire.

Atomic force microscopy (AFM) measurements made on standard bi-dimensional GaN are shown in Figure 2.12. Bi-atomic steps (seen as lines) and dislocations (dark dots) can be observed. The TD density of the samples grown during the validation process has been reduced to 6 x 10^8 cm^{-2}. Further optimisations could decrease this value to 2 x 10^8 cm^{-2}, which is stated as the TD density for optimised processes in the literature [Amano98, Iwaya98, Yang99a, Yang99b]. With a RMS of 0.42 nm (over 64 μm^2), the flatness of the sample is in the same order of magnitude as the flatness of the sapphire substrate (Kyocera).

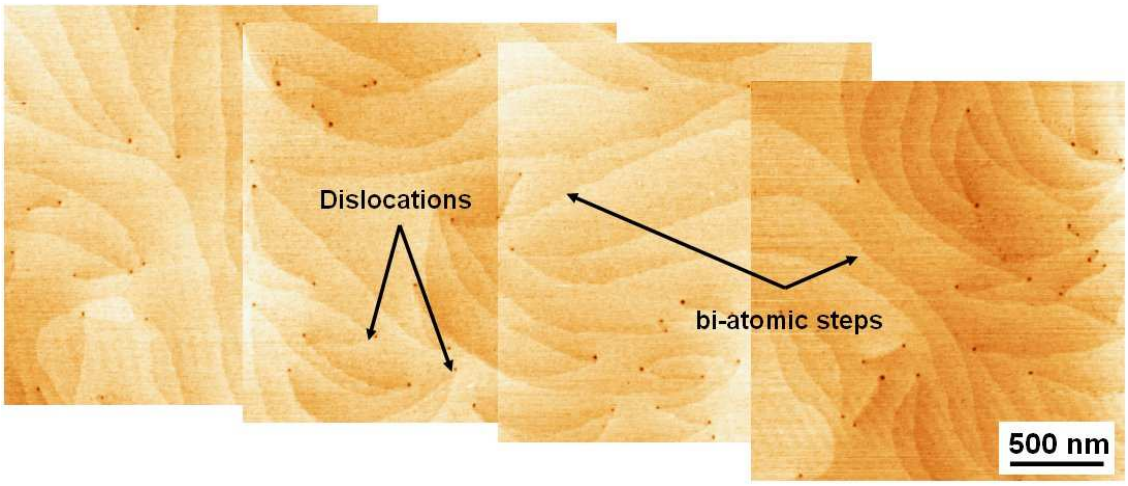

Figure 2.12 : AFM on a bi-dimensional GaN layer obtained during the validation period of the new MOCVD setup.

2.3.2. Doping of 2D GaN films

The doping control is an important factor for the carrier-density control in the fabrication of LEDs and laser diodes. Unintentionally doped GaN has been measured to be n-type with a concentration of about $3x10^{16}$ cm^{-3} in the present setup. Silicon and magnesium were used as common dopants of GaN for n- and p-type respectively. Carrier concentrations of 10^{19} cm^{-3} for n-doping and 10^{17} cm^{-3} for p-doping are currently reported in the literature [Lin93, Lee99].

n-doping

n-GaN is grown under the same growth conditions as u-GaN but at a pressure of 200 mbar and with the additional injection of silane. Silicon, a group-IV element, exhibits one valence electron more than Ga in group III. Therefore, incorporation of Si leads to an increase of electrons in the bulk and a decrease in electrical resistance. The carrier mobility, function of the Si concentration, is decreased with increasing doping level [Mnatsakanov03] and the final carrier concentration in the GaN layer directly depends on the silane molar flow [Nakamura00]. The resistance drops quickly with increasing doping level and is stabilised for values higher than 1 x 10^{18} cm^{-3}. For the present 3x2" CCS reactor, a molar

flow between 1.24 nmol/min and 6.26 nmol/min leads to a doping concentration in-between 1 x 10^{18} cm^{-3} and 5 x 10^{18} cm^{-3}.

p-doping

The growth of p-GaN is more difficult than n-GaN and was first achieved in 1989 with Mg as dopant followed by low energy electron beam irradiation (LEEBI) [Amano89]. In 1992, p-GaN was obtained by a thermal annealing under N_2 [Nakamura92a]. This process, much easier to integrate in a production flow than LEEBI, favoured the very strong development of the III-nitride devices.

p-GaN is grown at 920 °C, under a pressure of 200 mbar and a V/III ratio of 4000. The Cp_2Mg flow is 700 nmol/min. The post growth annealing is carried out at a temperature of 750 °C in an N_2 atmosphere for 20 min. During this annealing step, inactive hydrogen-donor complexes, responsible for low doping efficiency are dissociated [Nakamura92b, vanVechten92, Götz95]. p-GaN layers grown in the present MOVPE system exhibit a hole concentration of 4 x 10^{17} cm^{-3} and a mobility of 9-12 V cm^{-2}, consistent with the values reported in the literature [Nakamura00].

The Mg incorporation in the material is very bad because less than 1% of incorporated magnesium produces acceptor centres at room temperature due to a large activation energy of about 200 meV [Monroy04]. Fairly large quantities of magnesium must be incorporated to overcome the background-electron concentration due to residual donors of the unintentional doping. It is therefore difficult to achieve a hole concentration of 1 x 10^{18} cm^{-3} corresponding to a Mg incorporation of 1 x 10^{20} cm^{-3} because this value is near the solubility limit for Mg [VanDeWalle98]. In contrast to Si doping, the resistance of Mg-doped GaN increases for larger Mg content due to the increase of defects[20]. For all these difficulties, the heavy p-doping of bi-dimensional GaN is often restricted to the last 5 nm of a device to avoid material damaging.

[20] Moreover, the hole mobility is about a factor of 30 smaller than the electron mobility in Si-doped layers.

Summary of carrier concentrations and mobilities obtained in the MOCVD system

The carrier density and mobility of u-GaN; n-GaN and p-GaN were determined by Hall effect measurements carried out in the Van der Pauw configuration [VanDerPauw58]. The results of the measurements are given in the table below.

Sample	**GaN: nid**	**GaN:Si**	**GaN:Mg**
Type	u	n	p
Carrier concen. [cm^{-3}]	3 x 10^{16}	5 x 10^{18}	4 x 10^{17}
Mobility [cm^2/Vs]	132	320	9 - 12

Table 2.2 : Carrier concentration and carrier mobility for u-GaN (i.e. un-intentionally doped), n-GaN and p-GaN measured by Hall Effect in the Van der Pauw geometry

2.3.3. AlGaN growth

AlGaN is an interesting ternary alloy for applications in deep UV-light emitting devices with wavelengths down to 250 nm [Moe06]. Additionally, AlGaN films are used in blue laser diodes with Bragg mirror heterostructures [Nakamura99] and HEMT transistors [Li06b]. The band gap varies between 6.2 eV (AlN band gap) [Koide87] and 3.4 eV (GaN band gap) [Vurgaftman01] depending on the Al concentration. AlGaN was grown at the same temperature as GaN, at a pressure of 150 mbar with TMAl as aluminium precursor. The AlGaN layer was grown on a GaN template and examined by a symmetric X-ray ω - 2θ scan (see Figure 2.13). The aluminium concentration in the AlGaN layer has been calculated from the angular distance between the (002) peaks of GaN and AlGaN by using Vegard's law [Vegard21] linearly relating the alloy lattice-parameter to the Al-concentration. It was calculated to be 18.6 % whereas 20 % was targeted for the growth. The concentration homogeneity was very good as confirmed by four measurements on the 2-inch sample.

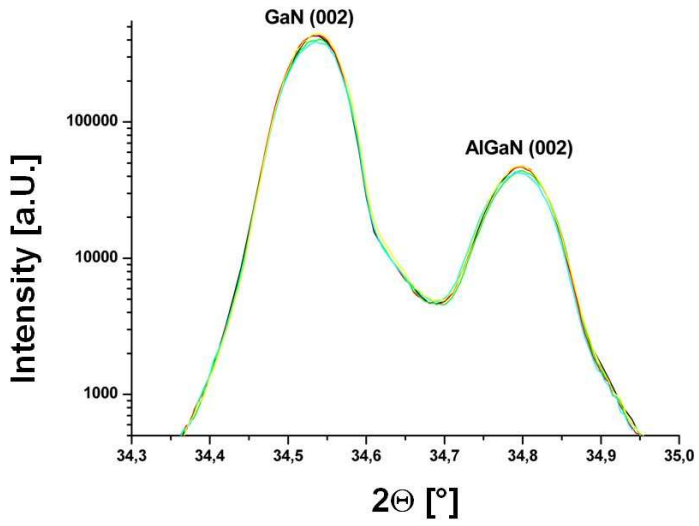

Figure 2.13 : X-ray ω - 2θ scan of AlGaN grown on GaN. The different measurements of the (002) reflection are taken at four positions on the 2-inch substrate. They are nearly superposed indicating a good homogeneity of the alloy composition.

2.4. InGaN properties

InGaN is the most important building-block for blue LEDs and laser diodes. By changing the In-concentration in the alloy, the light mission wavelength can be shifted from the near UV into the infrared spectra. The band gap energy E_g of $In_xGa_{x-1}N$ can be calculated by the following parabolic interpolation:

$$E_g(x) = E_{g,\,InN} + (1 - x)E_{g,\,GaN} - bx(1 - x) \qquad \text{(eq. 6)}$$

The values for $E_{g,InN}$, $E_{g,GaN}$ and the bowing parameter b are given in Table 1.4 and Table 1.6. The InGaN lattice parameter increases with x leading to strain between the GaN quantum barrier and the InGaN quantum box. Additionally, concentrations of over 20 % reveal the tendency of phase separation in bi-dimensional layers [Domracheva08]. In this chapter, the InGaN/GaN QW structure and growth for application in blue LEDs will shortly be discussed.

InGaN/GaN QW structure

As briefly discussed before, the GaN wurtzite crystal is polarised and exhibits piezoelectric fields in the material. The origin of this spontaneous polarisation lies in the strong ionic nature of the bond between the Ga- and the N-atoms. When the III-nitride lattice is deformed due to external forces such as compressive or tensile stress, a piezoelectric polarisation is induced to the crystal as a function of its orientation and the total polarisation is the sum of the spontaneous and the piezoelectric components [Harrison05]. In InGaN/GaN QW structures grown along the c-direction, the fields have a detrimental effect caused by the separation of the electron and hole-wave functions, a function of the QW thickness (see Figure 2.14). This effect reduces the overlapping of the electron and hole-wave functions decreasing the internal quantum efficiency of the structure [Berkowicz00]. Inside a QW the electrons and the holes accumulate at opposite sides and emission energy is smaller in comparison to the field-free case. Therefore the energy difference between the electron- and hole-states decreases causing a red shift in the emission spectrum of the structure. This phenomenon is known as the quantum confined stark effect (QCSE) [Takeuchi97, Chichibu00] first observed in GaAs-AlGaAs QWs [Chemla83].

Up to now, polarisation effects have not been of major concern in optoelectronic devices due to the high current densities at which these components are commonly operated (this influence will be discussed in chapter 4). Only recently, this issue has gained more attention due to the quest towards improved internal quantum efficiency in light-emitting devices targeted for general lighting applications.

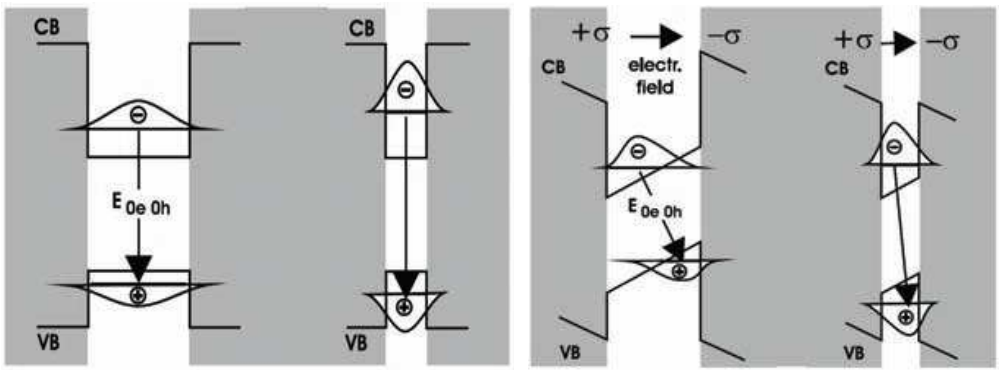

Figure 2.14 : Schematics of the energy band in a QW without (left) and with an internal electric field (right) and illustration of the impact of the QW thickness (figures taken from [Ambacher02])

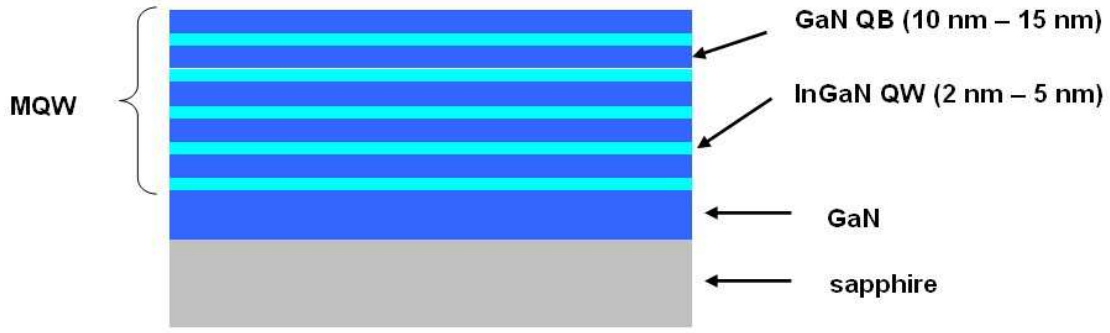

Figure 2.15 : Schematic of an InGaN/GaN MQW grown on sapphire

In the context of this project, a simple MQW structure composed of 5 InGaN/GaN layer grown on a 2" c-plane sapphire substrate was studied in order to validate the control of the growth process (see Figure 2.16).

The InGaN alloy growth is very sensitive to temperature [Kuykendall07]. The manufacturer of this equipment empirically observed that the optical emission wavelength of this alloy changes by about 1.5 nm per Kelvin. This means that both average temperature and homogeneity must be controlled during the process.

In these experiments, a growth temperature of about 750 °C was chosen for the InGaN well, the temperature variation being about 3 K on the 2" wafer. Nitrogen was used as the carrier gas instead of hydrogen, because H_2 has an etching behaviour for indium and would reduce its incorporation into the well [Koukitu99]. The growth rate was maintained to a low value to increase the structural quality of the layer and the typical thickness of the quantum well was between 2 and 5 nm.

The growth of the GaN needs higher growth temperatures to achieve a good structural quality. For the GaN barrier, a fast temperature ramping between the well and barrier growth is important to prevent a decomposition of the InGaN well and a compromise must be found for the barrier growth temperature: TEGa is preferred to TMGa as a Ga source to benefit from a higher decomposition rate at a lower temperature [Stockmann94] and the barrier growth temperature is set to about 860 °C. During the ramping (between 750 and 860 °C), a small amount of GaN is deposited to lock the indium in the well. The barrier is typically 10 to 15 nm thick.

Example of the photoluminescence measurement of a MQW

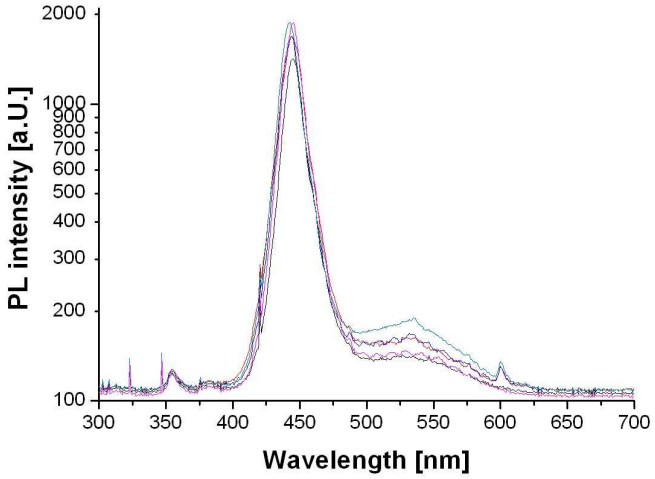

Figure 2.16 : RT PL of an InGaN/GaN x 5 MQW: The measurements are performed at different positions on the 2-inch wafer and show a shift of the InGaN emission wavelength of about 5 nm

Figure 2.16 shows a superposition of five RT PL measurements of an InGaN/GaN MQW (x 5) with a target thickness of 5 nm for the QW and 10 nm for the QB at different positions of the sample. A He-Cd laser with an emission wavelength of 325 nm (3.82 eV) (cut by a filter and not visible in the spectra) was used for PL excitation. The emission peaks are centred between 442 nm (2.81 eV) and 447 nm (2.78 eV) with a FWHM of 35 nm (20 meV). The different peak positions can be explained with a difference in temperature of ± 1.5 K at different positions of the sample. The MQW emission is about a factor of 15 stronger than the GaN NBE emission centred at 355 nm (3.497 eV).

2.5. Integration in a simple LED structure

The building blocks demonstrated previously (2D GaN film growth, doping control and MQW growth) have been combined in the single heterostructure shown in Figure 2.17 to obtain a simple blue LED.

Un-intentionally doped GaN is grown on a c-plane sapphire followed by two n-doped GaN layers: the first having a carrier concentration of 5 x 10^{18} cm^{-3} followed by a second with a smaller carrier concentration of 1 x 10^{18} cm^{-3}. The (InGaN/GaN) MQW (x 5) is grown on these layers. The use of several QWs increases the volume for electron-hole recombination and therefore the efficiency of the LED. For a convenient carrier injection, the QW number is usually lower than 7. The LED structure is finished by two layers of

p-doped GaN (200 nm thick), the Mg content being increased only at the top of the structure to avoid the material's degradation.

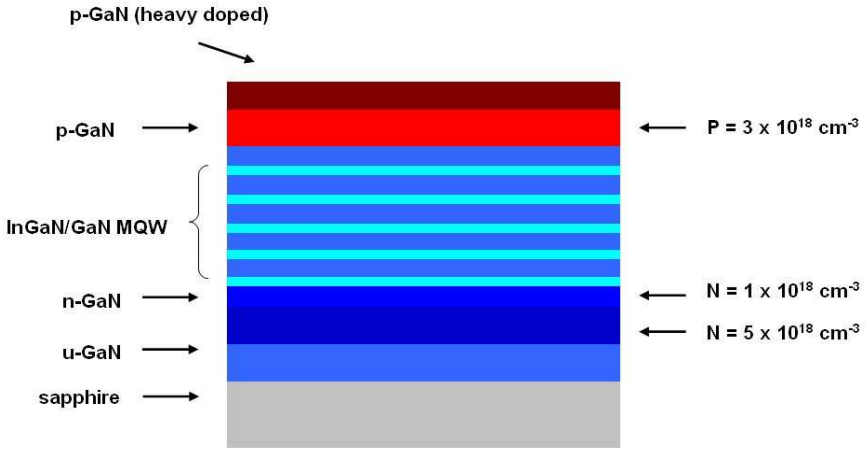

Figure 2.17 : Schematic of a simple GaN-based LED with an InGaN/GaN MQW as an active centre

The first layer has a carrier concentration of 3 x 10^{18} cm^{-3}. The second layer is much thinner but heavily doped for the later contacting in. Order to obtain the final LED-device the structure is etched down to the n-doped layer (that must be thick enough), a metal contact of Au/Ti is deposited at the bottom and the top p-doped layer is contacted by Au/Ni deposition as illustrated in the left of Figure 2.18. The right part in Figure 2.18 shows the blue electroluminescence of a LED structure grown on a 2" sapphire wafer electrically contacted at the CEA/LETI/DOPT department.

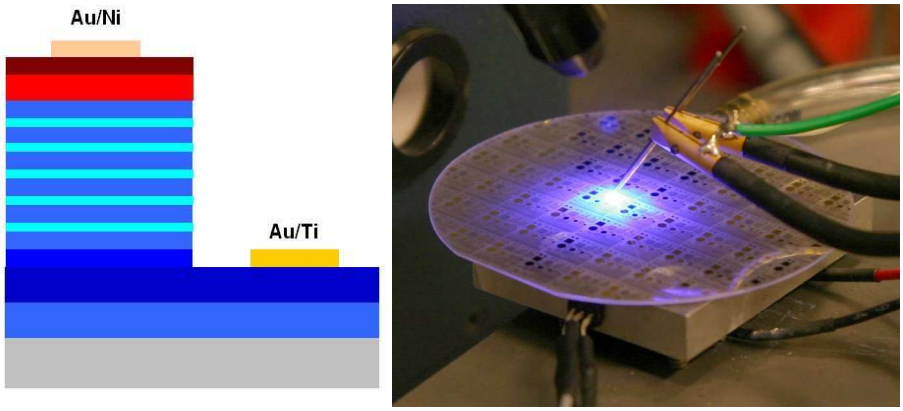

Figure 2.18 : Schematic view of the processed LED and the LED integrated by DOPT showing electro luminescence

2.6. Conclusions

During the validation period of the MOVPE system, the growth of the LED building blocks was demonstrated. Important points concerning the materials reproducibility and homogeneity over the whole 2" sapphire substrate have been demonstrated in terms of:

- Successful GaN film deposition using a low temperature GaN nucleation layer step (standard growth method in the literature). SEM and AFM have been performed to show the layer homogeneity and quality. The layers are flat (RMS 0.42 nm over 64 μm^2) and exhibit a dislocation density of 2 x 10^{8} cm^{-2}. AlGaN alloy layers with a maximum Al-concentration of about 20% have also been obtained.

- GaN doping control (n–type, but also p-type doping, which is more difficult to reach) with convenient concentration levels for device application (for example LED).

- Growth of InGaN/GaN multiple quantum wells with PL measurements evidencing emission wavelengths between 442 nm (2.81 eV) and 447 nm (2.78 eV) with a FWHM of 35 nm (20 meV). The different peak positions can be explained with a difference in temperature of ± 1.5 K over the total sapphire wafer.

- Combination of the different building blocks: 2D GaN film growth, doping control and MQW growth to get a blue electroluminescent LED (electrical contacting carried out at CEA/LETI/DOPT).

The MOVPE system has therefore fulfilled the desired specifications for GaN and InGaN growth with respect to crystal quality, doping level and In-percentage control. In the next chapters, these results will be adapted to the growth of GaN wires and InGaN/GaN heterostructures.

Chapter 3

Growth of self-assembled GaN wires

3.1. Introduction

In the literature, MOCVD and MOVPE GaN wires are usually grown with nickel and gold catalysts [Kuykendall03, Gottschalch08] or by catalyst-free approaches using an *ex situ* pre-patterned mask [Deb05, Hersee06]. During this PhD project, an original approach has been developed which does not require any *ex situ* substrate preparation before the growth. Actually, all surface preparations are carried out *in situ* inside the MOCVD reactor allowing an easier and faster growth of the wires.

The wires will be grown on a c-plane sapphire substrate as already discussed for the growth of 2D GaN films, taking advantage of the knowledge of this well understood process. This approach, based on *in situ* deposition of a thin SiN_x layer (around 2 nm) on a c-plane sapphire substrate, enables epitaxial growth of c-oriented wires with 200–1500 nm diameters and a large length/diameter ratio (>100). The wires grow randomly on the surface without any direct control of the seed position and have distributed diameters.

A detailed study of the growth mechanisms will show that a combination of key parameters is necessary to promote the vertical growth, in particular the duration of the SiN_x deposition prior to the wire growth, the GaN seed-nucleation time and a high Si-dopant concentration. This chapter will be focussed on the important steps controlling the wire growth and the structural properties of the wires.

3.2. General description of the wire growth method

Schematically, the growth of self-assembled wires can be divided into the three following main steps

- **Step I:** Surface preparation
- **Step II:** Nucleation of GaN seeds (Carrier gas: N_2, 1000 °C, V/III: 16.5, 800 mbar)
- **Step III:** Growth of GaN wires (with additional injection of SiH_4)

All these steps will be described in detail in the following.

3.2.1. The substrate

The c-plane sapphire substrates ("Crystec - alternative supplier" with a miscut of 0.25 °) were selected to grow the wires. As mentioned in chapter 2, GaN growth on sapphire leads to a high defect density in 2D layers due to the strain induced by the lattice mismatch of 13.9 % between the substrate and the GaN and due to the different thermal expansion coefficients of the materials [Ponce98]. For small wire lateral dimensions, the material is able to relax more easily from the free surface [Raychaudhuri06, Han09, Glass06, Li09] and the wires are less sensitive to substrate threading dislocations, which may curve at the bottom to reach the edge surface. Figure 3.1 below shows a 1D finite element calculation of the lateral strain without any defects. Luryi and Suhir [Li09] and Zubia, Hersee and co-workers [Zubia99, Zubia00, Hersee02, Hersee05] were able to show in theory that in a nanometer-scale heterojunction, the strain near the interface decays exponentially away from the interface. This strain decay length illustrated on the right part of the figure has the same order of magnitude as the lateral dimension of the nanojunction. Due to this exponential strain-decay at the junction, the wire is not affected by the interfacial lattice-mismatch strain or thermal strain, as long as the aspect ratio is greater than one.

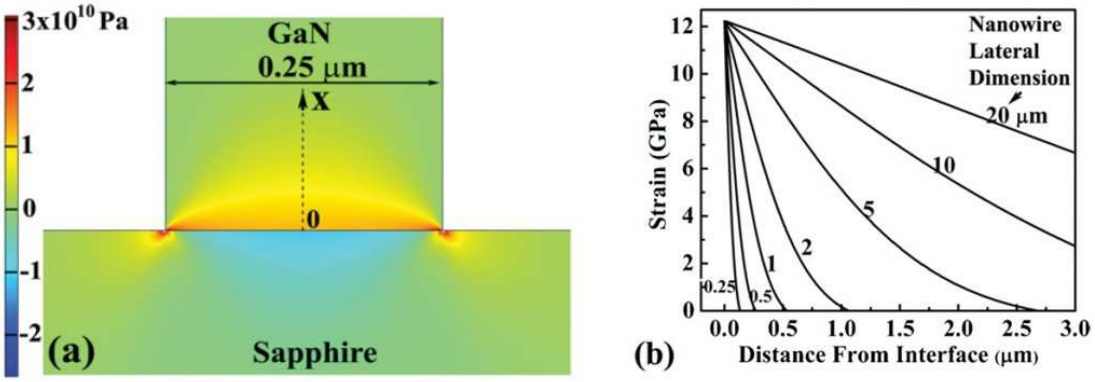

Figure 3.1: a) Finite element calculation of the lateral strain distribution induced by the lattice mismatch between sapphire and GaN for a wire with a diameter of 0.25 μm, b) strain along the wire (dotted line in a)) as a function of the distance between the sapphire/GaN interface for wires with different diameters [Li09]

From a practical point of view, the sapphire substrate is available at a low price (compared for example to SiC). Moreover, its transparency in the visible spectrum is convenient for light extraction and its smaller refractive index compared to GaN explains the general use of this substrate for LED device fabrication [Yang98].

The substrate does not have to be chemically cleaned before its introduction inside the reactor. An annealing under hydrogen at high temperature and the nitridation procedure described below prevent a contamination of the reactor chamber and allow a straightforward surface preparation before the wire growth.

3.2.2. Step I: Surface preparation

The surface preparation is subdivided into four steps:

- Surface cleaning: bake of sapphire under H_2 (100 mbar) during 20 min at 1050 °C
- Standard nitridation of the sapphire surface: annealing of sapphire under H_2 and NH_3 (1050 °C, 90 s, 100 mbar)
- SiN_x deposition (1040 °C, SiH_4: 200 nmol/min, NH_3: 4000 sccm, 133 mbar)
- Annealing of SiN_x (1040 °C, NH_3: 4000 sccm, 133 mbar)

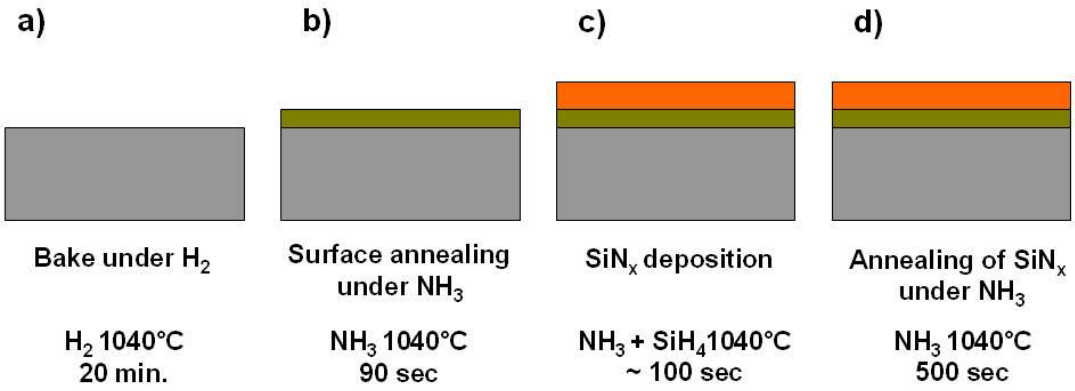

Figure 3.2: The four steps of the *in situ* surface preparation: a) bake under H_2 atmosphere, b) Surface annealing under NH_3 (leading to the AlN layer formation), c) SiN_x layer deposition and d) SiN_x layer annealing

3.2.2.1. Initial treatment of the sapphire surface

The sample is baked under H_2 at 1040 °C for 20 min to clean the substrate surface from contaminations: mainly dust, adsorbed gases and water remaining from the cleaving and transfer procedure. Additionally, due to enhanced surface diffusion, the surface topology is smoothed by removing some polishing defaults.

AFM measurements carried out on the untreated substrate (Figure 3.3 a)) and baked surface (Figure 3.3 b)) show a change in surface morphology induced by the bake, especially with the formation of pits (depth of about 1 nm and diameter of several tens of nm) with a density of about 125 pits / 100 μm^2. The sapphire terraces are nevertheless still visible on the baked surface and the flatness is maintained: the root mean square (RMS) roughness is about 0.15 nm (over 16 μm^2).

The bake is followed by an annealing step of 90 s under NH_3. During this step, a thin layer of AlN is formed on the substrate surface as already reported in the literature by different experimental techniques (RHEED, TEM, X-ray reflectivity and X-ray photoelectron spectroscopy) [Grandjean96, Vennegues99, Kim00, Dwikusuma03]. The typical staircase-like surface of the sapphire is still visible in AFM indicating a very thin and conformal layer (see Figure 3.3 c)). Even after doubling the nitridation time, the terraces still remain visible, indicating a self-passivation of the surface, which limits the thickness of the layer. The number of holes is increased with regard to the initial baked surface. These

defects can be viewed as preferential sites for the sticking of GaN during the nucleation step.

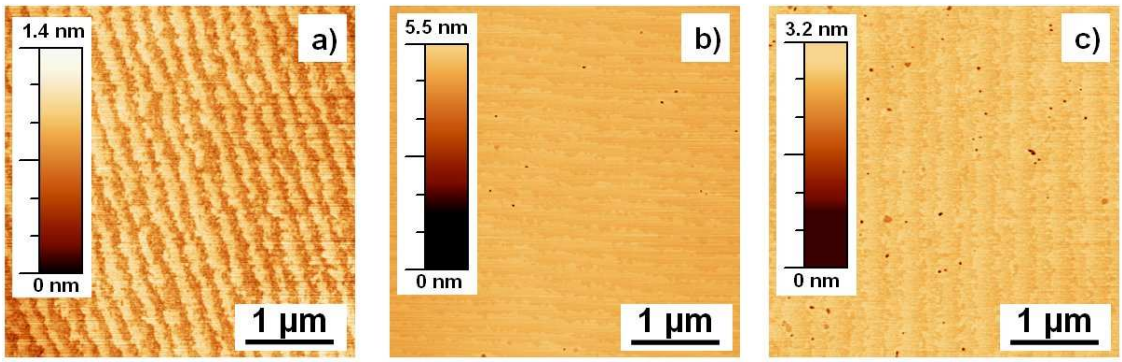

Figure 3.3 : Initial treatment of the sapphire surface: a) untreated sapphire, b) baked sapphire, c) baked and annealed sapphire

In order to initially demonstrate the formation of an AlN layer during the annealing step, the sample was studied by reflection high energy electron diffraction (RHEED)[21]. This experiment is generally not implemented in MOCVD reactors due to the large electron absorption induced by the working-pressure level. The samples have been transferred into a MBE growth chamber of the laboratory under inert gas, where the measurements were carried out. Three samples were measured by means of this technique: a) a bare sapphire, b) an AlN layer obtained by the annealing of the sapphire during 300 s under ammonia and c) a sapphire sample with the SiN_x deposition and annealing steps (corresponding to the complete surface preparation process). Figure 3.4 below shows the RHEED measurements performed in the <11-20> and the <1-100> AlN azimuths for the three samples. The diffraction strikes shown in b) demonstrate the crystalline nature of the nitridated sapphire. The diffraction pattern corresponds to the hexagonal lattice with parameters similar to AlN (the error bar is very large with this technique). These observations confirm the formation of an AlN layer already discussed in the literature [Grandjean96, Vennegues99, Kim00, Dwikusuma03]. In c), the AlN diffraction pattern became more diffuse indicating the amorphous or nanocrystalline nature of the deposited SiN_x layer. The nitridated layer signal is still visible underneath. It can be attributed to the very thin SiN_x layer thickness[22] as will be confirmed later by X-ray reflectivity experiments.

[21] Courtesy to M. Azize and E. Monroy

[22] An incomplete coverage can be excluded due to the results of AFM measurements.

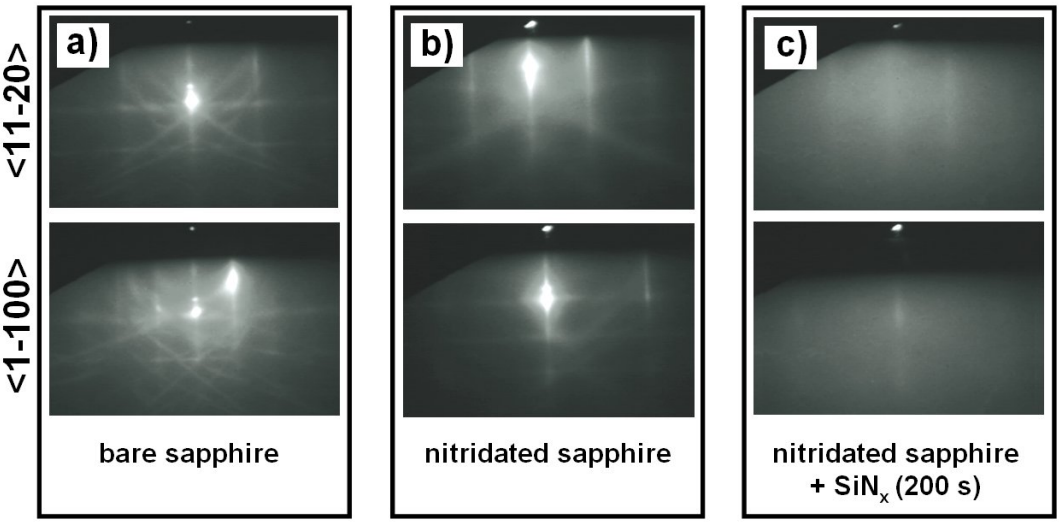

Figure 3.4 : RHEED patterns along the <11-21> (first line) and the <1-100> (second line) AlN directions for a) bare sapphire, b) annealed sapphire under NH_3 (300 s) and c) 1.5 nm SiN_X deposition on annealed sapphire [Courtesy to M. Azize and E. Monroy]

3.2.2.2. SiN_x deposition

After the annealing step under NH_3, the reactor conditions are immediately set for the deposition of SiN_x. Silane and NH_3 are simultaneously injected into the reactor leading to the formation of a thin SiN_x layer on the sapphire surface, as already reported in the literature by Haffouz and Beaumont [Haffouz98, Beaumont98].

Figure 3.5 shows AFM images (in tapping mode) of four SiN_x layers corresponding to different deposition times: a) 50 s, b) 100 s, c) 200 s and d) 400 s. A rough layer of SiN_x is observed irrespectively of the deposition time. At this observation scale the surface is homogeneously covered. The roughness is increased with respect to the initial surface: the RMS height is about 0.3 nm (integrated over 16 μm^2). The surface is crossed by linear marks, which are probably due to the preferential nucleation of defects along the polishing lines of the sapphire wafer.

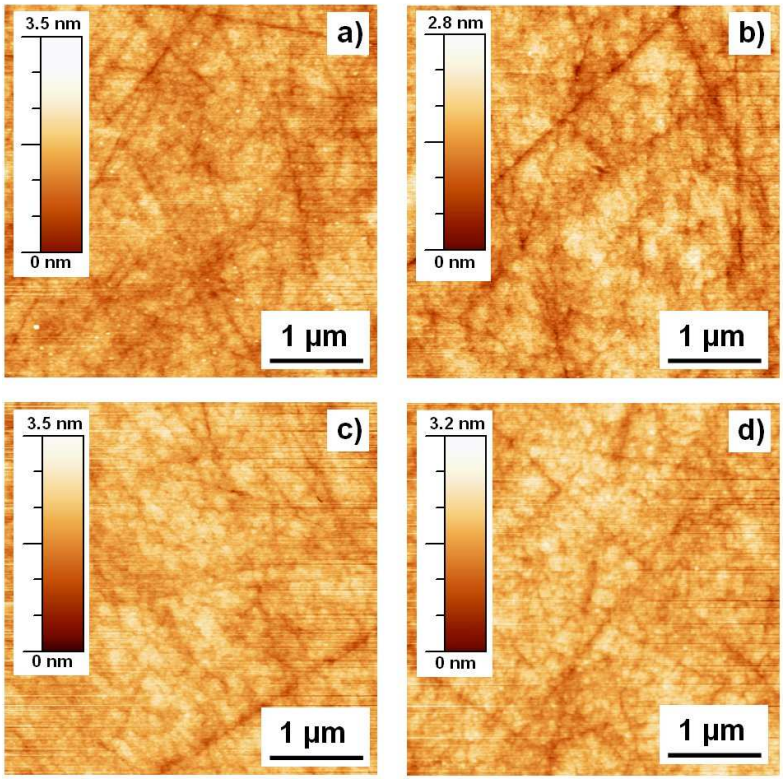

Figure 3.5 : AFM images (tapping mode) of SiN_x layers deposited on sapphire for a) 50 s, b) 100 s, c) 200 s and d) 400 s. All samples show a grain-like structure with scratches probably resulting from the polishing process during the sapphire-wafer production.

A systematic study of the wire growth exhibited a very high sensitivity to the initial SiN_x deposition time. Figure 3.6 shows tilted SEM views of wire growth on SiN_x layers deposited for different durations. The wire growth is not obtained for SiN_x layers deposited for durations shorter than 50 s which results in a rather a rough tri-dimensional growth instead (see Figure 3.6 a)). A SiN_x deposition for 100 s produces hexagonal shaped and vertically aligned wires as shown in Figure 3.6 b). A further increase to 200 s leads to highly defective wires with rough facets (Figure 3.6 c)). For 400 s (Figure 3.6 d), the quality of GaN wire growth is further degraded and additionally to the vertical growth, the growth of inclined wires can be observed. The origin of these inclined wires and their properties will be discussed below in this chapter.

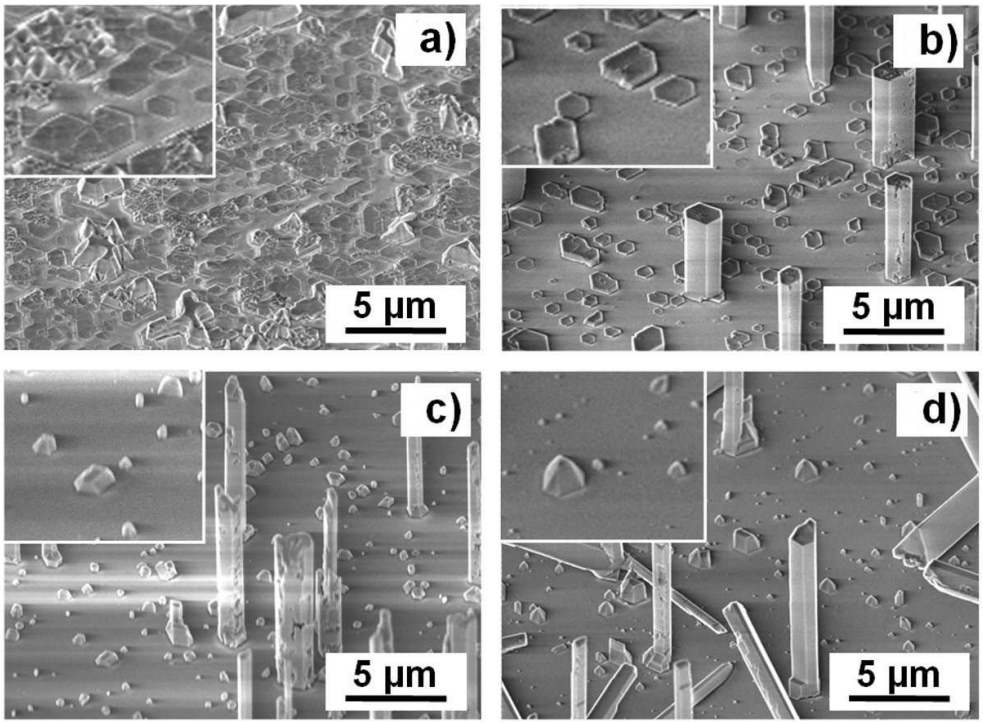

Figure 3.6 : GaN wire growth as a function of the SiN_x deposition time (50 s, 100 s, 200 s and 400 s). a) 50 s: three dimensional growth; no wires are visible. b) 100 s: well aligned hexagonal shaped wires. c) 200 s: wires with a high density of structural defects. d) 400 s or longer: non vertical growth occurs additionally to the vertical growth. The insets in the pictures show details of the nucleation seeds for each deposition time.

This initial surface preparation was analysed by specular X-ray reflectivity (XRR) to provide quantitative information on the surface electron-density in terms of layer density, thickness and roughness of the nitridation and SiN_x layers. The experiments were performed at the European Synchrotron Radiation Facility (ESRF, Grenoble France) on the French BM32 CRG beam line at 18 keV (*i.e.* λ=0.069 nm). Four samples were measured: the initial nitridated sapphire surface and the 100 s, 200 s, 800 s SiN_x depositions on nitridated sapphire.

Raw experimental curves are shown in Figure 3.7 a) as a function of the momentum transfer $Q = 4 \pi \sin\theta / \lambda$ where θ is the incidence angle. Fitted X-ray reflectivity curves are drawn in Figure 3.7 a) and show a very good agreement with experiments[23].

[23] In this analysis, the electron density profile is not *a priori* fixed - as is generally the case - by the superposition of step-like or Gaussian functions the parameters of which are numerically fitted. The drawback of this stochastic fit is to induce oscillations in the density profile which do not become visible in simplest box/roughness models. These two approaches produce similar values of the electron density profile.

The electron density profiles normalised to the sapphire substrate are depicted in Figure 3.7 b). It is shown that the initial nitridation step leads to a ~1.5 nm-thin layer with a lower density than sapphire, compatible with AlN electron density. It becomes evident that the surface roughness is quite low just after the nitridation process (see the abruptness of the profile at the sample surface). The following SiN_x deposition step increases the thickness by about 2 nm and significantly increases the surface roughness with respect to the initial nitridated surface. It turns out that the thickness of the SiN_x layer does not depend on the growth time. This indicates a self-passivation during deposition probably due to the limited reaction of diluted silane with the surface. The total thickness and the average density are slightly increased, especially for the 800 s SiN_x deposition time. This indicates that the thickness of the SiN_x layer is not the most important parameter for these wire growths but rather the roughness and density related to the chemical composition at the surface.

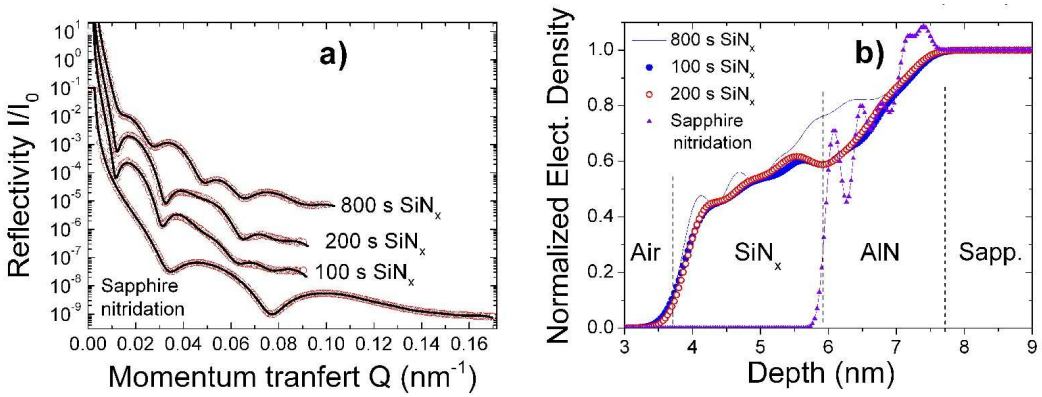

Figure 3.7 : (a) X-ray reflectivity curves I/I_0 of four templates before the wire growth: initial nitridated sapphire surface and 100, 200, 800 s SiN_x (annealed) deposition times on nitridated sapphire. Open symbols (resp. lines) correspond to experimental (fitted) data, b) Normalised electron-density profiles with respect to sapphire density extracted from the stochastic fit with 30 slabs

3.2.2.3. Annealing of the SiN_x layer

The SiN_x layer is annealed under NH_3 for 500 s directly after its deposition. This step is of high importance for the later wire growth: non-annealed SiN_x layers give rise to a growth mode in which not all the wires grow perpendicularly to the surface and may be branched from the same seed at different angles. This is called "multipod growth" and was already

observed and commented in ZnO wires [Xu05, Zheng08, Lyapina08, Wang08]. Figure 3.8 shows two SEM images of a growth of GaN wires on non-annealed SiN_x. Figure 3.8 a) shows a tilted view (45°) in which several configurations of inclined wires can be identified: 1) monopod, 2) tripod and 3) bipod with an additional wire emerging perpendicularly to the surface. Figure 3.8 b) shows a cross-section of the wire assembly viewed from the edge of a cleaved sample. The assembly growing perpendicularly to the surface is crossed by inclined wires with different angles.

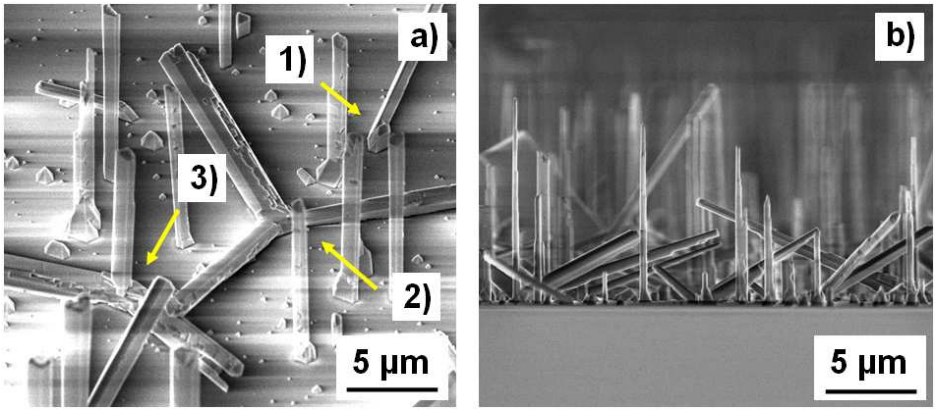

Figure 3.8 : Typical multipod growth on a c-plane sapphire: a) tilted (45°) and b) cross-section view

Figure 3.9 shows plane-view SEM images demonstrating the effect of SiN_x annealing on the GaN wire growth. In Figure 3.9 a), the surface was not annealed after the SiN_x deposition and thus the surface is completely covered with multipods. Figure 3.9 b) shows a GaN wire assembly grown on an annealed SiN_x layer on which the multipod growth is completely suppressed. The explanation of this behaviour will be discussed below in this chapter.

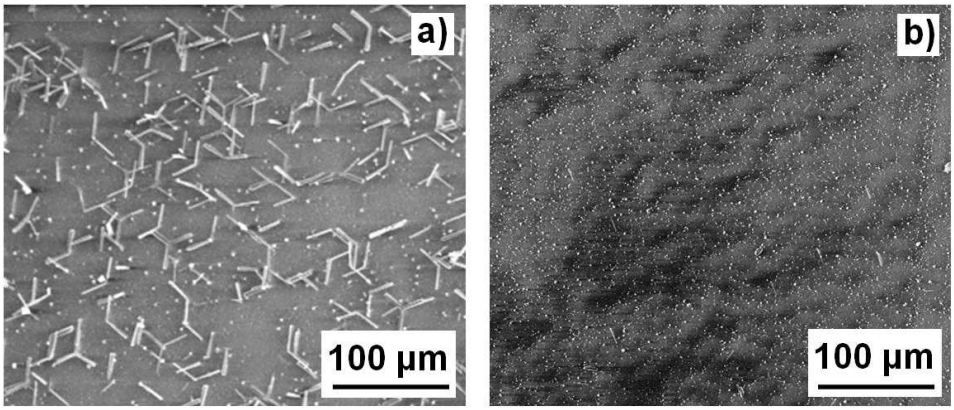

Figure 3.9 : GaN wire growth a) without annealing under NH_3: multipods are clearly visible and wires can be seen perpendicularly to the surface in the form of dots and b) with annealing under NH_3: multipod growth is completely suppressed and a very small number of non-perpendicular wires can be seen.

3.2.3. Step II - GaN seed nucleation for wire growth

The shape of the seeds between the wires strongly depends on the SiN_x deposition time, as shown in the insets of Figure 3.6. For 50 s of SiN_x deposition, a rough GaN bi-dimensional (2D) growth is observed indicating a coalescence of GaN (inset of Figure 3.6 a)). The GaN nucleates as hexagonal-shaped flat seeds for 100 s, whereas six-fold pyramidal-shaped seeds with $\{10\bar{1}1\}$ facets occur for durations longer than 200 s (insets of Figure 3.6 b) – d))). The seed shape appears to be critical for vertical wire growth. Indeed, only seeds with c-plane facets permit growth of c-oriented wires in contrast to the pyramids for which tilted growth was observed. The optimal SiN_x process corresponding to the growth of well-aligned hexagonal c-plane seeds is obtained for a SiN_x layer deposited for 100 s. Vertical wires can also emerge from the c-plane of truncated hexagonal pyramids as observed for 200 s and 400 s SiN_x deposition times, but for depositions longer than 200 s, most of the GaN seeds grow as hexagonal pyramids (without a c-plane facet) and lead to tilted wires.

The duration of the nucleation (hereafter called nucleation time) also appears as a critical parameter to decrease the mean wire size and to improve the crystalline quality. Figure 3.10 shows the wire growth using two different nucleation times a) 10 s and b) 100 s. The insets in Figure 3.10 show the surface morphology directly after the nucleation times of 10 and 100 s respectively.

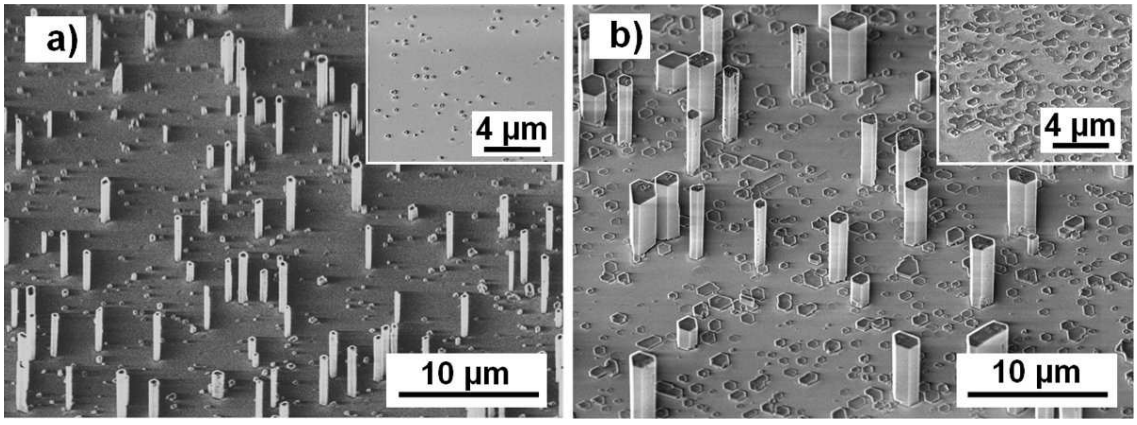

Figure 3.10 : Influence of the GaN nucleation time on the wire growth. a) 10 s and b) 100 s. The growth temperature is 1000°C. The insets show the seed morphology just after the nucleation step.

The mean-size of hexagonal GaN seeds is significantly reduced by decreasing the nucleation time, which certainly explains the reduction of the wire diameter. It is clearly

visible that an increase of the nucleation time enlarges the mean wire diameter from 500 ± 200 nm to 1.5 ± 0.4 µm and simultaneously decreases the wire density by a factor of two. Moreover, a deterioration of the crystalline quality with increasing nucleation time is observed.

To explain this phenomenon, one has to consider that the GaN seeds start to grow laterally just after the nucleation. Figure 3.11 shows SEM and AFM images of GaN nucleation seeds grown at 1000 °C during 100 s (this time suffices to develop the different types of defects). The surface is covered with oriented hexagonal shaped seeds.

The AFM images in the insets of Figure 3.11 show the surface of a seed and the surface in-between. The seed height is in the 50 - 200 nm range and the top has a grain-like structure with a RMS height of about 0.8 nm, whereas a flat surface (RMS height ≈ 0.2 nm) is observed in-between the seeds. Size and facet lengths are largely distributed explaining the difference of the wire's shape and size. The lateral growth of the seeds may encounter some surface defects such as pits, emerging dislocations and surface kinks, which may induce a cavity or an interface boundary (see white arrows in Figure 3.11) which propagates along the wire during the vertical growth [Tham06]. A second possible origin of defects is the coalescence of two or more seeds giving rise to grain boundaries which cannot be cured by a longer growth.

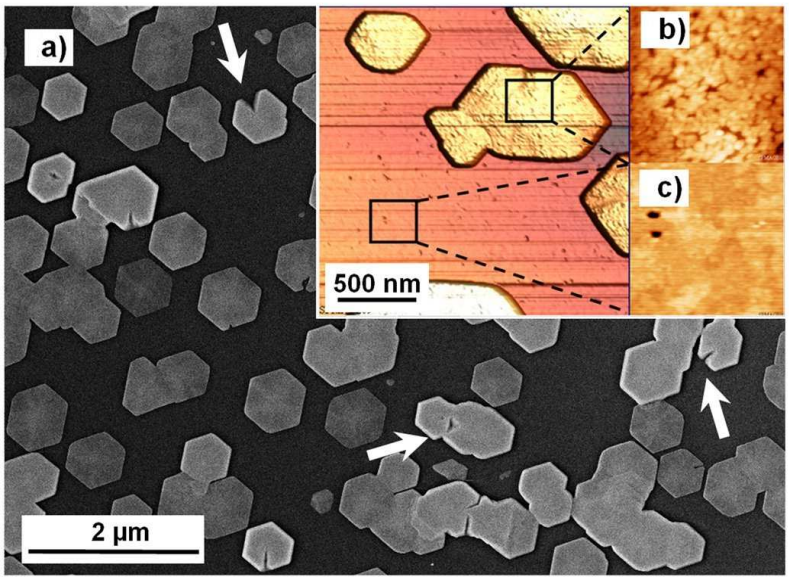

Figure 3.11 : SEM and AFM measurements of GaN seeds deposited for 100 s. This time is long enough to develop common defects. a) SEM image of GaN seeds. The white arrows point to defects. b) AFM images reveal the surface properties on and in-between the seeds.

In the same way, the origin of the distribution of the facet length can be partly explained by this coalescence. For these reasons, a shorter nucleation time leads to less seed defects and

consequently to better structural quality of the wire assembly. The optimal nucleation time is about 10 s to minimise the quantity of structural defects.

3.2.4. Step III: Growth of GaN wires

In the following the important process parameters to control the GaN wire growth: temperature, V/III ratio, carrier gas and precursor flows will be discussed. Moreover, the importance of silane injection in driving the vertical growth will be stressed. To simplify the presentation, the following parameters have been varied independently while keeping the others fixed:

- V/III ratio
- Silane injection
- Temperature
- Wire growth time
- Carrier-gas flow
- Precursor-flow rate
- Substrate miscut

This will allow some general conclusions about the growth mechanisms of the GaN wires, but it will also stress the complexity of the MOVPE growth technique.

3.2.4.1. V/III ratio

The V/III ratio corresponds to the molar ratio of group III (Ga) and group V (N) precursor flow. As already discussed in chapter 2, bi-dimensional GaN is grown with a V/III ratio around ~1000. For the one-dimensional wire growth, the V/III ratio must be decreased to about 16 to optimize the structural and optical properties (see chapter 4).

Experiments have shown that switching to a high V/III ratio during the wire growth immediately leads to strong lateral growth. This increase of the V/III ratio during the growth can be used to coalesce the upper part of a wire assembly in order to facilitate

the electrical contacting of the device [Bougrioua07].[24] In contrast, a decrease of the V/III ratio to 6 leads to laterally growing islands probably due to a GaN supersaturation of the sample surface.

3.2.4.2. Silane injection

The injection of silane during the growth is one of the most important parameters for the wire growth. Figure 3.12 shows three tilted SEM images showing the influence of silane on the growth with: a) no silane injected during the growth, b) 400 nmol/min silane injection, c) 4000 nmol/min silane injection. For no silane addition (Figure 3.12 a)), the formation of big GaN islands with a diameter of several μm is observed. The growth proceeds laterally and the islands show a tendency to coalesce.

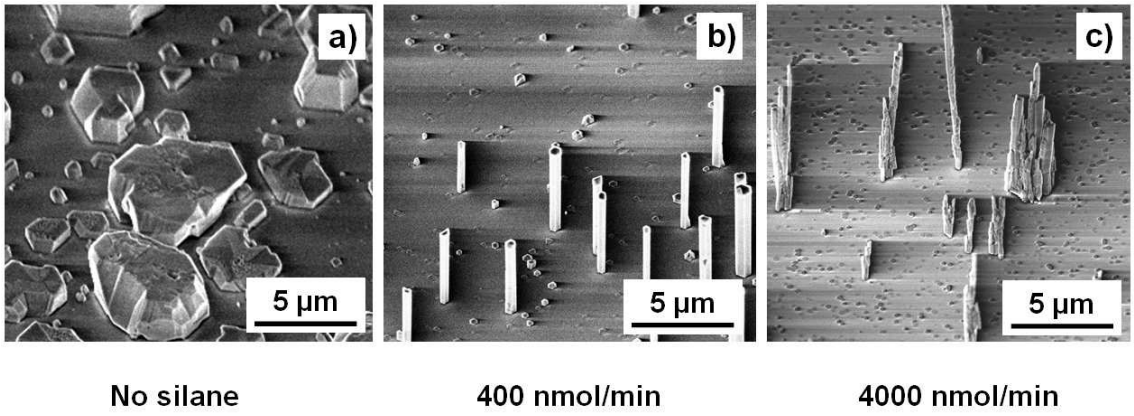

Figure 3.12: Silane plays an important role during the wire growth: a) no silane was injected into the reactor during the growth. The formation of big islands can be observed, b) Silane flow (400 nmol/ min): the wires grow in c-plane direction and the formation of islands is suppressed, c) Silane flow of 4000 nmol/min: wires are growing perpendicularly to the surface but are strongly degraded

For the silane flow of 400 nmol/min shown in Figure 3.12 b), the wires grow along the c-plane direction with a low number of defects on the side facets. The result is similar to the growth with a silane flow of 200 nmol/min (not shown here). Figure 3.12 c) finally shows the result for a silane flux of 4000 nmol/min, the highest flux that was possible to achieve with the MOCVD setup at that time. The wires have a very bad structural quality, facets are not flat and are covered with defects. The wire tops are not flat and some wires are tilted

[24] The coalescence of initial MBE nanocolumns using the MOCVD technique has also been proposed to decrease the number of dislocations and to obtain thick freestanding films by adding a HVPE deposition [Bougrioua97].

with respect to the substrate surface. Due to the high amount of defects, some wires stop growing, others show the tendency to coalesce.

The use of silane to favour the vertical growth has already been reported in the literature [Haffouz98]. Density-functional theory calculations have predicted that a Ga-polar c-plane surface is formed by a Ga bilayer with Si incorporated underneath under Ga-rich condition silane injection [Rosa06] and a catalytic role of this bi-layer can be suspected.

However, the impact of the Si incorporation under silane flow remains inexplicable at this point due to the lack of insights into the atomic configuration of the wire sides (e.g. m-plane) and the diffusion barriers on the present surface.

For very high silane flow (as observed with several thousands of nmol/min), it can be assumed that the high silicon content (> 10^{20} cm^{-3}) incorporated in the material leads to a high density of crystalline defects, which may prevent the growth of regular wires.

Further experiments showed that the silane source can be turned off after the wires have reached a length of about 5 μm. Why this continuation of growth without silane is possible and what mechanisms are involved, are presently open questions requiring deeper investigations.

3.2.4.3. Temperature

The reactor temperature is a fundamental parameter governing the process of chemical reactions. The reaction rates of the basic MOCVD mechanisms given in chapter 2 and the surface diffusion rates are strongly temperature dependent, both variables having a strong influence on the seed nucleation and the wire growth.

To evaluate the overall impact of the temperature on the applied technique, the reactor temperature was decreased in a first series of experiments by several tens of degrees during the nucleation and growth steps. Figure 3.13 compares a nucleation and growth carried out at 1000 °C and 970 °C, the other parameters being kept identical. In spite of the small temperature difference of 30 °C, a strong decrease in structural quality is observed (see the wire facets) and the wire diameter in b) is decreased by a factor two compared to a). Additionally, an increase of density by a factor five becomes evident. This strong influence of the temperature can probably be explained by a decrease of the surface

diffusion length at a lower temperature leading to both a decrease of the seed diameter and an increase of the seed density.

A decrease of temperature goes along with an increase of the deposition rate. The quantity of pre-reactions in the gas phase is reduced allowing more materials to reach the surface. This increase of deposition with a decreased surface-diffusion length impedes a proper crystal formation. Additionally, a higher seed density raises the risk of coalescence of two or more seeds, which also leads to the formation of defects.

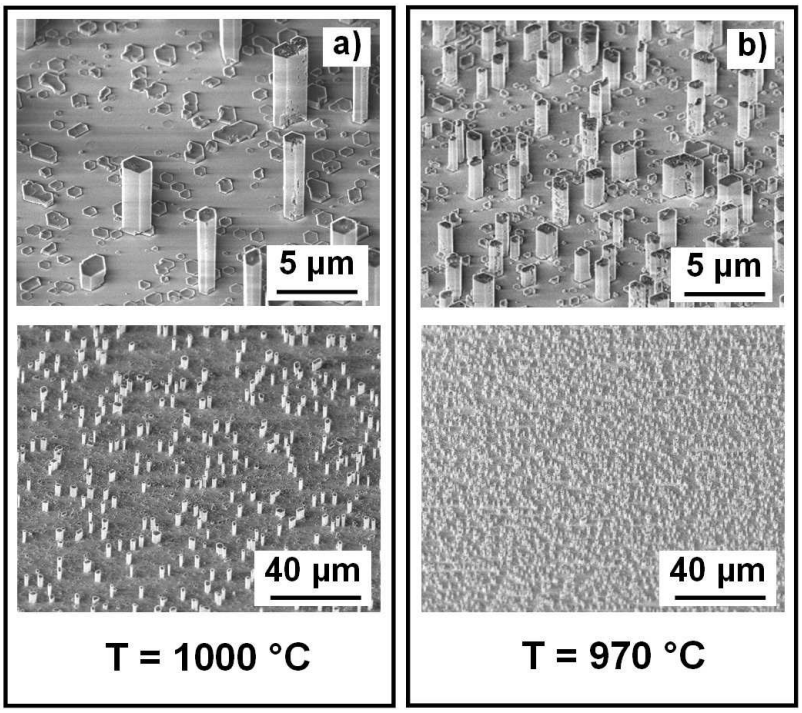

Figure 3.13 : Influence of nucleation and growth temperature (equal in these experiments) on wire density, diameter and structural quality for two temperatures: a) 1000 °C and b) 970 °C. The structural quality is decreased while the density is multiplied by a factor five.

In a second series of experiments, the temperature was stepwise decreased from 1000 °C to 800 °C during the wire growth for a given nucleation step. In this case, the temperature influence during the growth is decoupled from the seed nucleation step.

The growth temperature starting at 1000 °C was decreased in 50 °C steps down to 800 °C. At each temperature, GaN was deposited during 250 s and no precursors were injected into the reactor during the temperature ramping of 75 s. Figure 3.14 shows a SEM image of the resulting growth. The bottom part, grown at 1000 °C, shows the expected wire geometry: the side facets are smooth with a low defect density as in standard growth. With decreasing temperature, the material quality starts to deteriorate and forms foam-like

structures on top of the wires. As in the previous experiment, the deposition rate is increased with decreasing temperature.

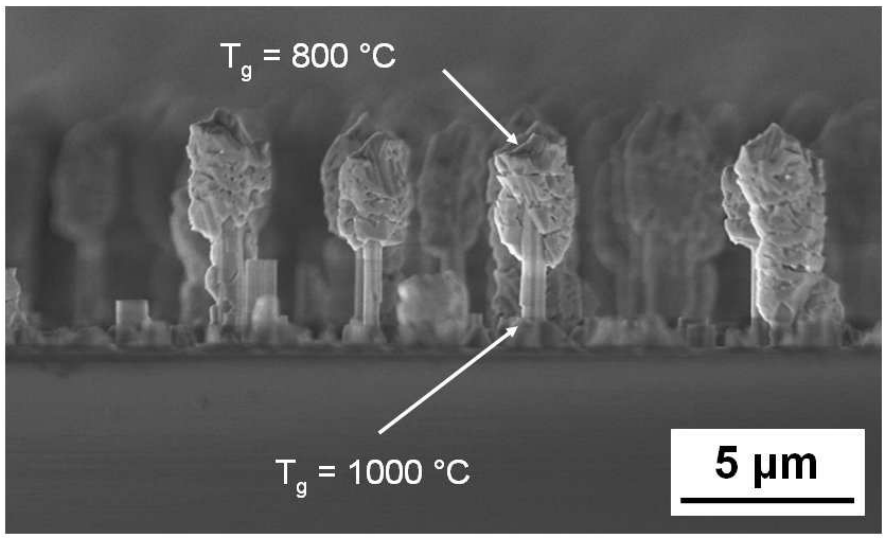

Figure 3.14 : Influence of a change of temperature during the wire growth. The temperature was stepwise reduced from 1000 to 800°C during growth (see text). The material quality is damaged at lower temperature forming tree-like structures.

3.2.4.4. Wire growth rate

As in 2D experiments, the growth rate depends on several parameters but is invariant in time as long as no parameter is changed. During 2D growth, this linear deposition of material as a function of time can be easily observed with the interferometer mounted on top of the reactor lid. For the present wire growth, this direct measurement is not possible, because the wire density does not sufficiently change the average refraction index of the substrate. To prove the linear evolution of the wire length as a function of time, the growth was interrupted after different times to measure the wire lengths by SEM cross-section images.

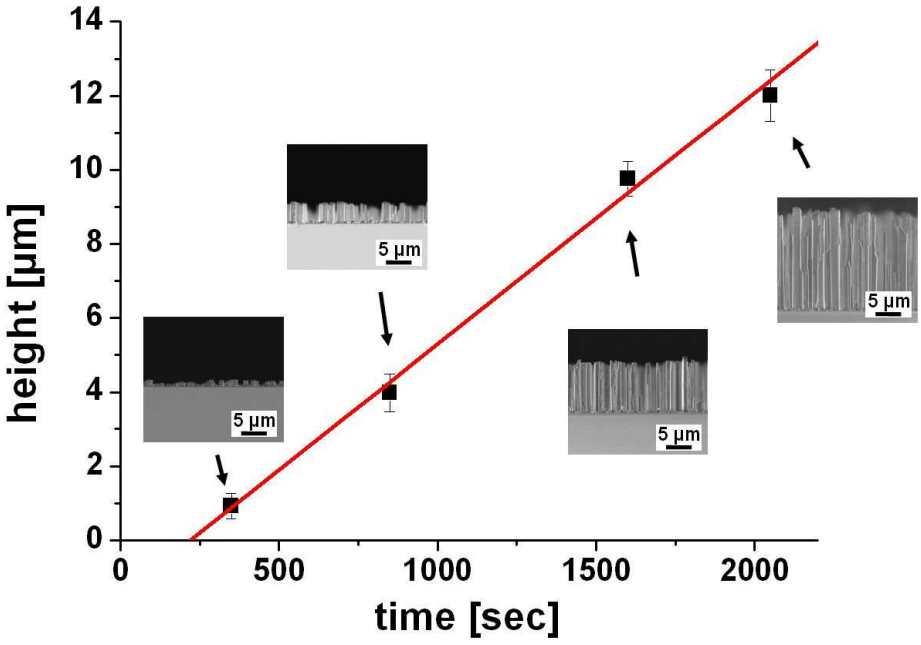

Figure 3.15: Linear relation of the wire height as a function of the deposition time defining a constant growth rate as in 2D growth.

The height of the wires is plotted as a function of the growth time in Figure 3.15. The red line represents the linear fit of the data. Small SEM images in the plot show the wire assembly related to every data point. An average length can be easily measured as well as its error bar. The growth rate is constant and the fitted line does not cross the origin of the time axis. This behaviour may be explained by the existence of a nucleation delay before the wire growth and also by the lateral growth occurring at the first stage of the growth: *i.e.* the wires do not directly start to grow in c-plane direction but the diameter of the seed is first increased. These arguments can explain the discrepancy between the observed initial seed diameter and the later diameter of the wires. This effect is particularly important for short nucleation times (for example 10 s), for which the initial seed diameter is quite low. As previously discussed in the context of temperature dependency (see Figure 3.13), a denser wire assembly leads to a lower growth rate (the wires grown at 970 °C are about two times shorter than the wires grown at 1000 °C) even if the overall material deposition is increased.

3.2.4.5. Carrier gas flow

The carrier-gas flow transports the precursors through the MO and hydrate lines into the reactor chamber. Its influence on the wire growth can be demonstrated using two different carrier gas flow rates. Figure 3. shows two cross-section view SEM images with a) 4000 sccm N_2 and b) 1000 sccm N_2 in the MO and hydrate line respectively. The growth rates are estimated respectively to 30 μm/h and 140 μm/h.

This increase in growth rate can be explained by the change of the precursor's dwell time and dilution inside the reactor chamber. The lower the carrier gas flow rate, the longer the precursors remain in the reactor chamber and contribute to the wire growth. In parallel, the precursors are less diluted, which increases the gas phase reaction rate. Figure 3. b) also contains some wires which stop to grow at a very early stage. All these wires exhibit a top facet which is not c-plane preventing the vertical growth. Simultaneously, the wires increase their diameters with increasing length. This effect can be observed in Figure 3. b) by comparing the bottom part of the wires with the top part. This effect however only occurs for wires with a length of several tens of μm. The origin of this very original increase of the lateral growth is not well understood but could be attributed to a gradient between the wire's temperature and the temperature of the surrounding gas. The GaN wire with its high heat conductivity probably exhibits the same temperature as the substrate (with reference to the calculations of [Glas06b]), whereas the gas phase is cooler due to the vertical gas stream in the reactor and the lower heat conductivity of the gases.

The wire shape featuring an increasing diameter with increasing length is of great importance in the attempt to establish a comparison between MOCVD mechanisms and MBE mechanisms. In MBE, the material's diffusion on the surface and on the wire edges (see Figure 3.16) may result in a cone shape with the exact opposite gradient in diameter and it may be concluded that these diffusion contributions are therefore not so important in our growth. The lengths of the wires are also significantly different, i.e. much longer, for MOCVD. With MBE, it is quite easy to reach the limit of the species diffusion at a given temperature but a saturation value of the length as a function of time was never reached. Further experiments with longer growth times will be necessary.

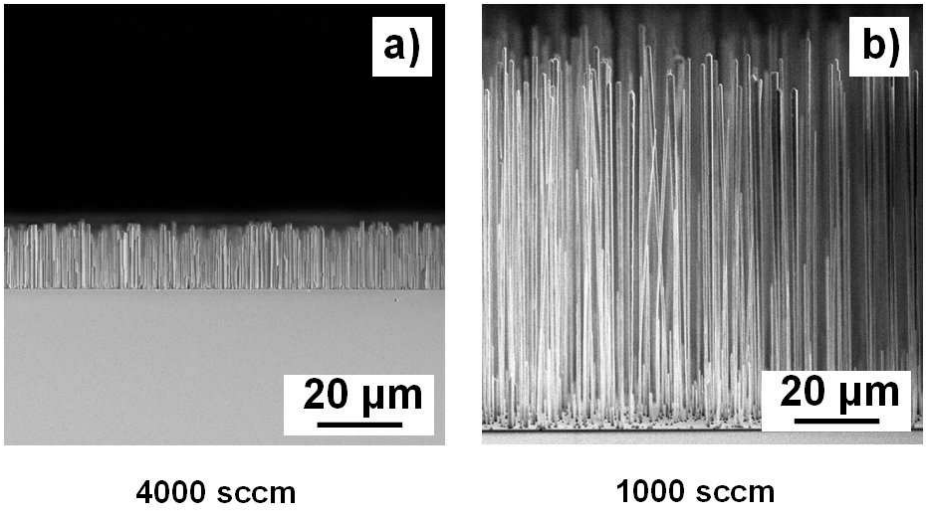

Figure 3.16 : Impact of carrier-gas flow on the growth rate: a) 4000 sccm N_2 and b) 1000 sccm N_2 in hydrate and MO line respectively. The growth time is 2000 s for both samples. The growth rate is increased by a factor of four.

3.2.4.6. Precursor flow rate

The precursor flow balance defining the overall material concentration in the gas phase was also expected to control the wire growth. This assertion has been checked by performing growth experiments with three different precursor-flow rates during the growth step keeping the V/III ratio constant at a value of 16. For simplicity, the precursor flows were not changed during the nucleation step and kept to TMGa: 60 sccm and NH_3: 50 sccm.

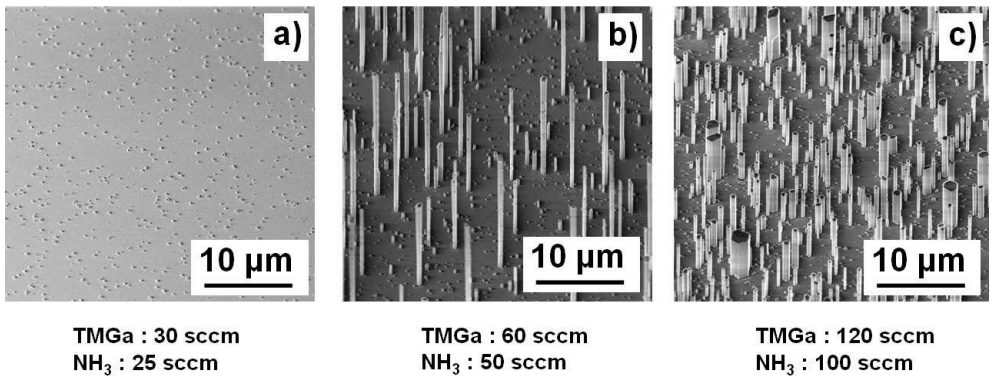

Figure 3.17 : SEM images of three growths carried out at different precursor-flow rates but identical V/III ratio of 16

Figure 3.17 shows SEM images of wire growths for the following wire-growth conditions: a) TMGa: 30 sccm, NH_3: 25 sccm, b) TMGa: 60 sccm, NH_3: 50 sccm (standard precursor flows) and c) TMGa: 120 sccm, NH_3: 100 sccm. During the growth, the N_2 carrier-gas flow was set to 1000 sccm both in the MO and Hydrate-lines. The growth times were 500 s. In case of the lowest precursor flow a), the surface is covered with seeds formed during the nucleation step and no wire growth is observed. The next higher flow rate b) corresponds to our reference standard giving acceptable wires and doubling the precursor flow in c) leads to an increase of the wire's assembly density compared to b) in parallel with a decrease in length. In agreement with the previous discussions, the distribution becomes broader and wires with a diameter of several μm can be observed.

In the case of a low precursor flow rate of a), most of the material is consumed during the pre-reaction in the gas phase and leaves the reactor chamber through the exhaust. The material-desorption rate is higher than the deposition rate and no wires can be grown.

The explanation of the difference between image b) and c) is more difficult to find. Of course, a higher precursor gas phase concentration leads to a higher material deposition and therefore to a higher wire density. But up to now, it is not understood why the wire's diameter distribution becomes larger and how this influences the growth.

3.2.4.7. Substrate miscut

In 2D GaN growth, a relatively low (~0.1 °) substrate miscut leads to a significantly rougher surface as already reported in the literature [Lu04]. To test the influence of the substrate, self-assembled GaN wire growths were carried out on different c-plane sapphire substrates in the same run. Figure 3.18 shows SEM images for growths on a) a Crystec alternative supplier substrate with a miscut of 0.25 ° and b) a Kyocera substrate with a miscut of less than 0.1 °. The wire density in a) is much higher compared to that in b). On the Kyocera substrates, the wires are generally larger and less dense. It shows that this self-organised method is sensitive to the substrate features in particular to the miscut, which may change the formation of the thin SiN_x layer and may drive the seed nucleation. This interpretation is also reinforced by the fact that pyramidal shaped seeds are measured in-between the wires in b) as opposed to a).

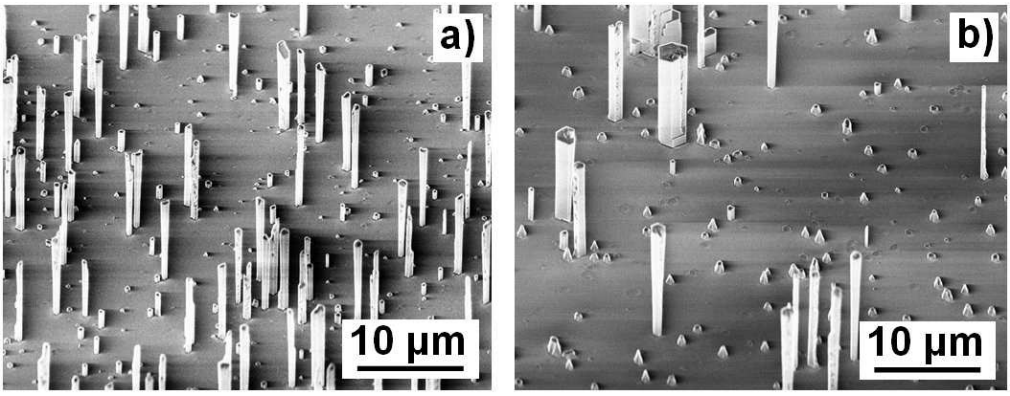

Figure 3.18 : Wire growth on a) Crystec – alternative supplier substrate (miscut 0,25°) and b) Kyocera substrate (miscut < 0,1°)

3.3. Structural characterisation of GaN wires

3.3.1. Epitaxial relationships

In order to determine the epitaxial relationship of the wires with respect to the substrate, the usual scan along the [0 0 L] direction of the sapphire in the standard θ–2θ geometry was first performed as a reference of a typical wire growth. Figure 3.19 shows that this scan can be indexed with the (0 0 6) and (0 0 12) α-Al_2O_3 Bragg reflections ($R\bar{3}c$, c = 1.299 nm) and the (0 0 2) and (0 0 4) wurtzite GaN Bragg reflections (P63mc, c = 0.5188 Å) indicating a growth along the c-axis.

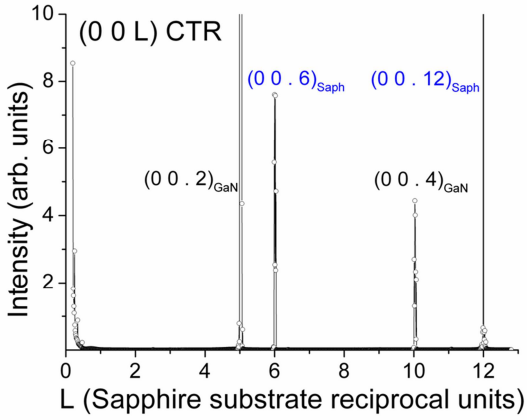

Figure 3.19 : Scan along the [0 0 L] direction of the sapphire substrate of a sample with GaN wires (standard Θ-2Θ geometry). Experiments were performed at ESRF with a wavelength of λ=0.06888 nm. GaN and sapphire indexations are in agreement with the usual bulk lattice parameters.

Grazing incidence (α_i) and emergence angles close to the critical angle of total reflection allow measurements of the diffraction of planes perpendicular to the surface for the sapphire substrate and the wires, as well as possible 2D or 3D substrate overgrowths. The beam footprint on the sample surface, which is about 10 x 0.5 mm^2, integrates the intensities of a very large number of wires. These wire growths exhibit quite narrow orientation distributions, which allow studying the wire's reciprocal space according to the substrate lattice [Eymery07]. Consider, as a reference, the conventional hexagonal c-plane sapphire surface unit cell (a = 0.4758 nm, c = 1.2991 nm), which is defined by (H K L) Miller indices. Radial scans along the (H 0 0) and (H H 0) sapphire in-plane Bragg reflections are shown in Figure 3.20 a) and b). For a small grazing incidence (α_i = 0.05°), only surface contributions are measured, whereas the substrate peaks can be recorded for α_i = 0.3°. The peak indexation shows that along the $(H\ H\ 0)_{Sap.}$ (resp. $(H\ 0\ 0)_{Sap.}$) scans, the $(H\ 0\ 0)_{GaN}$ (resp. $(H\ H\ 0)_{GaN}$) peaks can be measured, confirming the conventional 30° rotation around the c-axis between the two unit cells, *i.e.* $[1\bar{1}00]_{GaN}$ // $[1\bar{2}10]_{Al2O3}$ and $[0001]_{GaN}$ // $[0001]_{Al2O3}$. This measurement is also in agreement with Figure 3.11 in which the wire seeds were oriented in the same direction.

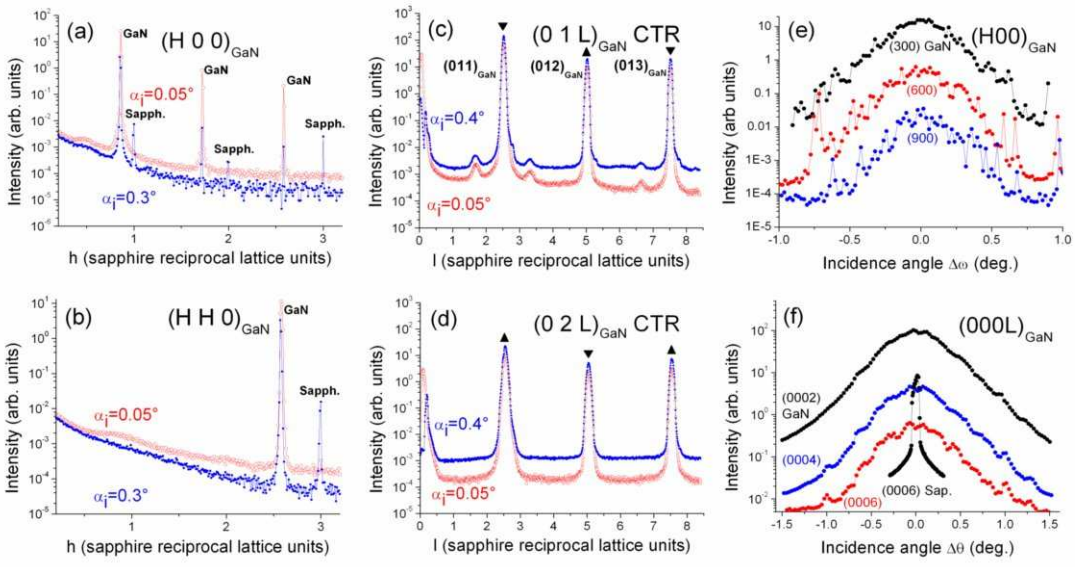

Figure 3.20 : X-ray diffraction measurements of GaN wires grown on c-sapphire. (a-b) In-plane grazing incidence X-ray diffraction measurements at two incidence angles (α_i=0.05, 0.3°) along the (a) [H 0 0] Sap. (resp. (b) [H H 0] Sap.) sapphire directions and corresponding to [H 0 0] GaN (resp. [H H 0] GaN) GaN lattice. (c-d) (0 1 L) and (0 2 L) crystal truncation rod.

The plane stacking along the wire c-axis can be analysed by means of the Crystal Truncation Rod (CTR) measurements [Feidenhans89]. The $(0\ 1\ L)_{GaN}$ CTR is measured for two grazing incidence angles (α_i= 0.05, 0.4°) in Figure 3.20 c). The three main peaks can be assigned to GaN (see the indexation given in the figure) and their positions are consistent with the bulk GaN parameters: for example, the third peak at L_3 = 7.528 in the sapphire reciprocal units corresponds to L = L_3 × 0.5188 / 1.2991 = 3.006 in the GaN reciprocal lattice units. It shows an almost complete relaxation emphasising the small influence of the sapphire/interfacial layer substrate strain as expected for wire geometry and the limited impact of Si incorporation on the lattice parameter. Moreover, these peaks reveal the wire characteristic features [Eymery07]: the intensity is not sensitive to α_i and a splitting of the peaks can be observed as a function of α_i for an improved instrumental resolution (not shown here). Due to symmetry considerations, hexagonal variants obtained by 60° in-plane rotations (see the ▼▲ notation shown in Figure 3.20 c) and d)) are present in equal proportions in the sample as confirmed by the measurements of the $(0\ 2\ L)_{GaN}$ CTR. Stacking defects along the c-plane direction give rise to a local cubic structure, which may be measured by means of CTRs. The (0 1 L) GaN CTRs show few stacking faults in the sample (see the small intensity peaks in Figure 3.20 c)), but they are not visible in the (0 2 L) CTR measured at another footprint position indicating a lateral heterogeneity. Moreover, these defect peaks can not be unambiguously attributed to the wires; they may also stem from the substrate overgrowth and further experiments are necessary to solve this point.

To further analywe the epitaxy, the twist and tilt of the wire assembly was measured. The twist is directly estimated from a rotation around the surface normal ($\Delta\omega$-scan) of in-plane reflections. Figure 3.20 e) shows the results for the (3 0 0), (6 0 0) and (9 0 0) peaks. Assuming a Gaussian peak shape, the FWHM corresponds to a 0.342 ± 0.015° twist angle. This result is significantly lower than the twist values obtained by MBE epitaxial growth of GaN wires on Si substrate [Songmuang07, Horak08] in spite of the growth through the thin silicon nitride layer openings.

The tilt is measured using typical rocking curves ($\Delta\theta$-scan) for (0 0 L) peaks using the Williamson–Hall plot [Cierchia03]. The GaN scans shown in Figure 3.20 f) for L = 2, 4, 6 gives a straight estimation of the wire tilt angle 0.61 ± 0.01° from the slope of the linear plot of the FWHM of the rocking curve as a function of the reflection order.

3.3.2. STEM studies on single wires

To gain a better understanding of the structural properties of the wires, scanning transmission electron microscopy (STEM) experiments were performed on single wires as shown in Figure 3.21. Convergent beam electron diffraction (CBED) measurements also revealed the existence of N-polar as well as Ga-polar side crystals on single wires. The N- and Ga-polar crystals are denoted by N and Ga respectively.

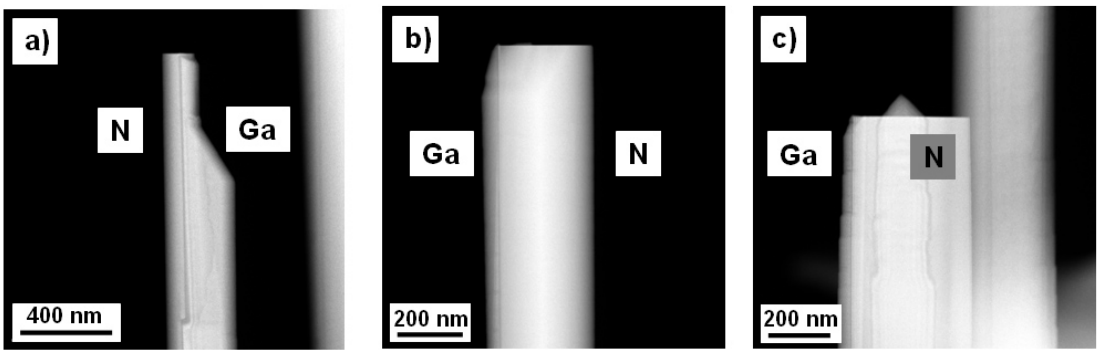

Figure 3.21: STEM images of single GaN wires. CBED measurements (not shown here) reveal N-polar as well as Ga-polar crystals.

From our MOVPE experiments, it seems that Ga-polar wire crystals are usually less stable than N-polar ones and show the tendency to develop non-c-plane facets at the top of the wires (visible in all three images, especially in Figure 3.21 a)). This observation may imply explanation for the change of facet orientation during the growth and thus the abrupt stop of wire growth. The origin of the formation of different polarities during wire growth is presently under study (PhD thesis of G. Perillat-Merceroz) and will be compared with polarity orientations in other systems, particularly in ZnO nanowires.

3.4. Seeds morphology and wire orientation

In section 3.2.3, the influence of the seed nucleation on the wire growth was discussed and it could be shown that the diameter and the structural quality were strongly related to this step. It also became evident that GaN nucleation on a non-annealed SiN_x mask gave rise to the growth of multipods. The multipod growth is a parasitic wire growth occurring in competition with the standard c-direction wire growth. Multipods may be prevented by an annealing under NH_3 directly after the SiN_x deposition. This type of growth has been mentioned for ZnO wires several times in the literature [Wang04b, Chen04, Xu05, Zheng08, Wang08, Feng09, Hongsith09] and occurs both, in the catalyst and catalyst-free approaches. For catalyst-driven growth of ZnO, the multipods exhibit complex configurations, in which the numbers of branches and the spatial orientations are not well defined. Hedgehog-like shapes can be observed. In contrast, the catalyst-free approach gives rise to tripods, tetrapods and hexapods with highly symmetrical configurations resulting from multi-facet nucleation centres.

For MOVPE GaN wires, the multipod wires are tilted with respect to the c-plane growth direction and have their origin in surface seeds. Even if this type of growth is not desirable, its study gives valuable information about the understanding of the nucleation seeds necessary for the wire growth. As demonstrated in Figure 3.6, the seed shape changes from a flat hexagonal shape to hexagonal shaped pyramids for SiN_x deposition times of 200 s or longer. In a deeper analysis of Figure 3.9 a) and Figure 3.23, a six-fold symmetry is visible in the multipod growth indicating an epitaxial relationship with the substrate. The origin of this six-fold symmetry can be found in the hexagonal shaped pyramids shown in Figure 3.6 c) and d), which will be studied in the following.

3.4.1. Experimental conditions for multipod growth

To test the assumption that hexagonal shaped pyramids give rise to the multipods, a growth on non-annealed SiN_x was interrupted at a very early stage, *i.e.* after 400 seconds in order to still be able to identify the seeds, and then observed by SEM. In Figure 3.22, four early stage multipods are imaged: a) shows the very beginning of a single tilted wire (monopod), b) the rise of a tripod and c) and d) the beginning of a bipod growth. It is clearly visible that the multipods grow from the pyramidal-shaped seed facets, similar to the catalyst free approach of ZnO growth. At their early growth stage, the wires are still

attached to the substrate with at least one of their facets. The emerging wire seems to nucleate on both the seed side facet and the substrate surface. During the growth, the wire will then rise from the substrate surface. The nature of the interface between the wire and the sample surface remain hitherto unknown and the continuity of the SiN_x layer could not be verified at this position. This point is probably a cause of the wires tilt angles varying from wire to wire.

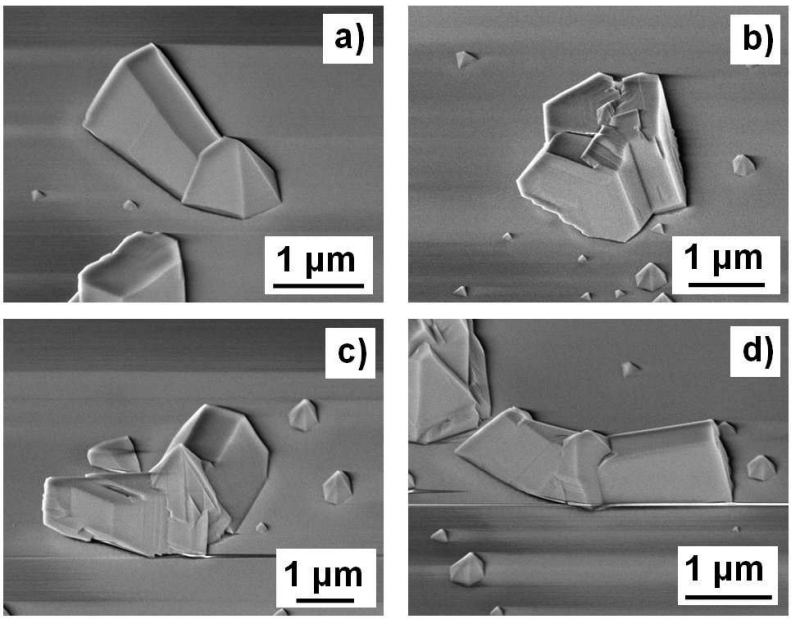

Figure 3.22 : Early stage of multipod growth from hexagonal shaped pyramids: a) monopod, b) tripod, c) and d) bipod.

As already seen in Figure 3.22, the multipods can be sorted in different subtypes. Figure 3.23 b) gives a plane view on a tripod assembly in which only five different types of multipods can be identified:1) tripod, 2) bipod, 3) monopod, 4) bipod with a c-plane wire on top and 5) monopod with a c-plane wire on top. A detailed description of the multipods' configurations is given in Table 3.1 below. The multipods have the same hexagonal shape and the same growth rate as the vertical wires grown along the c-direction. We can therefore assume that they exhibit the same crystalline orientation[25].

[25] Micro-Laue diffraction patterns have recently been obtained on the tripod branches at ESRF. The comparison of the Bragg peak positions with respect to those of the sapphire reference will allow the determination of the complete orientation matrix of the different crystals.

Figure 3.24 provides a detailed SEM view of the seeds growing in-between the tripod assembly. Three different types of seeds pointed at by arrows can be identified: a) a hexagonal shaped pyramid, b) a hexagonal shaped pyramid with c-plane on top and c) a triangular shaped pyramid. The identical orientation of the hexagonal seed is clearly visible indicating an epitaxial relationship with the underlying substrate. It explains the high symmetry of the in-plane orientation of the multipods.

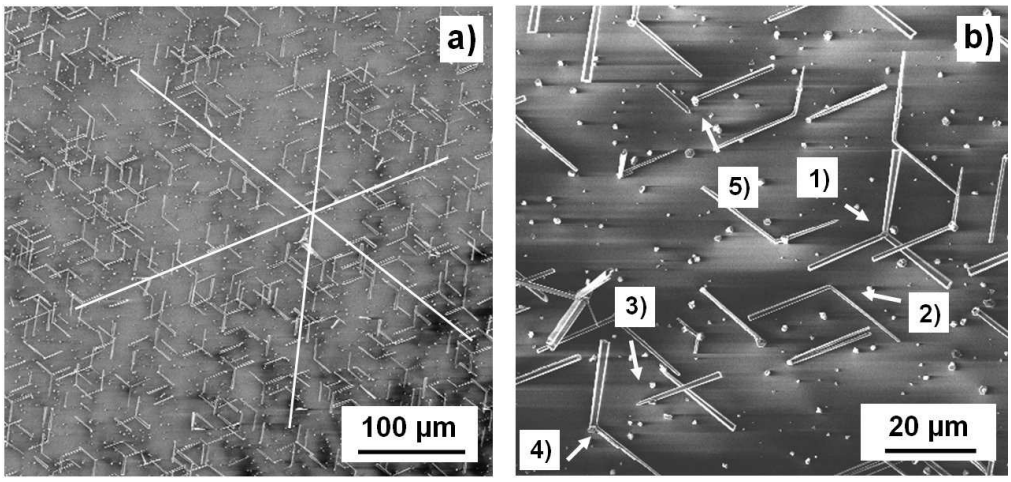

Figure 3.23 : Plane view of a tripod growth: a) general overview of the assembly. The three white lines indicate the six tripod-growth directions (from the top view), b) magnification of the assembly. Numbers denote the different types of tripod growth. 1) tripod, 2) bipod, 3) monopod, 4) bipod with c-plane wire on top and 5) monopod with c-plane wire on top. C-grown wires appear as white dots in this top-view picture.

Type	Notation	Appearance
1)	Tripod	Three tilted wires emerge from a nucleation centre.
2)	Bipod	Growth similar to tripod, one wire is missing.
3)	Monopod	Growth similar to tripod, two wires are missing.
4)	Bipod + c-wire	Bipod with additional wire along the c-plane direction.
5)	Monopod + c-wire	Monopod with additional wire along c-plane direction.

Table 3.1 : Type, notation and appearance of the multipod growth shown in Figure 3.23 b)

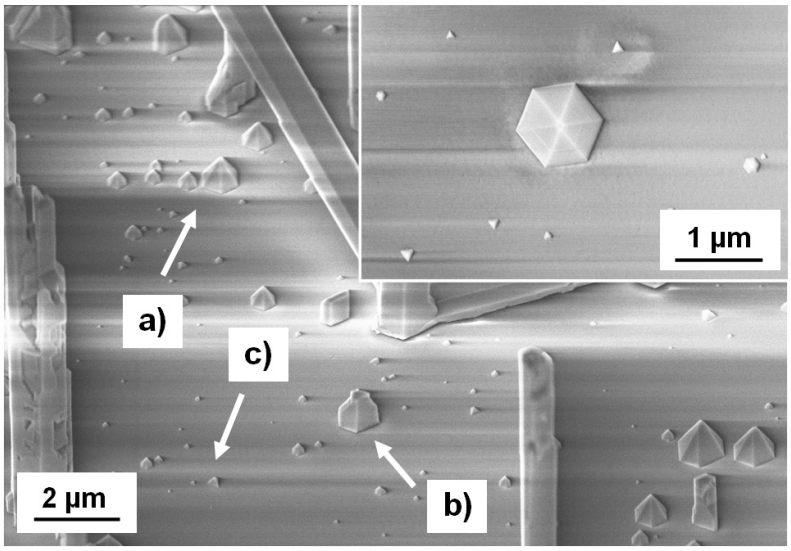

Figure 3.24 : Orientation of the seeds. White arrows point at different types of seeds growing in-between the wires: a) hexagonal shaped pyramid, b) hexagonal shaped pyramid with c-plane on top and c) triangular shaped pyramid. All seeds show the same in-plane orientation, the first hint of an epitaxial relationship with the surface.

Two hexagonal shaped pyramids are visible in the inset of Figure 3.24, a big on in the middle and a smaller one on the right side of the picture. Both are grown with the same in-plane orientation. They are surrounded by smaller triangular pyramids. The hexagonal shaped pyramids exhibit a six-fold symmetry. The triangular shaped pyramids only have a three-fold in plane symmetry and are two-fold degenerated (two sets of in-plane orientations). These three types of pyramid shaped seeds (see a schematic view in Figure 3.25) explain the origin of all the types of multipods in Figure 3.23. In principle, a tilted wire could emerge from any arbitrary facet meaning that we should be able to observe additional configurations like multipods with four, five or even six emerging wires. This is probably not possible due to steric constraints: when a facet grows, the neighbourhood facet can not grow anymore. For example, half of the facets will be blocked for tripod growth. The formation of bipods and monopods can be explained by some growth defects blocking the facets (see examples in Figure 3.22 c) and d) in which a bipod is growing instead of a tripod).

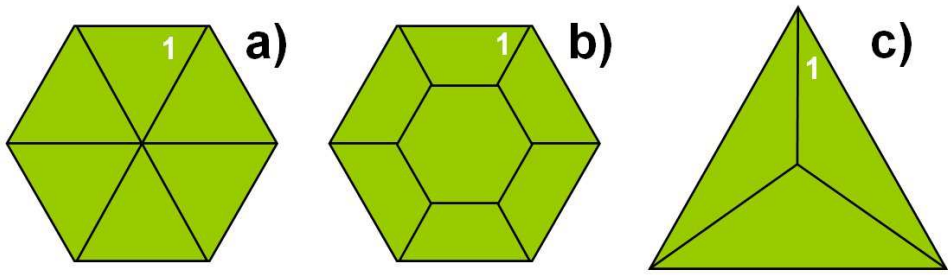

Figure 3.25 : The three different kinds of seeds responsible of the tripod growth: a) hexagonal pyramid, b) hexagonal truncated pyramid and c) triangular pyramid

3.5. Conclusions

In this chapter, a new approach for the growth of GaN wires by MOVPE has been presented. Compared to other techniques reported in the literature using metal catalysts or *ex situ* substrate pre-patterning, this method only uses *in situ* surface preparation (in the reactor) saving time and making this approach very efficient and fast. It was especially suitable for the study of the growth mechanisms, for which a huge number of runs were necessary in order to optimise the wire-growth quality. The wire-growth mechanisms were performed on c-plane sapphire substrates, commonly used in industry for 2D GaN film deposition. The deposition of an *in situ* SiN_x "mask" allows the GaN deposition at a high temperature and therefore the deposition of good quality materials.

Some important points published in [Koester10] were addressed:

- The initial surface preparation before the wire growth must be controlled in detail by specific annealing and silane treatments. The formation of a thin AlN layer on sapphire followed by a SiN_x "mask layer" has been studied by several techniques to gain a consistent insight into the mechanisms. A SiN_x deposition time of 100 s and an annealing under NH_3 for 500 s were found to be the optimal conditions for the formation of flat hexagonal shaped seeds during a GaN nucleation step, which has been demonstrated to be crucial to obtain high-quality wires. In the case of a longer SiN_x deposition time or by leaving out the annealing under NH_3, the seed shape can change to a pyramidal shape leading to parasitic multipod growth and highly defective wires.

- The deposition time during the nucleation step controls the seed size. SEM and AFM studies revealed the formation of defects by coalescence of seeds and the lateral growth pinning on surface inhomogeneities leading to defects in the later wire growth. For the process developed in this study, an optimal nucleation time has been found to be close to 10 s; in that case, the seeds are small enough to prevent coalescence.

- A low V/III ratio is essential for the wire growth. For these experiments a V/III ratio of 16 was applied leading to optimal growth. Experiments with V/III ratios of several hundreds gave rise to a strong lateral growth, whatever its application from the very beginning of the growth or at a later stage. For the later device fabrication, this behaviour could be used to coalesce the upper part of the wires assembly.

- The wire growth itself can be carried out under the same conditions as the seed nucleation, but with an additional injection of silane during the process. Silane is crucial for the wire growth since it favours a longitudinal growth along the c-direction. The optimal flow is several hundred nmol/min. The range of silane flows (from no silane to a very large amount of silane) has been studied.

- The nucleation step and the wire growth are both carried out at 1000 °C. Decreasing the temperature leads to a higher density of the assembly but in parallel to a decrease in structural quality. A higher growth and nucleation temperature leads to a strong evaporation rate of GaN making the material deposition difficult. Within these conditions, it has been shown that the growth rate of the wires was linear but directly influenced by the carrier gas flow rate.

The wires grown under these conditions have been studied by grazing incidence X-ray diffraction. The experiments evidenced a growth along the c-axis and revealed the epitaxial relationship of the wires with the surface and the typical 30 ° rotation of the GaN lattice with respect to the sapphire with low distributions of tilt (0.61 °) and twist (0.34 °) disorientations. STEM and CBED measurements revealed the coexistence of N- and Ga-polar crystals inside single wires. The observed instabilities of facets for Ga-polar crystals probably explain the top facet shape evolution of some wires and their tendency to stop growing.

SEM observations of the early stage of wire growth on non-annealed SiN_x revealed the origin of multipod formation and gave a deeper understanding of the importance of the seed nucleation on the wire growth. The 60 ° symmetry in the multipod orientation was the first evidence of the epitaxial relationship between the GaN growth and the sapphire substrate finally evidenced by x-ray diffraction.

Chapter 4

Optical properties of GaN wires and heterostructures grown by MOVPE

4.1. Introduction

The use of GaN wires - and heterostructures - in optoelectronic devices like LEDs, lasers and detectors (see chapter 1), it needs control of the optical properties of doped materials. This chapter will be dedicated to this field which constitutes a major concern for the use of MOCVD wires in applications.

The optical properties of "homogeneous" Si-doped wires (n-type), Si-doped/unintentionally-doped, Si-doped/Mg-doped (p-type) and InGaN/GaN multiple quantum well (MQW) heterostructures will be studied to demonstrate the potential use of MOCVD wires. Single wire measurements have been chosen to analyse their intrinsic properties. The main advantages of this approach are the removal of the parasitic signal which may stem from the overgrowth between the wires[26] and the gaining of information concerning the location of the optical emission at different wavelengths particularly important for heterostructures and the study of defects.

4.2. Si-doped/un-intentionally doped heterostructure growth

As already mentioned in chapter 3, the silane injection is a mandatory ingredient to fulfil the vertical growth [Haffouz98, Frayssinet02, Koester10]. This addition leads to a strong n-doping of the wires[27]. Nevertheless, it is possible to stop silane injection after the wire has reached a certain length.

---

[26] Due to the small density of the wires grown by the method described in chapter 3, macro-photoluminescence and cathodoluminescence measurements integrate both wire and overgrowth optical signals.

[27] The n-doped feature of strongly Si-incorporated wires has been estimated by four-probe electrical measurements [Zanin09]. The very small resistivity $\rho=10^{-3}$ $\Omega.cm^{-1}$ combined with the measured n-doped

Figure 4.1 shows a SEM image of such a wire growth. The initial n-doped part is grown at 1000 °C during 1000 s with a silane molar flow corresponding to the standard wire growth (200 nmol/min). The silane source is then switched off and the growth is continued for 500 s by keeping the other growth parameters unchanged. A small kink is visible in the upper part of the wire indicating the change of the growth conditions. The wire itself keeps on growing vertically without any significant change of shape: No strong lateral growth was observed equal to the conditions of no silane injection directly at the beginning of the growth.

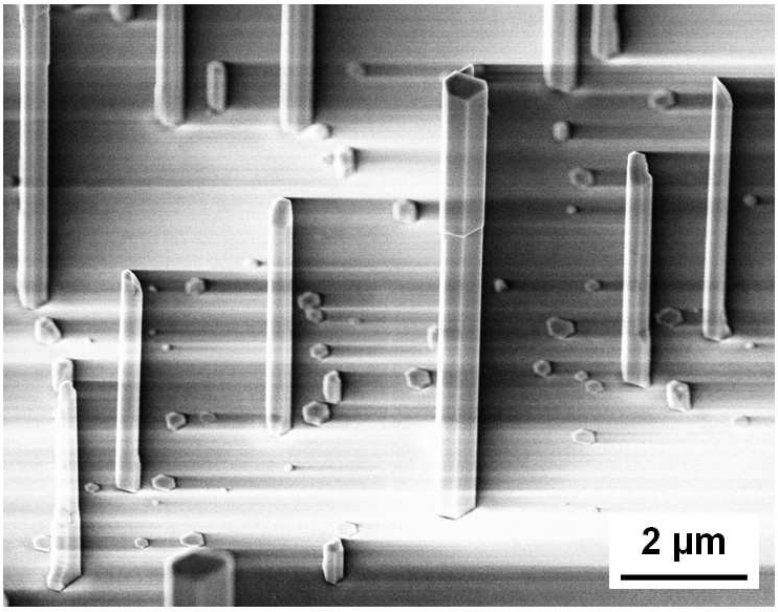

Figure 4.1 : Tilted (45°) SEM view of n/un-intentionally doped structures grown by stopping the silane flow after 1000 s of growth and continuing the growth for 500 s. The n-part uses the standard growth conditions given in chapter 3.

The wires were detached from the sapphire substrate by sonification in isopropanol and then dispersed on a conducting silicon substrate. The optical properties were studied by cathodo-luminescence (CL) measurements at Néel Institute, CNRS Grenoble[28]. Single wires are excited by an electron beam with a voltage of 20 kV and a current of less then 1 nA. Figure 4.2 shows the CL spectra integrated over four zones of a 9 µm long wire with equal areas (PO 1 to PO 4) regularly distributed along the growth axis (see inset in Figure 4.2). The PO 2 to PO 4 zones correspond to the n-doped part of the wire grown under

value of 2D layers (2-3 10^{19}cm-3) gives a mobility value of 200 $cm^2\ s^{-1}\ V^{-1}$ which is similar to bi-dimensional GaN (chapter 2) .

[28] In collaboration with F. Donatini, J S. Hwang and D. Le Si Dang, CNRS Institut Néel Grenoble.

silane injection (about 6 μm long). The PO 1 zone corresponds to the top part of the wire grown during 500 s (about 3 μm) without silane injection. A dominant band edge emission (around 350 nm (3.547 eV)) can be observed all along the wire with a negligible yellow band (YB) emission centred at 560 nm (2.217 eV). For 2D growths, the latter is commonly assigned to gallium and oxygen complexes [Polenta07], but for the MOVPE wire growths, a strong correlation between the observations of the band-defect emission with the occurrence of a large amount of structural defects was generally observed. The silicon doping coming from the silane injection produces an asymmetric band roughly centred at 350 nm (3.55 eV) nm with a broad low energy tail above the 350 nm (3.55 eV) band gap. This effect has been demonstrated to be due to the conduction band filling effect resulting from the heavy dopant concentration [Beaumont83, Leroux97]. Based on the optical study of silicon doped GaN thin films [Leroux97], the FWHM of 26 nm (120 meV) of the PO2 to PO4 curves suggests a carrier concentration of above $10^{20}/cm^3$ in this wire. The part of the wire grown without silicon injection (PO 1) has an emission peak at 355 nm (3.496 eV) and a FWHM of 14 nm (70 meV) corresponding to a carrier concentration in the $10^{19}/cm^3$ range much larger than the 2D residual doping given in chapter 2 (in the $10^{16}/cm^3$ range). Therefore, it seems that silicon continues to be incorporated even after stopping the silane flow. A possible source of this un-intentional doping may be the Si evaporation coming from substrate overgrowth (i.e. not incorporated in silicon nitride) which can be reincorporated mainly at the top of the wire or by Si diffusion on the wire edges or by solid silicon diffusion.

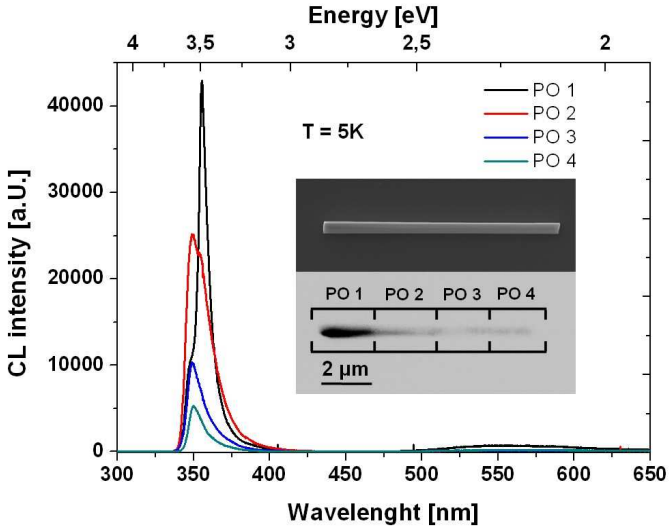

Figure 4.2 : CL emission spectra of a single wire with n-doped and un-intentionally doped segments. The integration areas are denoted PO 1 to PO 4. The insets show a SEM viewgraph and a CL mapping measured 355 nm (3.496 eV), respectively.

4.3. Si/Mg-doped heterostructure growth

After the demonstration of wire growth with Si-doping variation, the Mg-doping case will be discussed, now. Two types of growths will be discussed to study the influence of temperature on the surface morphology and on the optical signature of the wires. Firstly, Cp_2Mg injection will be started immediately after silane injection, keeping the standard growth temperature (1000°C). Second, the temperature will be decreased to 850 °C before the injection of Cp_2Mg.

Figure 4.3 shows tilted (45 °) SEM images of the grown structures. For the first growth, the longitudinal wire structure was grown at 1000 °C with silane injection for the first 1000 s, then the doping source was switched to Cp_2Mg with an additional wire growth of 500 s keeping the same temperature. The growth morphology is very similar to what has been observed for a Si-dopant variation along the wire. For the second growth, the bottom part of the structure was grown under silane injection at 1000 °C for 500 s. The temperature is then decreased to 850°C with a ramp of 60 s before opening the Cp_2Mg source for 300 s. In this case, a lollypop-like morphology is observed.

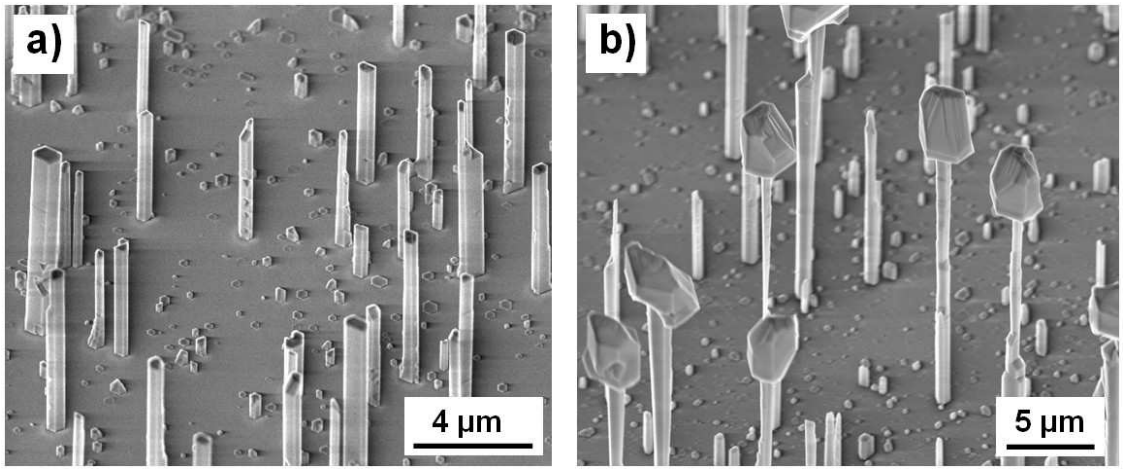

Figure 4.3 : Influence of temperature on Cp_2Mg–doped wire morphology. The base of the wire is grown during 1000 s (a) and 500 s (b) at 1000 °C. Then in a) Cp_2Mg is injected during 500 s at the same temperature and in b) Cp_2Mg is injected during 300 s after a decrease of temperature to 850 °C (a 60 s ramp is performed before opening the flow).

In order to study the optical properties of these two growths by CL, the wires were detached from the sapphire substrate by sonification in an isopropanol bath and dispersed on a conducting silicon substrate.

Figure 4.4 shows the CL spectra of a longitudinal wire taken from the first sample shown in Figure 4.3 a). The measurements have been performed on four positions along the wire, where PO 1 denotes the top and PO 4 the bottom region of the wire (see inset). PO 2 to PO 4 show the characteristic n-GaN emission with a near band edge emission centred at 350 nm (3.546 eV) and with a barley visible yellow band centred at 560 nm (2.217 eV). The overall CL emission is strongly reduced at PO 1 and a small additional peak can be seen centred at 375 nm (3.31 eV) next to the near band edge indicated with a black arrow in Figure 4.4. This peak can be attributed to the donor acceptor pair (DAP) recombination observed in p-doped GaN [Viswanath98, Reshchikov99]. The near-band edge itself is shifted to 355 nm (3.496 eV) due to the absence of silicon doping. The inset in Figure 4.4 shows a SEM image and its corresponding CL emission at 350 nm (3.55 eV). The wire exhibits an overall length of 8 µm whereas the top part grown under the Cp_2Mg injection is about 2 µm long.

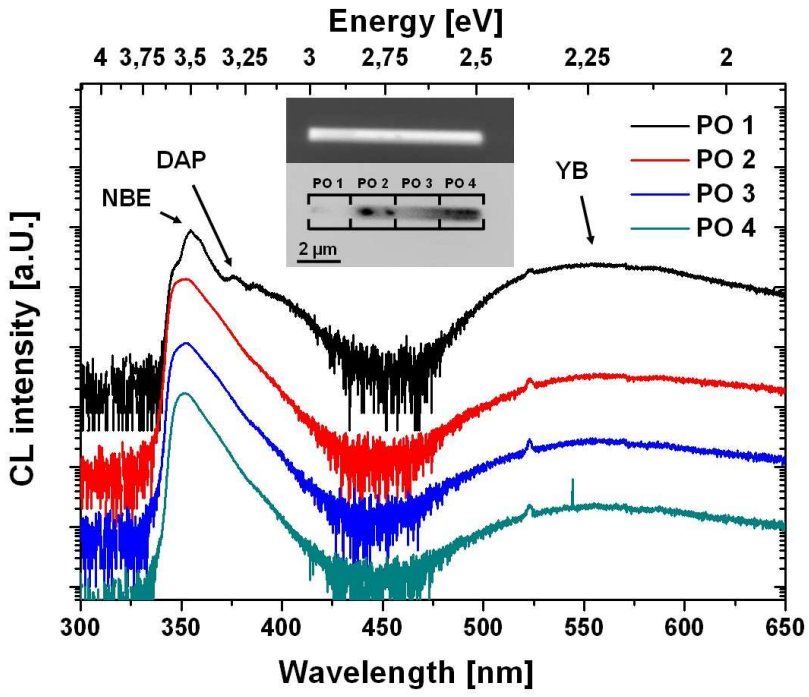

Figure 4.4 : CL (5 K) spectra of a longitudinal wire structure for the positions PO 1 to PO 4 indicated in the CL image (inset) measured for 350 nm emission. For comparison, the SEM image of the wire is given at the top of the inset.

Figure 4.5 shows the CL spectra corresponding to the second sample (see Figure 4.3 b). The part of the wire grown under injection of silane exhibits a strong near band edge emission (see Figure 4.5 a)) centred at 350 nm (3.546 eV) and a FWHM of 14 nm (70 meV), characteristic for heavily n-doped GaN. The yellow band is very small showing the good optical (and structural) quality of the wire. The CL image shows that the 350 nm emission is homogeneous over the whole wire length except at the very top region where Cp_2Mg injection occurred. Figure 4.5 b) details the emission of the top of the wire: the near band edge emission is strongly reduced and is accompanied by an additional emission centred at 370 nm (3.355 eV), which is about three times more intense. This region also exhibits a very strong YB emission centred at 560 nm probably related to the low growth temperature of 850 °C, which decreases the structural (and optical) quality of the wires. The CL image under the spectra shows the wire emission recorded at 370 nm showing the widened shape of the upper part of the wire. The shape of the n-doped part is also measured due to the tail of the near band edge emission, which reaches up to 400 nm as shown in the spectrum of Figure 4.5 a).

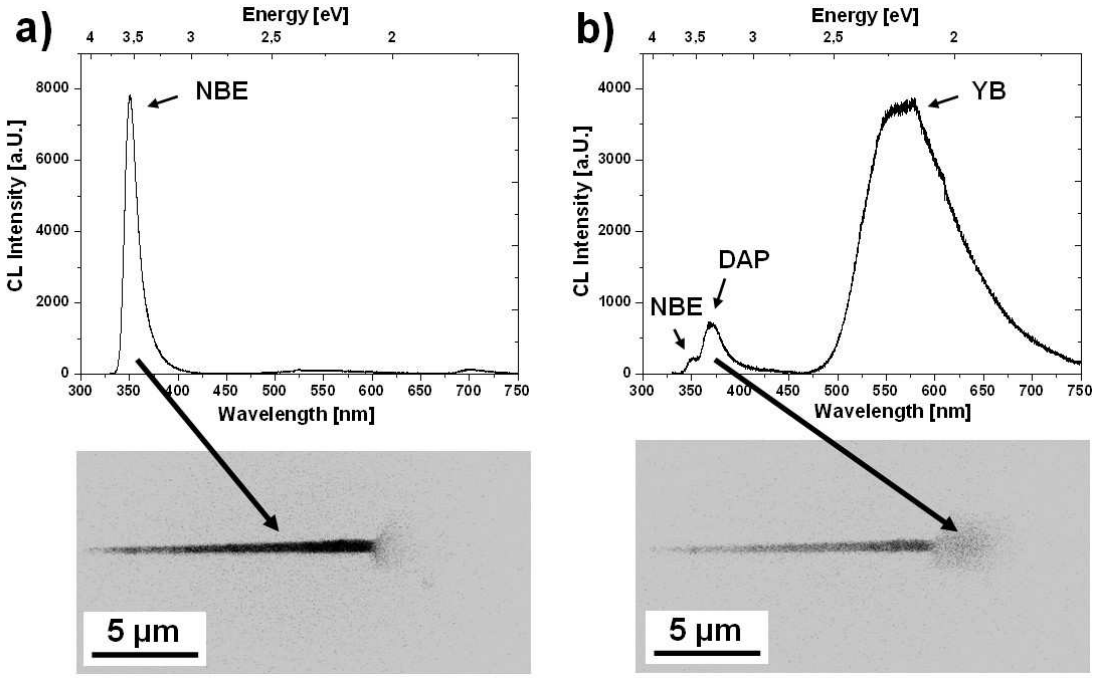

Figure 4.5 : a) CL (5 K) spectra of the n-doped GaN wire with a strong near band edge emission. The CL image shows the emission at 350 nm. b) CL spectra of the top of the wire grown under Cp_2Mg injection at 850 °C. The spectra show an emission peak at 370 nm three times stronger than the near band edge emission and a strong yellow band centred at 560 nm. The CL image shows the emission at 370 nm.

The strong peak centred at 370 nm can be attributed to the DAP recombination. The strong increase of the signal compared to the sample displayed in Figure 4.3 a) is probably related to the higher Mg incorporation due to the lower growth temperature. LO-phonon replicas as reported in the literature [Viswanath98, Reshchikov99] were not observed. These results are a first hint at successful p-doping, nevertheless further experiments (*i. e.* electrical measurements and secondary ion mass spectroscopy (SIMS) on single wires) are necessary to prove this assumption and to estimate the p-doping level. These results also evidence the difficulty to achieve a good structural and optical quality of the Mg-doped part. Like in 2D materials, the p-doped crystal should probably be limited to its minimal volume in order to establish good contacts in the devices.

4.4. InGaN/GaN multi quantum wells

InGaN/GaN MQW heterostructures constitute one of the most important building blocks for blue and white LEDs. In this section, the growth of such InGaN/GaN heterostructures on wire templates will be discussed in terms of morphological and optical properties. The influence of In-concentration and quantum well thickness on the optical properties will be studied by varying the InGaN growth temperature and time respectively.

4.4.1. InGaN/GaN MQW growth on GaN wires

The GaN wires, the growth of which was discussed in chapter 3, can be used as templates for InGaN/GaN MQW heterostructures. The bottom of the wires is n-doped and the structure is ended with an un-intentionally doped top part (see section 4.3). The standard growth process for 2D InGaN/GaN MQW growth described in chapter 2 was chosen as a first attempt to grow MQWs on the wire templates. The resulting In-incorporation, thickness and growth morphology (radial or longitudinal heterostructures) were open questions in this new MOVPE process.

The important features of the growth conditions can be summarised as follows: the InGaN growth temperature is set to about 750 °C (leading to a indium incorporation of about 18 % in 2D growth), TEG is used as a Ga precursor instead of TMG. In order to effectuate a higher decomposition rate at a lower temperature, the reactor pressure is set to 400 mbar under N_2 atmosphere instead of H_2 to prevent indium etching during the growth. For a first demonstration, the QW and QB growth times were set to 2D nominal values corresponding to 5 nm (QW) and 10 nm (QB) thicknesses respectively.

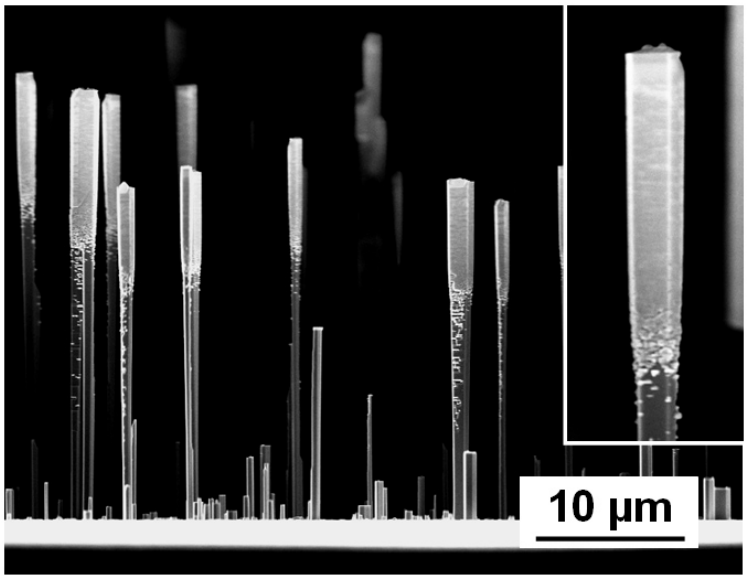

Figure 4.6 : SEM image corresponding to InGaN/GaN MQW (5x) grown on GaN wires. The MQW is located in the upper part of the wires (see the diameter enhancement and the contrast difference). The inset shows a detailed view of a MQW structure.

MQW morphology

The growth of five InGaN/GaN MQWs reveals a matchstick-like structure located at the upper part of the wires (see the SEM image of Figure 4.6). Single QW structures (not shown here) exhibit the same morphology. This radial overgrowth is smooth and continuous at the top, but becomes more and more irregular at the bottom part of the structure. A grain-like structure and surface defects can be seen in Figure 4.6 as well as a diameter increase at the top of the structure (see Figure 4.7).

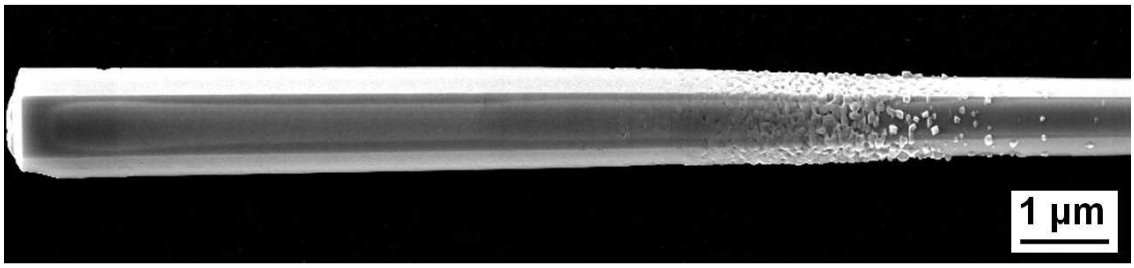

Figure 4.7 : SEM image of the MQW region located at the upper part of a GaN wire template.

Scanning transmission electron microscopy (STEM) measurements performed in the SEM setup revealed the existence of the initial GaN wire surrounded by the InGaN/GaN superlattice. A single wire was thinned by Focused Ion Beam (FIB) and transferred into the SEM equipment. This surface preparation allows measurements of the wire edges but unfortunately not the top of the wire which has been removed. Figure 4.8 shows the GaN core of the wire and the alternating layers of InGaN and GaN on the edges. From this STEM image, the InGaN QW (resp. GaN QB) thickness can be estimated to be about 6 nm (resp. 18 nm) showing that the lateral growth rate is not too far from the nominal 2D values.

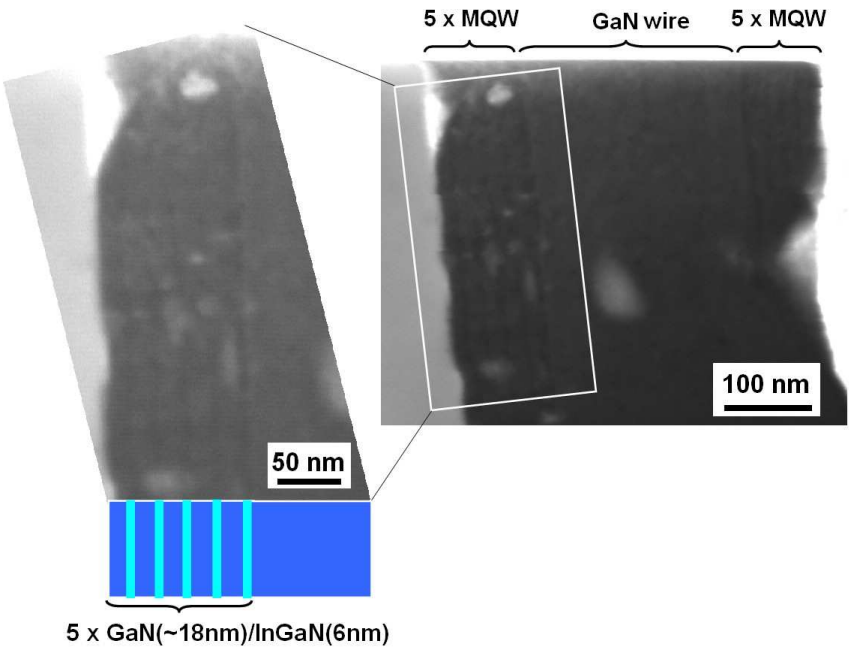

Figure 4.8 : STEM image of InGaN/GaN MQW grown around a GaN wire template. The enlarged picture (on the left) shows the InGaN/GaN superlattice stacking.

Figure 4.9 shows the room temperature μ-PL measurement on InGaN/GaN MQW grown on a GaN wire (T_g = 759 °C). A strong emission peak is centred at 415 nm (2.99 eV) with a FWHM of 26 nm (190 meV). A small emission tail reaching up to a wavelength of 500 nm does not have a clear origin but may be attributed to the nitrogen vacancies during the growth [Nakamura92c]. The near band edge emission located at 355 nm (3.497 eV) stems from the un-doped GaN core. No YB emission was observed in these samples.

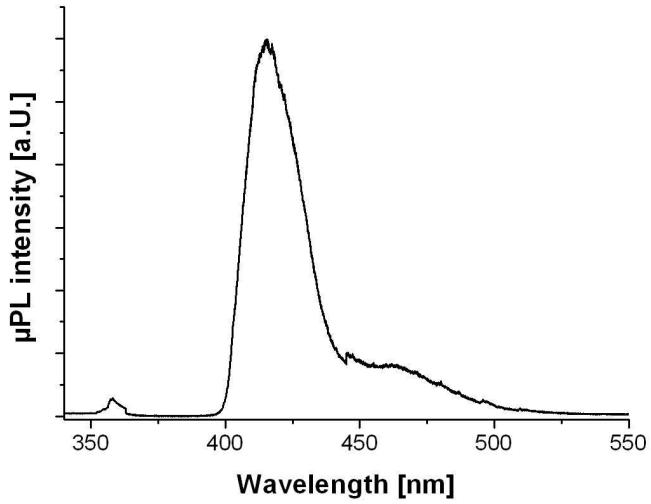

Figure 4.9 : Room temperature µ-PL spectra of a 5 x InGaN/GaN MQW grown on a GaN wire template.

CL measurements were used to study the spatial distribution of the MQW emission. Figure 4.10 shows the CL images and spectra for heterostructures having gone through two times spans of InGaN-QW growth 20 s and 120 s respectively with a fixed nominal QB thickness of 10 nm (value of 2D MQW growth). As will be discussed below, it is assumed that this change of duration will be proportional to the change of thickness. The top of the figure shows standard SEM images taken in the CL setup illustrating the overall shape and size of the wire. The CL graphs at the bottom of the figure show the CL spectra for seven different positions along the MQW heterostructure. The sample holder was maintained at a fixed position allowing a comparison of the spatial distribution at the different wavelengths. Positions PO 1 and PO 7 are indicated by arrows in the SEM viewgraphs. The positions PO 2 to PO 6 lie in-between these two positions.

Four main emission features can be directly identified in the CL spectra:

- 348-350 nm emission corresponding to the n-GaN NBE (a,b))
- 356-358 nm emission corresponding to the u-GaN NBE (c,d)
- a broad and intense peak around 400 nm related to the InGaN QW emission (e,f)
- a yellow band centred at 560 nm commonly attributed to defects (and generally to the deep-level acceptors) (g,h).

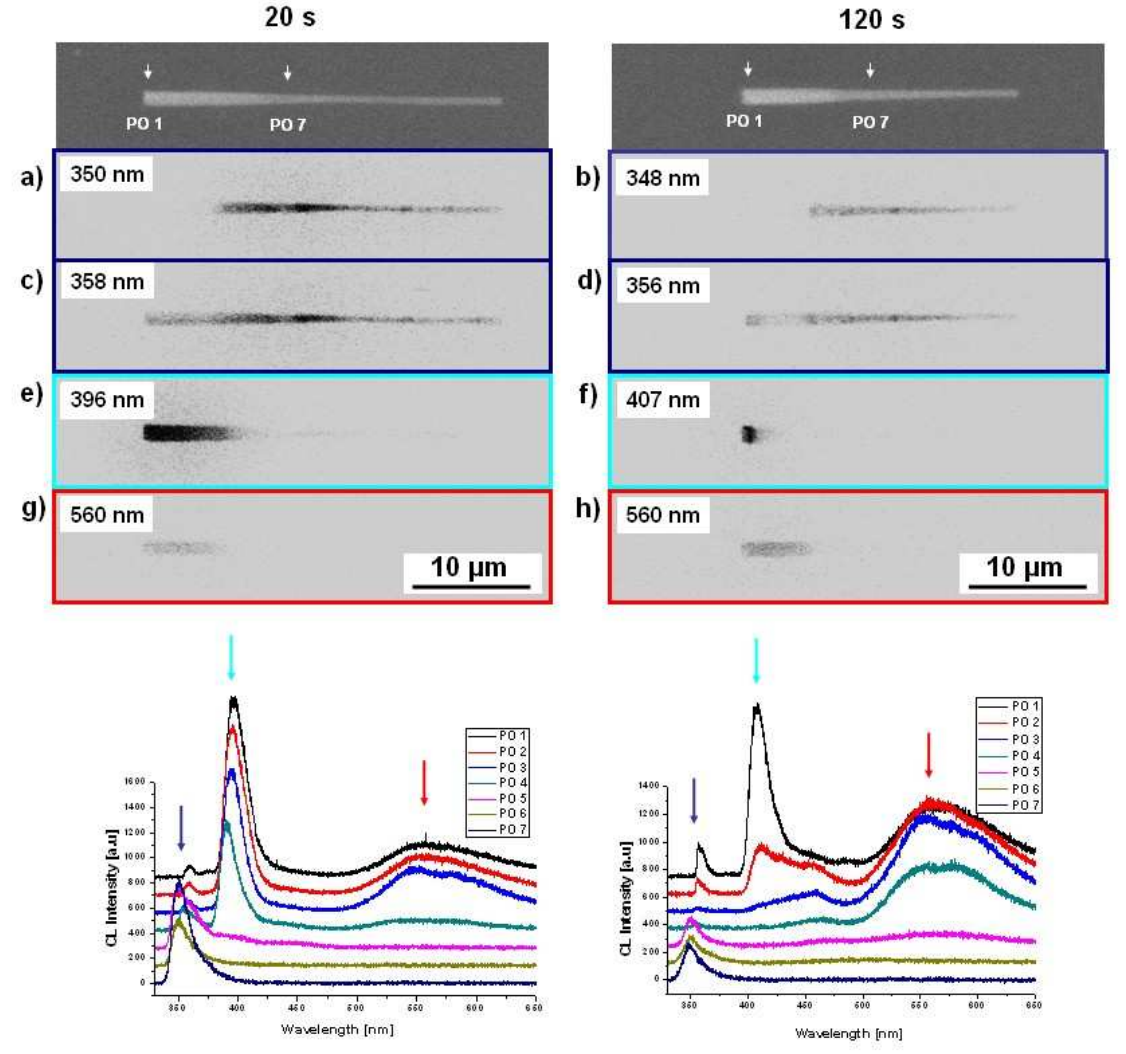

Figure 4.10 : Spatial distribution of the MQW emission measured by CL (5 K) on single wires for 20 s and 120 s QW-growth time.

The CL mapping analysis for the 20 s and 120 s samples allows the following remarks:

- The 350 nm (3.55 eV) emission mapping (see a) and b)), which is attributed to the n-GaN emission, shows that the top of the wires does not emit light at this wavelength. It confirms the change of growth conditions at the top of the wire during u-GaN growth.
- The whole wires show light emission in the 358 - 356 nm (3.487 – 3.468 eV) range and not only in the top part because of the tail of the NBE peak at 350 nm (3.55 eV) originating from the n-doped part. It is therefore difficult to see the direct signature of the non-intentionally doped part at the top of the GaN template.

- The YB centred at 560 nm (2.217 eV) mainly originates from the u-GaN part located on the top of the wires.

- The 396-407 nm (3.135 – 3.05 eV) emission corresponding to the emission of InGaN/GaN MQWs changes as a function of the QW-growth duration. It is localised more or less at the top of the wire: for the 20 s QW growth, the emission covers one third of the wires length. For the 120 s QW growth, on the contrary, the emission is only located at the extreme top of the wire, although the MQW growth extends over the top third of the wire length.

As already shown in Figure 4.7, an increasing gradient of defect density is observed in the direction of the bottom of the wire. The bottom part of the defective region is certainly non-radiative and may explain the gradient of the MQW-emission intensity along the structure. The main difference between the 20 s and the 120 s samples comes from the time spent at low temperature. For the 120 s QW growth time, the non-radiative region will be larger due to the increased low temperature defect formation. Note that the longitudinal extension of the 120 s MQW structure is slightly smaller than for the 20 s sample. This probably indicates that the surface diffusion does not change significantly in-between these two InGaN/GaN samples. The quantitative interpretation of these effects will require further studies in the future.

The standing wires were measured by cathodo luminescence in order to carry out complementary measurements. In this case, the electron beam is oriented perpendicularly to the top-facet plane.

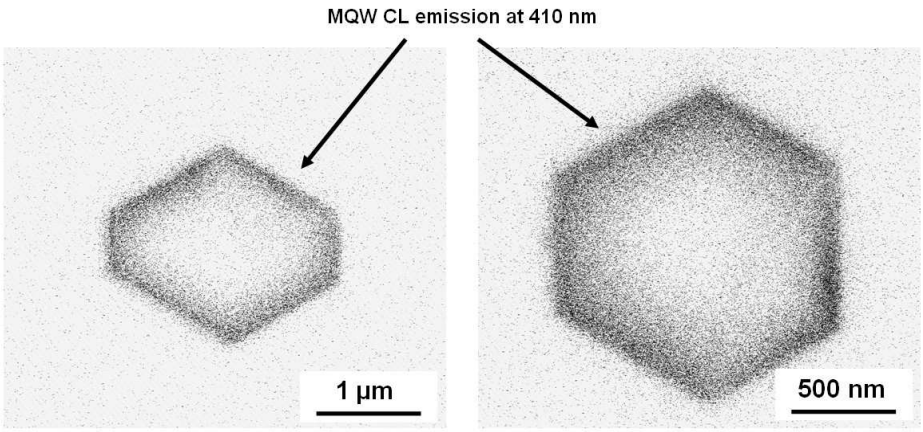

Figure 4.11 : CL measurements performed on the top of standing wires in epitaxy on sapphire substrates. The characteristic multiple quantum well emission at 410 nm is located at the side facets.

Figure 4.11 shows two CL images taken at a wavelength of 410 nm corresponding to the MQW emission of this sample. The hexagonal shape of the wires is clearly visible and the side facets exhibit a strong emission. The top c-facet exhibits no MQW emission at this wavelength, indicating the absence of active material on the top.

Combining this information with the CL emission mappings measured on the dispersed wires and by SEM and STEM observations, core-shell geometry of the MQW growth around the top part of the wire template can be concluded. A schematic of the structure is given in Figure 4.12. The MQW superlattice is grown around the wire and an about the superlattice thickness gradient between the top and the bottom of the active MQW remains hitherto impossible. But it seems that the non-radiative part has a bad structural quality, which is deteriorated into a grain-like structure at the bottom of the MQW.

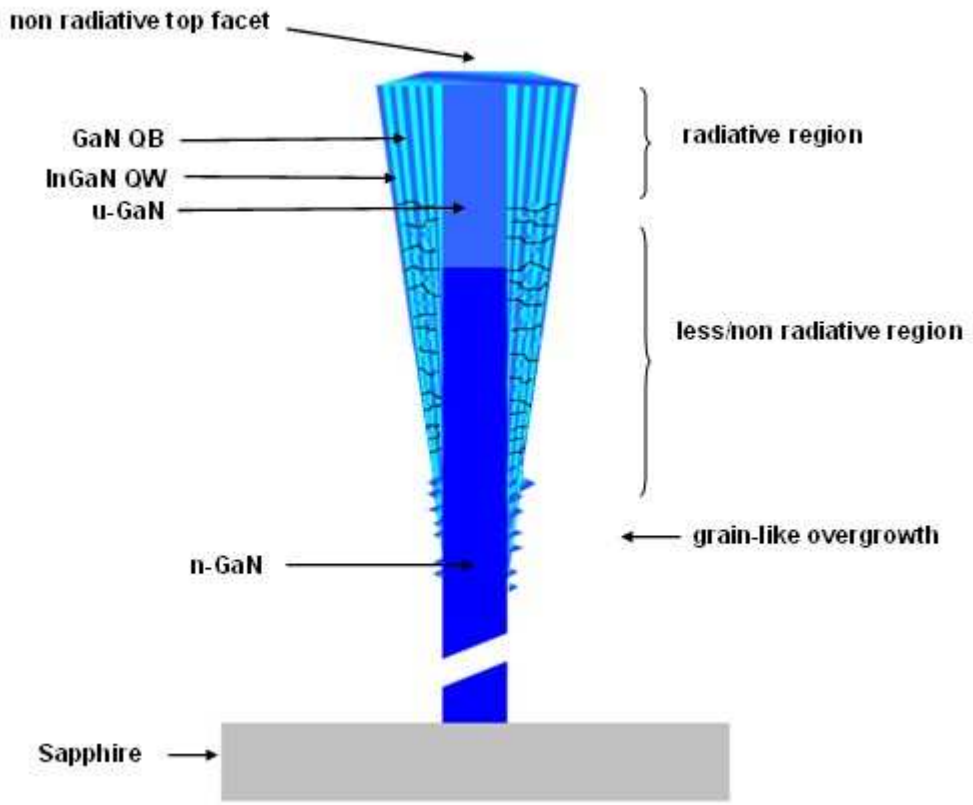

Figure 4.12 : Schematic view of an InGaN/GaN MQW grown by MOVPE around a GaN wire template. The black lines in the MQW structure represent defects. The wire n-GaN part is two times longer than the MQW region (not shown here).

4.4.2. Variation of the indium concentration (QW growth temperature)

Opto-electronic device fabrication is based on 2D GaN film growth whereby the emission wavelength is generally controlled by the indium concentration in the QWs. As already mentioned in chapter 2, indium incorporation is very sensitive to the temperature during the QW growth: the wavelength is shifted by about 1.5 nm/K. Therefore, the indium concentration can be increased by decreasing the InGaN QW growth temperature. This temperature effect on the light emission properties of InGaN/GaN MQWs grown around GaN wires was studied in order to determine the wavelength range (and to estimate the In concentration) which can be reached in the MOVPE wires.

For this experiment, four samples with a 2D QW target thickness of 5 nm were grown at decreasing QW growth temperatures: 759, 747, 735 and 723 °C respectively. Figure 4.13 shows the normalised μPL intensities measured on single wires at 5 K for the different QW growth temperatures. The MQW emission is clearly shifted and the yellow band emission (not shown here) is very low as presented in the last sample. The deep-level emission band next to the emission peak may be attributed to nitrogen vacancies [Yoshimoto91].

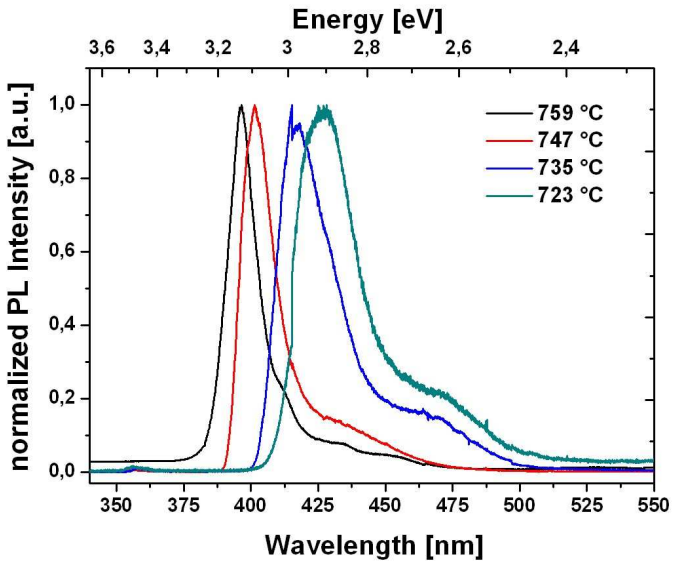

Figure 4.13 : μ-PL (5 K) spectra of MOVPE single wires containing radial InGaN/GaN MQWs grown at different growth temperatures.

As expected, the wavelength of MQW emission increases with decreasing growth temperature as well as the FWHM of the emission peak. A strong decrease (~ 10^3) of the emission efficiency was observed as a function of the temperature decrease (not shown in

these normalised data). The emission peak wavelengths are plotted as a function of the InGaN growth temperature in Figure 4.14 a) as well as the FWHM in Figure 4.14 b). The variation of the emission wavelength as a function of the QW-growth temperature is clearly linear. In a first approximation and with a direct comparison with 2D materials, this behaviour can be attributed to a variation of the In incorporation in the InGaN layers.

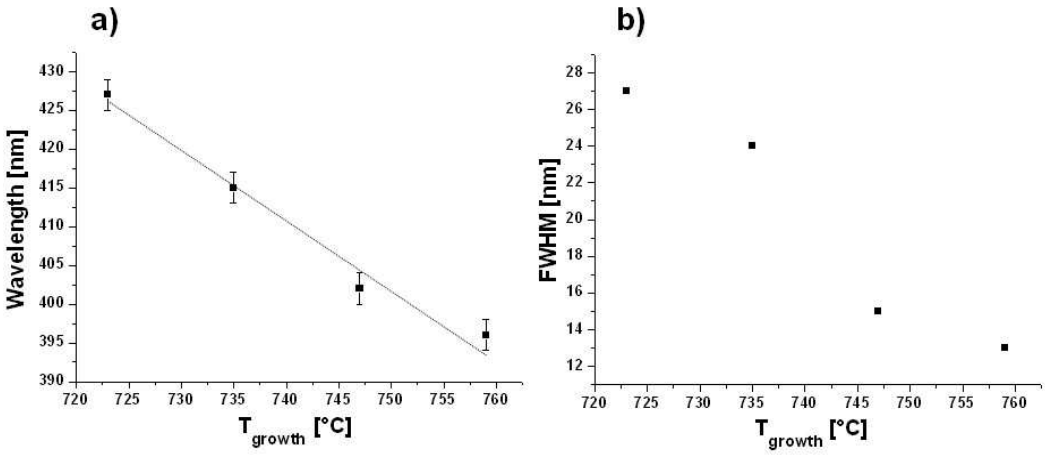

Figure 4.14 :a) InGaN MQW emission peak wavelength as function of the growth temperature. b) FWHM of the emission peak as function of the growth temperature. The measurements were done at 5 K.

Figure 4.15 indeed shows the RT μPL emission wavelength as a function of the In molar fraction measured by X-ray diffraction in 2D InGaN films. The emission peak wavelength is shifted to higher energies with decreasing indium concentration in the layer.

Figure 4.14 b) shows the FWHM of the MQW emission as a function of the growth temperature. As already reported in the literature, the FWHM of the MQW peak emission is increased with the In mole fraction in the QW [Yoshimoto91, Nakamura92c]. The broadening of the FWHM may also be due to the increase of structural and chemical (like clustering) defects induced by low temperature growth.

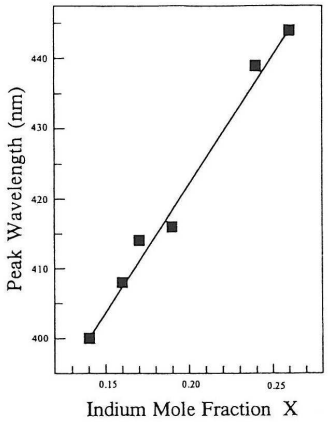

Figure 4.15: RT PL emission wavelengths of InGaN 2D layers as a function of the indium mole fraction measured by X-ray diffraction [Nakamura92c].

The In-concentration in the presented QWs can be roughly estimated from the InGaN PL emission peak wavelength in Figure 4.15, supposing that quantum and localisation effects do not play an important role in these samples[29]. The RT MQW emission reported in Figure 4.9 is located at 415 nm (2.99 eV) which gives, in comparison with Figure 4.15, an In concentration of 18 %. We can assume that the indium concentration in the QWs is in the same order of magnitude as in 2D structures grown at the same temperature.

4.4.3. Variation of the QW thickness by changing the QW growth time

The CL spectra in Figure 4.10 revealed different MQW emission curves for the two different QW growth times. For 20 s of QW growth, the maximum is close to 396 nm (3.135 eV), whereas for 120 s of deposition, the peak is centred at 407 nm (3.05 eV). For a deeper understanding, the MQW emission, the 80 s and 40 s intermediate values of QW deposition times were also measured by CL. In Figure 4.16, the normalised MQW CL spectra are plotted as a function of the wavelength. A shift to lower wavelengths is observable with decreasing QW growth time, which becomes stronger for low QW deposition times (40 s and 20 s). Figure 4.17 plots the position of the maximum of the emission peak as a function of the QW growth time. For deposition times longer than 80 s, the emission wavelength does not change significantly. For shorter growth times, a drastic

[29] QW target thickness is 5 nm

drop of the emission wavelength can be seen. The FWHM of the CL emission is about 20 nm (see Table 4.1) and does not vary with the growth time, contrary to the dependency on the indium concentration at a given thickness (see section 4.4.2).

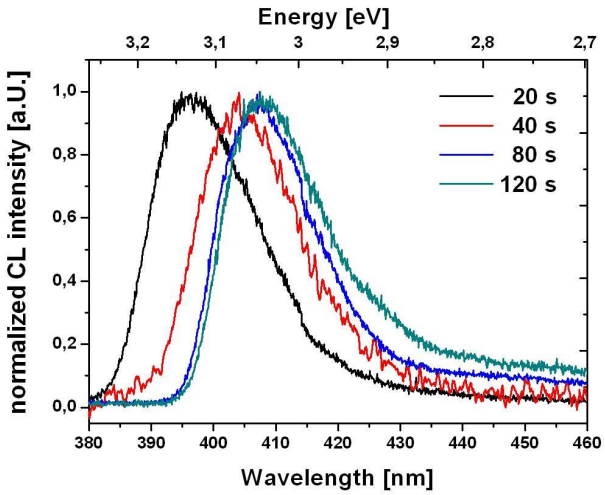

Figure 4.16 : MQW (x 5) CL (5 K) spectra for several QW growth times (20 to 120 s). The QW target thickness is 5 nm.

This observation tends to indicate that the In-concentration in the QW is roughly constant in all the samples and that the shift of the emission peak should not be attributed to a change of the InGaN alloy composition. It can be most probably attributed to a decrease of the QW thickness with decreasing growth time[30], which leads to a quantum confinement [Takeuchi97, Chichibu99]. Table 4.1 gives the nominal QW thickness corresponding to 2D growth on the c-plane surface for the different growth times, the measured emission wavelength and the corresponding FWHM.

[30] The precise measurements of the core/shell superlattice thicknesses are under way. MOVPE grown samples are too thick to be directly measured by TEM without any thinning. Focused Ion Beam (FIB) preparations will be performed to obtain longitudinal slices of the wires. They will allow the comparison of the real thickness values with the nominal ones and the verification of the proportionality of growth time and thickness on the m-plane edges of the wires. SIMS profiling is also under way with 2D references to obtain these values.

QW growth time (s)	Nominal QW thickness (nm) target value for 2D (0001) growth	Emission wavelength (nm)	FWHM (nm)
120	7.5	408.3	20
80	5	407.3	19
40	2.5	404.7	20
20	1.25	396.5	19

Table 4.1 : QW growth time, nominal QW thickness from 2D growth in [0001] direction, CL (5 K) MQW emission wavelength and corresponding FWHM.

Figure 4.17 a) and b) respectively show the MQW emission wavelength and energy as a function of the QW growth time. For longer QW growth times, the emission peak position has an asymptotic behaviour to reach a value of about 408 nm (3.04 eV).

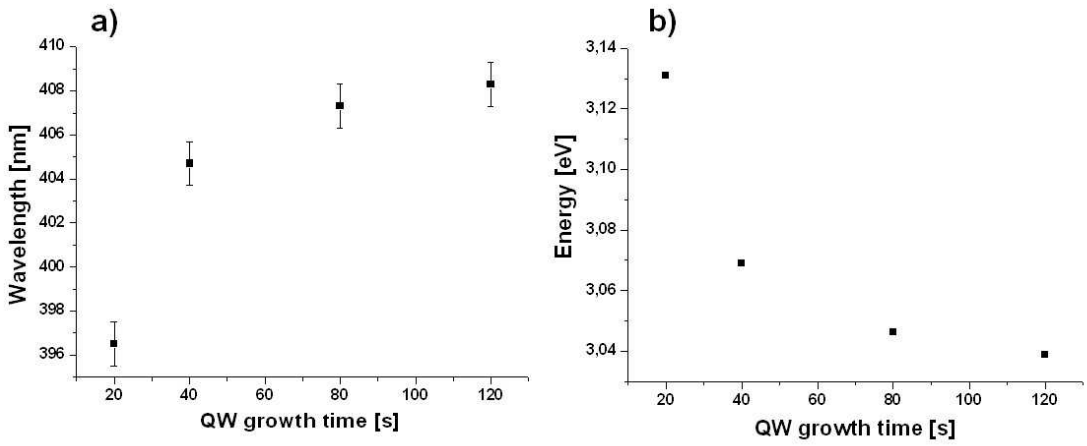

Figure 4.17 : a) Wavelength and b) energy evolution of InGaN QW transition as a function of growth time. These CL measurements have been obtained at 5K.

Figure 4.18 shows the calculated QW emission energy and the PL measurements for an $In_{0.13}Ga_{0.87}N/Ga_{0.97}In_{0.03}N$ MQW grown in c-plane direction as a function of the QW thickness [Takeuchi97]. The solid curve represents the peak evolution under the presence of a piezoelectric field of 1.08 MV/cm. The transition energy without any electric field is shown by the dashed line. The white and black squares represent PL measurements with low (2 W/cm^2) and high (200 kW/cm^2) excitation power for different QW thicknesses.

In a first approximation, the transition energy E in a QW is given by the following equation:

$$E = E_g + E_{e1} + E_{h1} - eFd \qquad \text{(eq. 7)}$$

where E_g is the strained fundamental band gap of the strained well material, E_{e1} (E_{h1}) are the first confinement energy levels of the electrons (holes) and the last term represents the influence of the quantum-confined Stark effect (QCSE) as a function of the piezoelectric field F and the QW thickness d.

With a piezoelectric field in the QWs, the QCSE term becomes dominant for thick QWs, which results in a constant decrease of the QW transition energy as shown by the solid curve in Figure 4.18. Without a piezoelectric field, the last term falls apart and the curve progression only depends on the electron and hole confinement energies, which are constant for thick QWs due to the lack of quantum confinement (see the dashed curve in Figure 4.18).

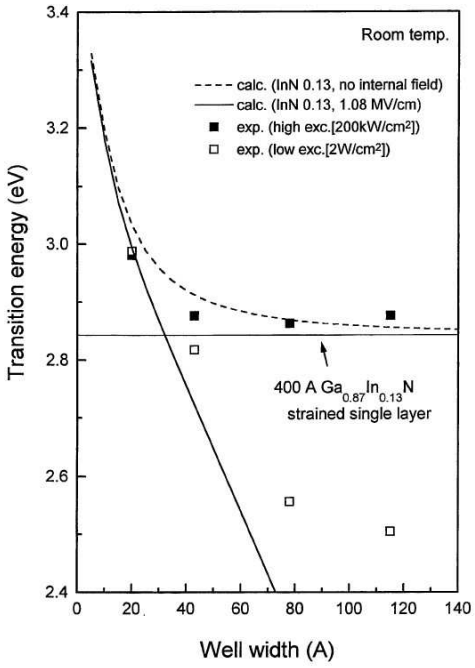

Figure 4.18 : Calculated and experimental transition energy of an $In_{0.13}Ga_{0.87}N/Ga_{0.97}In_{0.03}N$ MQW as a function of the QW thickness. The solid and the dashed line represent the calculated transition with a piezoelectric field of 1.08 MV/cm and without any field. The white and black squares represent PL measurements for different QW thicknesses at low and high excitation powers of 2 W/cm² and 200 kW/cm² [Takeuchi97].

The CL measurements given in Figure 4.17 b) are therefore consistent with a very small (or null) piezoelectric field in the MOVPE grown MQW structures that may result from the m-plane growth on the edge of the GaN wire templates. To confirm this interpretation, power-dependent CL measurements have been performed on the 120 s MQW heterostructure.

As calculated and measured in Figure 4.18 for PL experiments, the electron-hole pair concentration in the QWs increased with excitation power should screen the piezoelectric field. In this case, a blue shift of the emission peak position should be observed. The CL spectra for excitation powers from 0.019 kW/cm^2 up to 60 kW/cm^2 are plotted in Figure 4.19. No blue shift of the MQW emission peaks is observed, which excludes the presence of a significant piezoelectric field in the QWs.

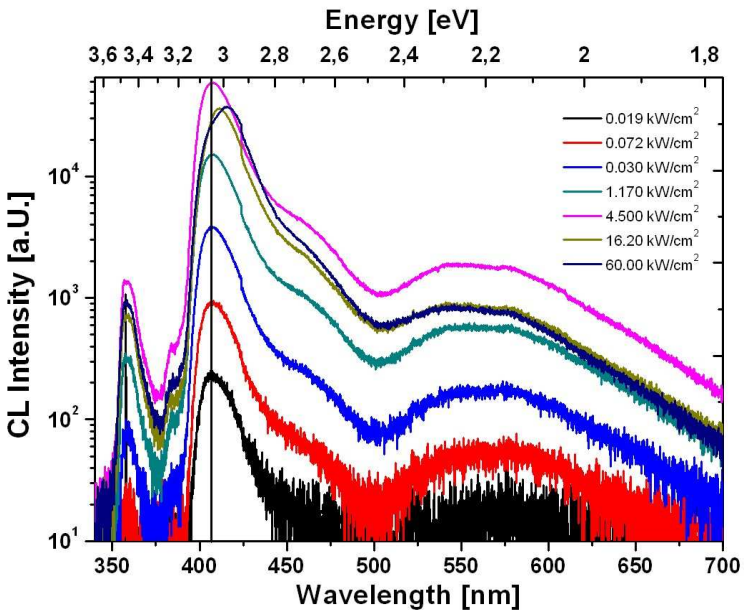

Figure 4.19: Power-dependent CL (5 K) measurements on the MQW (x 5) structure with a QW growth time of 120 s.The line at 407 nm (3.05 eV) indicates the position of the MQW emission peak.

4.5. Conclusions

The optical properties of several wire-based heterostructures were studied in this chapter.

- n/un-intentionally doped axial heterostructures were produced by stopping the silane flow after the first part of the wire had been grown under silane injection. To maintain the wire geometry, this stop of silane injection can only be performed after the n-doped part has reached a length of at least 5 μm. Stopping the silane flow at an earlier stage of the growth leads to the formation of GaN island with a strong lateral growth.

CL measurements (5 K) revealed a characteristic n-GaN emission over the bottom part of the wire grown under silane injection: the near band edge emission is located at 350 nm (3.55 eV) with a FWHM of 16 nm (120 meV) indicating a doping level of about $10^{20}/cm^3$. A continuation of the growth without silane injection (maintaining the growth temperature of 1000 °C) does not lead to a significant change of the wire shape. The NBE emission is more intense and shifted to 355 nm (3.496 eV) with a FWHM of about 7 nm (70 meV). A carrier concentration in the $10^{19}/cm^3$ range can be estimated and it can be concluded that this part is un-intentionally n-doped in practice.

- n-doped/Mg-doped heterostructures were realised by Cp_2Mg injection at the n-doped top part of the wire. The growth temperature of the Mg-doped part was shown to be very important for both structural and optical properties (growth temperatures of 1000 °C and 850 °C were tested).

CL measurements reveal a very weak emission at the Mg-doped top part of the wires: an emission peak at 375 nm (3.31 eV) can be observed close to the near band edge emission at 355 nm (3.497 eV). At high temperature growth (1000 °C), the wire geometry is preserved (like the n/un-intentionally doped heterostructure) whereas the growth at lower temperature (850 °C) leads to the formation of a lollypop-like morphology on top of the wire (with enhanced lateral growth). CL measurements on top of a wire grown at 850 °C show a 370 nm (3.36 eV) emission peak similar to the peak observed for the growth at 1000 °C but with a much stronger intensity. These emission peaks can be attributed to the DAP transition and can be taken as a first hint of successful p-doping of the material. The increase of the DAP emission with decreasing growth temperature leads to the conclusion of the decrease of Mg incorporation with increasing growth temperature.

Complementary experiments in terms of secondary ion mass spectroscopy (SIMS) on single wires and electrical measurements to estimate the dopant concentrations and

activities are presently under way. The properties of p – u – n photodetector devices are also presently studied in a project of the French Research Agency (ANR).

- InGaN/GaN MQW heterostructures were deposited on wire templates by applying the 2D MQW growth technique described in chapter 2. The spatial distribution of the emission was studied by CL on single wires; the growth temperature was changed to vary the indium concentration and growth time to change the QW thickness.

The MQW lateral overgrowth at the top of the wire in the core/shell geometry was evidenced by CL and SEM observations: characteristic MQW emission is located on the side facets and not on the wires tops. The MQW structure grows on the m-plane facets of the wires, not along the c-direction and therefore significantly different piezo-electric contributions influence the optical emission.

μ-PL measurements on single MQW structures with different QW growth temperatures revealed a shift of the MQW emission peak to higher energies with increasing growth temperature, which was attributed to a change of the In concentration.
The decrease of the QW growth time led to the blue shift of the QW transition energy attributed to quantum confinement in the wells. The asymptotic behaviour at larger thickness of this QW transition energy and the absence of a blue shift at a high CL excitation power excluded the presence of a significant piezoelectric field in the QWs, in agreement with the radial growth of InGaN/GaN MQWs on the m-plane side facets of the GaN wires.

Chapter 5

Conclusions and perspectives

This work demonstrated the MOVPE catalyst-free self-assembled growth of GaN wires.

The GaN wire growth was achieved in a new Thomas Swan (Aixtron) 3x2" CCS MOCVD reactor. This reactor was the first one of this type in the laboratory and was installed in 2007. The system is originally designed for bi-dimensional growth of GaN, AlN, InN and their alloys. During the validation process of the MOCVD system, the growth of the building blocks of blue LEDs was achieved.

- Reproducibility of the GaN layers in terms of material composition, thickness, structural quality and homogeneity over a whole 2" sapphire wafer was fulfilled using a low temperature GaN nucleation layer, the standard growth method in the literature. SEM and AFM measurements quantified the layer morphology in terms of homogeneity and roughness. The layers are flat with a RMS of 0.42 nm over 64 μm^2 and exhibit a standard dislocation density of 2×10^8 cm^{-2}.

- The control of n- and p-doping in GaN was achieved by convenient concentrations for device applications. The residual n-doping of un-intentionally doped GaN as well as related carrier mobilities were quantified.

- InGaN/GaN MQWs grown with the MOCVD system exhibit RT PL emission wavelengths between 442 nm and 447 nm (2.81 eV - 2.78 eV) depending on the position on the 2" sapphire substrate. The FWHM is about 35 nm (20 meV) and independent from the measured position. These results confirm the homogeneity of the MQW layers in terms of composition and quality over the whole wafer.

- After having checked that the MOCVD system fulfils the desired specifications for GaN and InGaN growth with respect to crystal quality, doping level and In-concentration control, these building blocks were combined to realise a blue LED, showing a strong blue electro-luminescence[31].

The catalyst-free self-assembled approach to grow GaN wires by MOVPE, developed during this thesis, was not reported in the literature. A systematic study was performed to understand the key parameters controlling the growth of these one-dimensional structures. Schematically, the developed approach can be divided into three main steps:

- (I) Surface preparation: bake, annealing under NH_3 and the deposition of a thin dielectric SiN_x layer followed by an annealing under NH_3
- (II) Nucleation of GaN islands
- (III) GaN wire growth.

(I) The thin dielectric SiN_x layer, deposited during the surface preparation step, behaves like a (selective) mask for the later GaN deposition. The SiN_x deposition time (100 sec where found to be close to the optimum) and the annealing of the resulting layer under NH_3 are both crucial parameters for the wire growth.

(II) During the nucleation step, a deposition time between 10 s and 100 s was found to be the optimum for the formation of hexagonal shaped GaN seeds, which determine the later GaN wires' shape and diameter.

(III) Several growth parameters were identified to be crucial for the GaN wire growth:

- A V/III ratio lower than a few tens is essential for the wire growth: a too high value (several hundreds) leads to lateral growth, whereas values below ten lead to the formation of laterally growing islands.

[31] Lithography and electrical contacting was performed by CEA/DOPT.

- Within the mentioned experimental conditions (in particular: a low hydrogen content in the carrier gas, and no patterned surface for selective area growth), the wire growth is only observed under injection of silane. The optimal silane flow was found to be several hundreds of nmol/min. A too low silane flow leads to strong lateral growth and for flows of several thousands of nmol/min, the structural quality (and morphology) of the wires is strongly degraded.

- The growth temperature affects the structural quality of the wires. The wires' structural quality is good at a high temperature (1000 °C) growth, but a decrease of only some tens of degrees leads to an increase of structural defects (kinks along the wires, irregular shapes…) accompanied by an increase of the wire density. A higher temperature leads to material evaporation without the formation of wires.

- Within these optimised growth conditions, the growth rate is constant but strongly dependent on the carrier-gas flow: a decrease of the carrier-gas flow increases the dwell time of the materials in the reactor and leads to a large increase of the wire-growth rate.

From the structural point of view, the as-grown wires have been studied by grazing incident x-ray diffraction. The experiments evidenced the wires' growth direction along the c-axis and revealed the epitaxial relationships of the wires with the substrate. The wires show the typical 30 ° rotation of the GaN lattice with respect to the sapphire, and the assembly has a low distribution of tilt- and twist-disorientations corresponding to about 0.61 and 0.34 ° FWHM respectively. STEM and CBED measurements revealed the coexistence of N- and Ga-polar crystalline c-orientations in the wires. It is proposed that the instabilities of the Ga-polar facets may explain the evolution of the top wire facets and their tendency to stop growing.

To conclude, the developed approach may be viewed as a fast and reproducible technique to grow GaN wires by MOVPE. Compared to other techniques, it allows the systematic study of the growth parameters' influence without being dependent on time consuming *ex situ* surface preparations like surface patterning used in SAG. Nevertheless, the controls of density and the diameter distribution as well as the reduction of the overgrowth in-between the wires have not been completely solved.

The growth of heterostructures as longitudinal n-u and "n-p" wires as well as a core-shell InGaN/GaN MQW using the wires as templates was demonstrated.

The longitudinal n/un-intentionally doped heterostructures were grown by stopping the silane flow after the wires had reached a length of about 5 μm. At this stage of the growth, the absence of silane does not lead to lateral growth which would occur without silane injection directly at the beginning of the growth. The doping variation in the longitudinal structure was evidenced by cathodo luminescence measurements on single wires at 5 K. The bottom part of the wire, grown under silane injection, shows a near band edge emission located at 350 nm (3.55 eV) with a FWHM of 16 nm (120 meV) consistent with a doping level of about 10^{20} cm^{-3}. This value has been confirmed by electrical transport measurements on single wires at the Néel Institute, CNRS Grenoble. A continuation of the growth without silane injection (maintaining the growth temperature at 1000 °C) does not result in a significant change of the wire shape. The NBE emission is shifted to 355 nm (3.496 eV) with a FWHM of about 7 nm (70 meV) indicating a carrier concentration of about 10^{19} cm^{-3}. It can be concluded that this part is un-intentionally n-doped at a much higher level than the conventional un-doped layers (around 10^{16} cm^{-3}).

In parallel, an attempt was taken to develop n-p heterostructures by switching from silane to Cp_2Mg and keeping the other growth conditions fixed. At a growth temperature of 1000 °C, the wires' geometry is preserved (like for the n/un-intentionally doped heterostructure) whereas the growth at a lower temperature (850 °C) leads to a lollypop-like morphology on top of the wire. CL measurements revealed a small emission peak centred at 375 nm (3.31 eV) next to the NBE emission centred at 355 (3.496 eV) for the structure grown at 1000 °C and a peak with a larger intensity at 370 nm (3.36 eV) for the structure grown at 850 °C. These emission peaks can be attributed to the DAP transition and can be taken as a first hint for successful p-doping of the material. Electrical measurements now have to be performed to confirm these preliminary experiments.

InGaN/GaN MQW heterostructures were grown on wire templates by applying the 2D MQW growth parameters. The spatial distribution of the QW emission was studied on single wires by μPL and CL. The In-concentration in the QWs and their thickness was controlled by changing the QW growth temperature and growth time respectively. The lateral core/shell overgrowth on top of the wires has been evidenced by SEM and CL measurements.

The characteristic MQW emission is located at the side facets of the structure but not on the top facet. The core/shell structure is grown on the m-plane facets of the wire and not on the c-plane as is the case for 2D materials with the same sapphire substrate. Consequently, different piezoelectric contributions influence the wires' emission properties.

- μPL measurements on single MQW structures grown with different QW growth temperatures revealed a shift of the MQW emission to higher energies with increasing growth temperature. This shift can be attributed to a change of the indium concentration in the QWs.

- A decrease of the QW growth time led to a blue shift of the emission attributed to quantum confinement in the wells. The asymptotic behaviour for larger QW thicknesses and the absence of a blue shift for higher excitation powers in that region excludes the presence of a significant piezoelectric field in the QWs, in agreement with the m-plane growth direction.

The growth of the fundamental building blocks of a wire-based blue LED was demonstrated during this thesis. The realisation of an efficient device still requires a deeper understanding and optimisation of the parameters controlling the material growth and an optimisation of the electrical contacts, difficult to achieve directly on sapphire substrates.

This work opens new opportunities for nitride nanowires grown by MOCVD. The control of the diameter, position and assembly density is strongly limited by the self-assembled approach described in this thesis. A possibility to overcome these limits is the use of SAG[32]. The position and diameter of the wires are defined by a pre-patterned mask generated *ex situ* by lithographic techniques allowing a deeper study of the nucleation and its influence on wire growth. Experiments with different assembly densities could clarify how the material is incorporated at the top of the wire structure and what the role of surface diffusion is [Borgström07]. A higher density of the assembly could also allow the coalescence of the top of the wires to obtain a bi-dimensional layer, much more convenient for later electrical contacting of the devices.

[32] This SAG approach, using nano-imprint for substrate patterning is presently under development by Xiaojun Chen (PhD student, CEA Grenoble INAC/SP2M/NPSC).

Doping control, especially the growth of intrinsic materials and p-doping, still has to be optimised. In the case of p-doping, the incorporation of Mg and its activation after annealing has to be confirmed electrically. These results should be compared with advanced characterisation techniques such as secondary ion mass spectrometry (SIMS), x-ray fluorescence and electron microscopy holography performed on single wires.

Concerning the InGaN/GaN MQW growth, a few questions remain open: Why do the materials grow in core/shell geometry and not longitudinally as is the case for MBE and why is the core/shell structure only located in the upper third of the wire and what is the influence of the growth parameters on this effect? To answer these questions, the influence of the growth parameters such as temperature, pressure and carrier-gas flow should be studied in more detail.

Finally, the growth of an AlGaN-based wire heterostructure seems to be interesting for future explorations because of the smaller difference in growth temperature between AlGaN and GaN compared to the InGaN/GaN system.

Glossary

AFM – atomic force microscopy

AM – air mass

CBED – convergent beam electron diffraction

CCS – close coupled showerhead

CL – catodoluminescence

CTR – crystal truncation rod

CVD – chemical vapour deposition

DAP – donor acceptor pair

DBR – distributed bragg reflector

EL – electroluminescence

FET – field effect transistor

FIB – focused ion beam

FWHM – full width at half maximum

HCP – hexagonal closed packed

HEMT – high electron mobility transistor

HT – high temperature

HVPE – hydrate vapour phase epitaxy

LED – light emitting diode

LEEBI – low energy electron beam irritation

LPCVD – low pressure chemical vapour deposition

LT – low temperature

MBE – molecular beam epitaxy

MO – metal organics

MOCVD – metal organic chemical vapour deposition

MO-HVPE – metal organic hydride vapour phase epitaxy

MOVPE – metal organic vapour phase epitaxy

MQW – multi quantum well

NBE – near band edge

PAA – porous anodic alumina

PL – photoluminescence

μPL – micro photoluminescence

QB – quantum barrier

QCSE – quantum confined stark effect

QW – quantum well

RHEED – reflection high energy electron diffraction

RMS – root mean square

RT – room temperature

SAG – selective area growth

SEM – scanning electron microscope

SIMS – secondary ion mass spectroscopy

SOG – spin-on glass

STEM – scanning transmission electron microscopy

TD – threading dislocation

TEM – transmission electron microscope

VLS – vapour liquid solid

VS – vapour solid

VSS – vapour solid solid

XPS – X-ray photoelectron spectroscopy

XRR – X-ray reflectivity

YB – yellow band

References

[Allwood05] D. A. Allwood, G. Xiong, C. C. Faulkner, D. Atkinson, D. Petit and R. P. Cowburn, *Magnetic Domain-Wall Logic*, Science 309 1688 (2005)

[Amano89] H. Amano, M. Kito, K. Hiramatsu, *P-Type Conduction in Mg-Doped GaN Treated with Low-Energy Electron Beam Irradiation (LEEBI)*, Japanese Journal of Applied Physics 28 2112 (1989)

[Amano98] H. Amano, M. Iwaya, T. Kashima, M. Katsuragawa, I. Akasaki, J. Han, S. Hearne, J. A. Floro, E. Chason and J. Figiel, *Stress and Defect Control in GaN Using Low Temperature Interlayers*, Japanese Journal of Applied Physics 37 1540 (1998)

[Ambacher98] O. Ambacher, Growth and applications of Group III nitrides, *Journal of Physics D 31 2653 (1998)*

[Ambacher00] O. Ambacher, B. Foutz, J. Smart, J. R. Shealy, N. G. Weimann, K. Chu, M. Murphy, A. J. Sierakowski, W. J. Schaff, L. F. Eastman, R. Dimitrov, A. Mitchell and M. Stutzmann, *Two dimensional electron gases induced by spontaneous and piezoelectric polarization in undoped and doped Al-GaN/GaN heterostructures*, Journal of Applied Physics 87 334 (2000)

[Ambacher02] O. Ambacher, J. Majewski, C. Miskys, A. Link, M. Hermann, M. Eickhoff, M. Stutzmann, F. Berardini, V. Fiorentini, V. Tilak, B. Schaff and L. F. Eastman, *Pyroelectric properties of Al(In)GaN/GaN hetero- and quantum well structures*, Journal of Physics: Condensed Matter 14 3399 (2002)

[Aschenbrenner09] T. Aschenbrenner, C. Kruse, G. Kunert, S. Figge, K. Sebald, J. Kalden, T. Voss, J. Gutowski and D. Hommel, *Highly ordered catalyst-free and mask-free GaN nanorods on r-plane sapphire*, Nanotechnology 20 075604 (2009)

[Avramescu09] A. Avramescu, T. Lermer, J. Müller, S. Tautz, D. Queren, S. Lutgen and U. Strauß, InGaN *laser diodes with 50 mW output power emitting at 515 nm*, Applied Physics Letters 95 071103 (2009)

[Barrelet04] C. J. Barrelet, A. B. Greytak and C. M. Lieber, *Nanowire Photonic Circuit Elements*, Nano Letters 4 1981 (2004)

[Beaumont83] B. Beaumont, G. Nataf, J. C. Guillaume and C. Verie, *Low temperature photoluminescence of n-type GaInAsP layers grown on InP by liquid phase epitaxy*, Journal of Applied Physics, 54 5363 (1983)

[Beaumont98] B. Beaumont, M. Vaille, G. Nataf, A. Bouillé, J.-C. Guillaume, P. Vénnègues, S. Haffouz and P. Gibart, *Mg-enhanced lateral overgrowth of GaN on patterned GaN/sapphire substrate by selective Metal Organic Vapor Phase Epitaxy*, MRS Internet Journal Nitride Semiconductor Research 3 20 (1998)

[Berkowicz00] E. Berkowicz, D. Geshoni, G. Bahir, E. Lakin, D. Shilo, E. Zolotoyabko, A. Abare, S. DenBaars, L. Coldren, *Measured and calculated radiative lifetime and optical absorption of $In_xGa_{1-x}N/GaN$ quantum structures*, Physical Review B 61 10994 (2000)

[Bernardini97] F. Bernardini, V. Fiorentin and D. Vanderbilt, *Spontaneous polarization and piezoelectric constants of III-V nitrides*, Physical Review B 56 10024 (1997)

[Bertness06] K. A. Bertness, A. Roshko, N. A. Sanford, J. M. Barker and A. V. Davydov, *Spontaneously grown GaN and AlGaN nanowires*, Journal of Crystal Growth 287 522 (2006)

[Bloom74] S. Bloom, G. Harbeke, E. Meier and I. Ortenbur, *Band-structure and reflectivity of GaN*, Physica Status Solidi B-Basic Research 66 161 (1974)

[Borgström07] M. T. Borgström, G. Immink, B. Ketelaars, R. Algra and E. P. A. M. Bakkers, *Synergetic* nanowire *growth*, Nature Nanotechnology 2 541 (2007)

[Bougrioua07] Z. Bougrioua, P. Gibart, E. Calleja, A. Trampert, J. Ristic, M. Utrera and G. Nataf, *Growth of freestanding GaN using pillar-epitaxial lateral overgrowth from GaN nanocolumns*, Journal of Crystal Growth 309 113 (2007)

[Caetano07] C. Caetano, L. K. Teles, M. Marques, A. D. Pino and L. G. Ferreira, *Theoretical support for the smaller band gap bowing in wurtzite InGaN alloys*, AIP Conference Proceeding 893 257 (2007)

[Calleja00] E. Calleja, M. A. Sanchez-Garcia, F. J. Sanchez, F. Calle, F. B. Naranjo and E. Munoz, *Luminescence properties and defects in GaN nanocolumns grown by molecular beam epitaxy*, Physical Review B 62(24) (2000)

[Chemla83] D. S. Chemla, T. C. Damen, D. A. B. Miller, A. C. Gossard and W. Wiegmann, *Electroabsorption by Stark effect on room-temperature excitons in GaAs/GaAlAs multiple quantum well structures*, Applied Physics Letters 42 864 (1983)

[Chen04] Z. Chen, Z. Shan, M. S. Cao, L. Lu and S. X. Mao, *Zinc oxide nanotetrapods*, Nanotechnology 15 365 (2004)

[Cheng07] A. T. Cheng, Y. K. Su and W. C. Lai, *MOVPE growth of InGaN/GaN multiple quantum wells for the blue laser diode applications*, Journal of Crystal Growth 298 508 (2007)

[Chichibu99] S. F. Chichibu, A. C. Abare, M. P. Mack, M. S. Minsky, T. Deguchi, D. Cohen, P. Kozodoy, S. B. Fleischer, S. Keller, J. S. Speck, J. E. Bowers, E. Hu, U. K. Mishra, L. A. Coldren, S. P. DenBaars, K. Wada, T. Sota and S. Nakamura, *Optical properties of InGaN quantum wells*, Material Science and Engineering B 59 298 (1999)

[Chichibu00] S. Chichibu, A. Shikanai, T. Deguchi, A. Setoguchi, R. Nakai, H. Nakanishi, K. Wada, S. DenBaars, T. Sota and S. Nakamura, *Comparison of Optical Properties of GaN/AlGaN and InGaN/AlGaN Single Quantum Wells*, Japanese Journal of Applied Physics 39 2417 (2000)

[Chien96] F. R. Chien, X. J. Ning, S. Stemmer, P. Pirouz, M. D. Bremser and R. F. Davis, *Growth defects in GaN films on 6H–SiC substrates*, Applied Physics Letters 68 2678 (1996)

[Cierchia03] R. Chierchia, T. Böttcher, H. Heinke, S. Einfeldt, S. Figge and D. Hommel, *Microstructure of heteroepitaxial GaN revealed by x-ray diffraction*, Journal Applied Physics 93 8918 (2003)

[Cordier09] Y. Cordier, F. Semond, J. - C. Moreno, E. Frayssinet, B. Benbakhti, Z. Cao, S. Chenot, L. Nguyen, O. Tottereau, A. Soltani, K. Blary, *Selective area growth of GaN-based structures by molecular beam epitaxy on micrometer and nanometer size patterns*, Materials Science in Semiconductor Processing 12 16 (2009)

[Daulesberg08] M. Dauelsberg, C. Martin, H. Protzmann, A. R. Boyd, E. J. Thrush, J. Kaeppeler, M. Heuken, R. A. Talalaev, E. V. Yakovlev and A. V. Kondratyev, *Modeling and process design of III-Nitride MOVPE at near-atmospheric pressure in Close Coupled Showerhead and Planetary Reactors*, ICMOVPE 13 poster (2008) (http://aixtron.com/fileadmin/user_upload/pdf/Publications/ICMOVPE_13__Poster__Modeling_GaN_High_Pressure_MOVPE.pdf)

[Deb05] P. Deb, H. Kim, V. Rawat, M. Oliver, S. Kim, M. Marshall, E. Stach and T. Sands, *Faceted and Vertically Aligned GaN Nanorod Arrays Fabricated without Catalysts or Lithography*, Nano Letter 5(9) 1847 (2005)

[Dobrokhotov06] V. Dobrokhotov D. N. McIlroy, M. G. Norton, A. Abuzir, W. J. Yeh, I. Stevenson, R. Pouy, J. Bochenek, M. Cartwright, L. Wang,J. Dawson, M. Beaux and C. Berven, *Principles and mechanisms of gas sensing by GaN nanowires functionalized with gold nanoparticles*, Journal of Applied Physics 99 104302 (2006)

[Domracheva08] Y. V. Domracheva, V. N. Jmerik, T. B. Popova and M. V. Zamoryanskaya, *Cathodoluminescent investigations of $In_xGa_{1-x}N$ layers*, Journal of Materials Science: Materials in Electronics 19 319 (2008)

[Dong09] Y. Dong, B. Tian, T. J. Kempa and C. M. Lieber, *Coaxial Group III-Nitride Nanowire Photovoltaics*, Nano Letters 9(5) 2183 (2009)

[Duan00a] X. Duan and C. M. Lieber, *General Synthesis of Compound Semiconductor Nanowires*, Advanced Materials 12(4) 298 (2000)

[Duan00b] X. Duan and C. M. Lieber, *Laser-Assisted Catalytic Growth of Single Crystal GaN Nanowires*, Journal of Ameriacan Chemical Society, 122(1) 188 (2000)

[Dubrovskii08] V. G. Dubrovskii, N. V. Sibirev, J. C. Harmand and F. Glas, *Growth kinetics and crystal structure of semiconductor nanowires*, Physical Review B 78 235301 (2008)

[Dwikusuma03] F. Dwikusuma and T. F. Kuech, *X-ray photoelectron spectroscopic study on sapphire nitridation for GaN growth by hydride vapor phase epitaxy: Nitridation mechanism*, Journal of Applied Physics 94 5656 (2003)

[Eterkin05] E. Ertekin, P. A. Greaney and D. C. Chrzan, *Equilibrium limits of coherency in strained nanowire heterostructures*, Journal of Applied Physics 97 114325 (2005)

[Eymery07] J. Eymery, F. Rieutord, V. Favre-Nicolin, O. Robach, Y.-M. Niquet, L. Froberg, T. Martensson and L. Samuelson, *Strain and shape of epitaxial InAs/InP nanowire superlattice measured by grazing incidence X-ray techniques*, Nano Letters 7 2596 (2007)

[Feidenhans89] R. Feidenhans'l, *Surface structure determination by X-ray diffraction*, Surface Science Reports 10 105 (1989)

[Feng09] L. Feng, A. Liu, J. Wei, M. Liu, Y. Ma and B. Man, *Synthesis, characterization and optical properties of multipod ZnO whiskers*, Applied Surface Science 255 8667 (2009)

[Fert99] A. Fert and L. Piraux, *Magnetic nanowires*, Journal of Magnetism and Magnetic Materials 200 338 (1999)

[Frayssinet02] E. Frayssinet, B. Beaumont, J. P. Faurie, P. Gibart, Z. Makkai, B. P´ecz, P. Lefebvre and P. Valvin, *Micro epitaxial lateral overgrowth of GaN/sapphire by metal organic vapour phase epitaxy*, MRS Journal of nitride semiconductors 7 1 (2002)

[Geelhaar07] L. Geelhaar, C. Chèze, W. M. Weber, R. Averbeck, and H. Riechert, Th. Kehagias, Ph. Komninou, G. P. Dimitrakopulos and Th. Karakostas, *Axial and radial growth of Ni-induced GaN nanowires*, Applied Physics Letters 91 093113 (2007)

[Givargizov75] E. I. Givargizov, *Fundamental aspects of VLS growth, Journal of Crystal Growth* 31 20 (1975)

[Glas06a] F. Glas, *Critical dimensions for the plastic relaxation of strained axial heterostructures in free-standing nanowires*, Physical Review B 74 121302 (2006)

[Glas06b] F. Glas and J. C. Harmand, *Calculation of the temperature profile in nanowhiskers growing on a hot substrate*, Physical. Review B 73, 155320 (2006)

[Gottschalch08] V. Gottschalch, G. Wagne, J. Bauer, H. Paetzelt and M. Shirnow**,** *VLS growth of GaN nanowires on various substrates***,** Journal of Crystal Growth 310 5123 (2008)

[Götz95] W. Götz, N. M. Johnson, J. Walker, D. P. Bour, H. Amano and I. Akasaki, *Hydrogen passivation of Mg acceptors in GaN grown by metalorganic chemical vapor deposition*, Applied Physics Letters 67 2666 (1995)

[Gradečak05] Silvija Gradečak, Fang Qian, Yat Li, Hong-Gyu Park, and Charles M. Lieber, *GaN nanowire lasers with low lasing thresholds*, Applied Physics Letters 87 173111 (2005)

[Grandjean96] N. N. Grandjean, J. Massies, P. Vennègues, M. Laugt and M. Leroux, *Effect of the Nitridation of the Sapphire (0001) Substrate on the GaN Growth*, Applied Physics Letters 69 2071 (1996)

[Guo94] Q. Guo and A. Yoshida, *Temperature dependence of band gap change in InN and AlN, Japanese* Journal of Applied Physics 33 2453 (1994)

[Haffouz98] S. Haffouz, B. Beaumont and P. Gibart, *Effect of magnesium and silicon on the lateral overgrowth of GaN patterned substrates by metal organic vapor phase epitaxy*, Journal of Nitride Semiconductor Research 3(8) (1998)

[Han09] Y. Han, L. Pengfei, Y. Zhongyuan, S. Yuxin, W. Donglin and W. Shumin, *Critical Thickness and Radius for Axial Heterostructure Nanowires Using Finite-Element Method*, Nano Letters 9 1921 (2009)

[Harmand07] J. C. Harmand, M. Tchernycheva, G. Patriarche, L. Travers, F. Glas and G. Cirlin, *GaAs nanowires formed by Au-assisted molecular beam epitaxy: Effect of growth temperature*, Journal of Crystal Growth 301–302 853 (2007)

[Hersee02] S. D. Hersee, D. Zubia, X. Y. Sun, R. Bommena, M. Fairchild, S. Zhang, D. Burckel, A. Frauenglass and S. R. J. Brueck, *Nanoheteroepitaxy for the integration of highly mismatched semiconductor materials*, IEEE Journal of Quantum Electronics 38 1017 (2000)

[Hersee05] S. D. Hersee, X. Y. Sun, X. Wang, M. N. Fairchild, J. Liang and J. Xu, *Nanoheteroepitaxial growth of GaN on Si nanopillar arrays*, Journal of Applied Physics 97 124308 (2005)

[Hersee06] S. D. Hersee, X. Sun and X. Wang, *The Controlled Growth of GaN Nanowires, Nano Letters* 6 1808 (2006)

[Heying96] B. Heying, X. H. Wu, S. Keller, Y. Li, D. Kapolnek, B. P. Keller, S. P. D. Baars and J. S. Speck, *Role of threading dislocation structure on the xray diffraction peak widths in epitaxial GaN films*, Applied Physics Letter 68 643 (1996)

[Hiramatsu91] K. Hiramatsu, S. Itoh, H. Amano, I. Akasaki, N. Kuwano, T. Shiraishi and K. Oki, *Growh mechanism of GaN grown on sapphire with AlN buffer layer by MOVPE*, Journal of Crystal Growth 115 628 (1991)

[Hirato03] K. Hirato, H. Fujioka, S. Ito, J. Ohta and M. Oshima, *Characteristics of AlN buffer layers for GaAs epitaxial growths on MnZn ferrite substrates*, Thin Solid Films 435 131 (2003)

[Hiruma96] K. Hiruma, H. Murakoshi, M. Yazawa and T. Katsuyama, *Self-organized growth of GaAs/InAs heterostructure nanocylinders by organometallic vapor phase epitaxy*, Journal of Crystal Growth 163 226 (1996)

[Hoffmann08] V. Hoffmann, A. Knauer, F. Brunner, C. Netzel, U. Zeimer, S. Einfeldt, M. Weyers, G. Tränkle, J. M. Karaliunas, K. Kazlauskas, S. Jursenas, U. Jahn, J. R. van Look and M. Kneissl, *Influence of MOVPE growth temperature on the structural and optical properties of InGaN MQW laser diodes*, Journal of Crystal Growth 310 452 (2008)

[Holmes09] M. J. Holmes, Y. S. Park, J. H. Warner, R. A. Taylor, *Quantum confined Stark effect and corresponding lifetime reduction in a single $In_xGa_{1-x}N$ quantum disk*, Applied Physics Letters 95 18190 (2009)

[Hongsith09] N. Hongsith, T. Chairuangsri, T. Phaechamudd and S. Choopun, *Growth kinetic and characterization of tetrapod ZnO nanostructures*, Solid State Communication 149 1184 (2009)

[Horak08] L. Horák, V. Holý, C. R. Staddon, N. R. S. Farley, S. V. Novikov, R. P. Campion and C. T. Foxon, *X-ray in-plane scattering investigation of GaN nanorods*, Journal of Applied Physics 104 103504 (2008)

[Iwaya98] M. Iwaya, T. Takeuchi, S. Yamaguchi, C. Wetzel, H. Amano and I. Akasaki , *Reduction of Etch Pit Density in Organometallic Vapor Phase Epitaxy-Grown GaN on Sapphire by Insertion of a Low-Temperature-Deposited Buffer Layer between High-Temperature-Grown GaN*, Japanese Journal of Applied Physics 37 316 (1998)

[Jahn07] U. Jahn, J. Ristić and E. Calleja, *Cathodoluminescence spectroscopy and imaging of GaN/(Al,Ga)N nanocolumns containing quantum disks*, Applied Physics Letters 90 161117 (2007)

[Jiang07] X. Jiang, Q. Xiong, S. Nam, F. Qian, Y. Li and C. M. Lieber, *InAs/InP Radial Nanowire Heterostructures as High Electron Mobility Devices*, Nano Letters 7 3214 (2007)

[Johnston32] W. C. Johnston, J. B. Parsons, and M. C. Crew, *Nitrogen compound of Gallium*, Journal of Physics and Chemistry 234 2651 (1932)

[Johnson02] J. C. Johnson, H. K. Choi, K. P. Knutsen, R. D. Schaller, P. Yang and R. J. Saykally, *Single gallium nitride nanowire lasers*, Nature Materials 1 106 (2002)

[Kapolnek95] D. Kapolnek, X. H. Wu, B. Heying, S. Keller, B. P. Keller, U. K. Mishra, S. P. DenBaars and J. S. Speck, *Structural evolution in epitaxial metalorganic chemical vapor deposition grown GaN films on sapphire*, Applied Physics Letters 67 1541 (1995)

[Kapon89] E. Kapon, D. M. Hwang, and R. Bhat, *Stimulated emission in semiconductor quantum wire heterostructures*, Physcal Review Letters 63 430 (1989)

[Keller96] S. Keller, B. P. Keller, Y.-F. Wu, B. Heying, D. Kapolnek, J. S. Speck, U. K. Mishra and S. P. DenBaars, *Influence of sapphire nitridation on properties of gallium nitride grown by metalorganic chemical vapor deposition*, Applied Physics Letters 68 1525 (1996)

[Kempa08] T. J. Kempa, B. Tian, D. R. Kim, J. Hu, X. Zheng and C. M. Lieber, *Single and Tandem Axial p-i-n Nanowire Photovoltaic Devices*, 8 3456 (2008)

[Kim00] K.-S. Kim, S.-H. Kim and D.-R. Lee, *Structures of nitridated layers on sapphire studied by x-ray reflectivity and diffraction*, Applied Physics Letters 76 1552 (2000)

[Kim04] H.M. Kim, Y.H. Cho, H. Lee, S.I. Kim, S.R. Ryu, D.Y. Kim, T.W. Kang, and K.S. Chung, *High-brightness light emitting diodes using dislocation-free indium gallium nitride/gallium nitride multiquantum-well nanorod arrays*, Nano Letters 4 1059 (2004)

[Kim06] T.-W. Kim, N. Matsuki, J. Ohta and Hiroshi Fujioka, *Characteristics of AlN/Ni(111) Heterostructures and their Application to Epitaxial Growth of GaN*, Japanese Journal of Applied Physics 45 396 (2006)

[Kishino08] K. Kishino, T. Hoshino, S. Ishizawa and A. Kikuchi, *Selective-area growth of GaN nanocolumns on titanium-mask-patterned silicon (111) substrates by RF-plasma-assisted molecular-beam epitaxy*, Electronic Letters 44 819 (2008)

[Koester10] R. Koester, J. S. Hwang, C. Durand, D. Le Si Dang and J. Eymery, *Self-assembled growth of catalyst-free GaN wires by metal-organic vapour phase epitaxy*, Nanotechnology 21 015602 (2010)

[Koide87] Y. Koide, H. Itoh, M. R. H Khan, K. Hiramatu, N. Sawaki and I. Akasaki, Energy *band-gap bowing parameter in* an $Al_xGa_{1-x}N$ *alloy*, Journal of Applied Physics 61 4540 (1987)

[Koukitu99] A. Koukitu, T. Taki, N. Takahashi and H. Seki**,** *Thermodynamic study on the role of hydrogenduring the MOVPE growth of group III nitrides***,** Journal of Crystal Growth 197 99 (1999)

[Kuo02] Y.-K. Kuo and W.-W. Lin, *Band-Gap Bowing Parameter of the $Al_xIn_{1-x}N$ Derived from Theoretical Simulation*, Japanese Journal of Applied Physics 41(Part 1, No. 9), 5557 (2002)

[Kuykendall03] T. Kuykendall, P. Pauzauskie, S. Lee, Y. Zhang, J. Goldberger and P. Yang, *Metalorganic Chemical Vapor Deposition Route to GaN Nanowires with Triangular Cross Sections*, Nano Letters 3 1063 (2003)

[Kuykendall04] T. Kuykendall, P. J. Pauzauskie, Y. Zhang, J. Goldberger, D. Sirbuly, J. Denlinger and P Yang, *Crystallographic alignment of high-density gallium nitride nanowire arrays*, Nature Materials 3 524 (2004)

[Kuykendall07] T. Kuykendall, P. Ulrich, S. Aloni and P. Yang, *Complete composition tunability of InGaN nanowires using a combinatorial approach*, Nature Materials 6 951 (2007)

[Landré08] O. Landré, R. Songmuang, J. Renard, E. Bellet-Amalric, H. Renevier and B. Daudin, *Plasma-assisted molecular beam epitaxy growth of GaN nanowires using indium-enhanced diffusion*, Applied Physics Letters 93 183109 (2008)

[Landré2010] O. Landré, V. Fellmann, P. Jaffrennou, C. Bougerol, H. Renevier, A. Cros, and B. Daudin, *Molecular beam epitaxy growth and optical properties of AlN nanowires,* Applied Physics Letters 96 061912 (2010)

[Lee04] S. K. Lee, H. J. Choi , P. Pauzauskie, P. Yang, N. K. Cho, H. D. Park, E. K. Suh, K. Y. Lim, H. J. Lee, *Gallium nitride nanowires with a metal initiated metal-organic chemical vapor deposition (MOCVD) approach*, physica status solidi (b) 241(12) 2775 (2004)

[Lee97] S.-K Lee, T.-H Kim, S.-Y Lee, K.-C Choi and P. Yang, *High-brightness gallium nitride nanowire UV-blue light emitting diodes*, Philosophical Magazine 87(14) 2105 (1997)

[Lee99] I.-H. Lee, J. J. Lee, P. Kung, F. J. Sanchez and M. Razeghi, *Band-gap narrowing and potential fluctuation in Si-doped GaN*, Applied Physics Letters 74 102 (1999)

[Leroux97] M. Leroux, B. Beaumont, N. Grandjean, P. Lorenzini, S. Haffouz, P. Vennéguès, J. Massies and P. Gibart, *Luminescence and reflectivity studies of undoped, n- and p-doped GaN on (0001) sapphire*, Materials Science and Engineering B, 50 97 (1997)

[Leroux99] M. Leroux, N. Grandjean, B. Beaumont, G. Nafat, F. Semond, J. Massies and P. Gibart, *Temperature quenching of photoluminescence intensities in undoped and doped GaN*, Journal of Applied Physics 86 3721 (1999)

[Li06a] Y. Li and F. Qian, J. Xiang and C. M. Lieber, *Nanowire electronic and optoelectronic devices*, Materials Today 9 18 (2006)

[Li06b] Y. Li, J. Xiang, F. Qian, S. Gradečak, Y. Wu, H. Yan, D. A. Blom, and C. M. Lieber, *Dopant-Free GaN/AlN/AlGaN Radial Nanowire Heterostructures as High Electron Mobility Transistors*, Nano Letters, 6 1468 (2006)

[Li08] Q. Li and G. T. Wang, *Improvement in aligned GaN nanowire growth using submonolayer Ni catalyst films*, Applied Physics Letters 93 043119 (2008)

[Li09] Qiming Li, Y. Lin, J. R. Creighton, J. J. Figiel and G. T. Wang, Nanowires-templated lateral epitaxial growth of low-dislocation density nonpolar a-plane GaN on r-plane sapphire, Advanced Materterials 21(23) 2416 (2009)

[Lin93] M. E. Lin, G. Xue, G. L. Zhou, J. E. Greene, H. Morkoc, *p-type zinc-blende GaN on GaAs substrates*, Applied Physics Letters 63(7) 932 (1993)

[Liou05] B.-T. Liou, S.-H. Yen, Y.-K. Kuo, J. quan Yao, Y. J. Chen and S. Lee, *Vegard's law deviation in band gaps and bowing parameters of the wurtzite III-nitride ternary alloys*, Semiconductor Lasers and Applications II 5628 296 (2005)

[Lu04] D. Lu, D. I. Florescu, D. S. Lee, V. Merai, J. C. Ramer, A. Parekh and E. A. Armour**,** *Sapphire substrate misorientation effects on GaN nucleation layer properties*, Journal of Crystal Growth 272 353 (2004)

[Luryi86] S. Luryi and E. Suhir, *New approach to the high quality epitaxial growth of lattice mismatched materials*, Applied Physics Letters 49 140 (1986)

[Lyapina08] O. A. Lyapina, A. N. Baranov, G. N. Panin, A. V. Knotko and O. V. Kononenko, *Synthesis of ZnO nanotetrapods*, Inorganic Materials 44 846 (2008)

[Manasevit71] H. M. Manasevit, F. M. Erdmann, and W. I. Simpson, *The use of metalorganics in the preparation of semicondutor materials*, Journal of Electrochemistry Society 118 1864 (1971)

[Maruska71] H. P. Maruska and J. J. Tietjen, *The preparation and properties of vapordeposited single-crystalline GaN*, Applied Physics Letter 15, 327 (1971)

[Mnatsakanov03] T. T. Mnatsakanov, M. E. Levinshtein, L. I. Pomortseva, S. N. Yurkov, G. S. Simin and Asif, *Carrier mobility model for GaN*, Solid-State Electronics 47 111 (2003)

[Moe06] C. G. Moe, M. C. Schmidt, H. Masui, A. Chakraborty, K. Vampola, S. Newman, B. Moran, L. Shen, T. Mates, S. Keller, S. P. Denbaars and D. Emerson, *Optimized doping and contact scheme for low-voltage 275-nm deep ultraviolet LEDs*, Journal of Electronic Materials 35(4) 750 (2006)

[Monroy04] E. Monroy, T. Andreev, P. Holliger, E. Bellet-Amalric, T. Shibata, M. Tanaka and B. Daudin, *Modification of GaN(0001) growth kinetics by Mg doping*, Applied Physics Letters 84 2554 (2004)

[Moret09] M. Moret, B. Gil, S. Ruffenach, O. Briot, C. Giesen, M. Heuken, S. Rushworth, T. Leese and M. Succi**,** *Optical, structural investigations and band-gap bowing parameter of GaInN alloys*, Journal of Crystal Growth 311 2795 (2009)

[Morko94] H. Morko¸c, S. Strite, G. B. Gao, M. E. Lin, B. Sverdlov, and M. Burns, *Large-band-gap SiC, III-V nitride, and II-VI ZnSe-based semiconductor device technologies*, Journal of Applied Physics 76 1363 (1994)

[Nakamura00] S. Nakamura, S. Pearton and G. Fasol, *The blue Laserdiode*, Springer (2000)

[Nakamura92a] S. Nakamura, T. Mukat, M. Senoh, *In situ monitoring and Hall measurements of GaN grown with GaN buffer layers*, Journal of Applied Physics 71 5543 (1992)

[Nakamura92b] S. Nakamura, N. Iwasa, M. Senoh and T. Mukai, *Hole Compensation Mechanism of P-Type GaN Films***,** Japanese Journal of Applied Physics 31 1258 (1992)

[Nakamura92c] S. Nakamura and T. Mukai, High *quality InGaN films grown on GaN films*, Japanese Journal of Applied Physics 31 1457 (1992)

[Patolsky06] F. Patolsky, B. P. Timko, G. Yu, Y. Fang, A. B. Greytak, G. Zheng and C. M. Lieber, *Detection, Stimulation, and Inhibition of Neuronal Signals with High-Density Nanowire Transistor Arrays*, Science 313 1100 (2006)

[Pauzauskie06] P. J. Pauzauskie and P. Yang, *Nanowire photonics*, Materials Today 9 36 (2006)

[Petroff84] P. M. Petroff, A. C. Gossard, and W. Wiegmann, *Structure of AlAs-GaAs interfaces grown on (100) vicinal surfaces by molecular beam epitaxy*, Applied Physics Letters 45 620 (1984)

[Polenta07] L. Polenta, A. Castaldini and A. Cavallini, *Defect characterization in GaN: Possible influence of dislocations in the yellow-band features*, Journal of Applied Physics 102 063702 (2007)

[Ponce96] F. A. Ponce, D. Cherns, W. T. Young, and J. W. Steeds, *Characterization of dislocations in GaN by transmission electron diffraction and microscopy techniques*, Applied Physics Letters 69 770 (1996)

[Pugh99] S. K. Pugh, D. J. Dugdale, S. Brand, and R. A. Abra, *Electronic structure calculations on nitride semiconductors*, Semiconductor Science Technology 14(23) 631 (1999)

[Qian04] F. Qian, Y. Li, S. Gradečak, D. Wang, C. J. Barrelet and C. M. Lieber*, Gallium Nitride-Based Nanowire Radial Heterostructures for Nanophotonics*, Nano Letters 4 1975 (2004)

[Qian05] F. Qian, S. Gradečak, Y. Li, C. Y. Wen and C. M. Lieber, *Core/Multishell Nanowire Heterostructures as Multicolor, High-Efficiency Light-Emitting Diodes*, Nano Letters 5 2287 (2005)

[Qian08] F.Qian, Y. Li, S. Gradečak, H. G. Park, Y. Dong, Y. Ding, Z. L. Wang and C. M. Lieber, *Multi-quantum-well nanowire heterostructures for wavelength-controlled lasers*, Nature Materials 7, 701 (2008)

[Raychaudhuri06] S. Raychaudhuri and E. T. Yu, *Critical dimensions in coherently strained coaxial nanowire heterostructures*, Journal of Applied Physics 99 114308 (2006)

[Reed88] M.A. Reed, J. N. Randall, R. J.Aggarwal, R. J. Matyi, T. M. Moore, A. E. Wetsel, *Observation of discrete electronic stated in zero-dimensional semiconductor nanostructure*, Physical Review Letters 60 535 (1988)

[Renard08] J. Renard, R. Songmuang, C. Bougerol, B. Daudin and B. Gayral, *Exciton and Biexciton Luminescence from Single GaN/AlN Quantum Dots in Nanowires*, Nano Letters 8 2092 (2008)

[Renard09] J. Renard, R. Songmuang, G. Tourbot, C. Bougerol, B. Daudin, B. Gayral, *Evidence for quantum-confined Stark effect in GaN/AlN quantum dots in nanowires*, Physical Review B 80 121305 (2009)

[Reshchikov99] M. A. Reshchikov, G.-C. Yi and B. W. Wessels, *Behavior of 2.8- and 3.2-eV photoluminescence bands in Mg-doped GaN at different temperatures and excitation densities*, Physical Review B 59 (1999)

[Ristic05] J. Ristic, E. Calleja, A. Trampert, S.Fernandez-Garrido, C. Rivera, U. Jahn and K. H. Ploog, *Columnar AlGaN/GaN Nanocavities with AlN/GaN Bragg Reflectors Grown by Molecular Beam Epitaxy on Si(111)*, Physical Review Letters 94 146102 (2005)

[Ristic08] J. Ristic, E. Calleja, S. Fernandez-Garrido, L. Cerutti, A. Trampert, U. Jahn and K. H. Ploog, On the mechanisms of spontaneous growth of III-nitride nanocolumns by plasma-assisted molecular beam epitaxy, Journal of Crystal Growth 310 4035 (2008)

[Romanov06] A. E. Romanov, T. J. Baker, S. Nakamura, and J. S. Speck, *Strain-induced polarization in wurtzite III-nitride semipolar layers*, Journal of Applied Physics 100 023522 (2006)

[Rosa06] A. L. Rosa and J. Neugebauer, *Understanding Si adsorption on GaN(0001) surfaces using first-principles calculations*, Physical Review B 73 205314 (2006)

[Sekiguchi08] H Sekiguchi, K Kishino and A Kikuchi, *Ti-mask Selective-Area Growth of GaN by RF-Plasma-Assisted Molecular-Beam Epitaxy for Fabricating Regularly Arranged InGaN/GaN Nanocolumns*, Applied Physics Express 1 124002(2008)

[Seon00] M. Seon, T. Prokofyeva, M. Holtz, S. A. Nikishin, N. N. Faleev and H. Temkin, *Selective growth of high quality GaN on Si(111) substrates*, Applied Physics Letters 76(14) 1842 (2000)

[Sheleg79] A. V. Sheleg and V. A. Savastenko, *Determaination of elastic-constants of hexagonal crystals from measured values of dynamic atomic displacements*, Inorganic materials 15 1598 (1979)

[Simpkins07] B. S. Simpkins, K. M. McCoy, L. J. Whitman and P. E. Pehrsson, *Fabrication and characterization of DNA-functionalized GaN nanowires*, Nanotechnology 18 355301 (2007)

[Songmuang07] R. Songmuang O. Landré and B. Daudin, *From nucleation to growth of catalyst-free GaN nanowires on thin AlN buffer layer*, Applied Physics Letters 91 251902 (2007)

[Stockmann94] S. A. Stockman, A. W. Hanson, C. M. Colomb, *A comparison of TMGa and TEGa for low-temperature metalorganic chemical vapor deposition growth of CCI4-doped inGaAs*, Journal of Electronic Materials 23 791 (1994)

[Su05] J. Su, M. Gherasimova, G. Cui, H. Tsukamoto, and J. Hana, T. Onuma, M. Kurimoto, and S. F. Chichibu, C. Broadbridge, Y. He and A. V. Nurmikko, *Growth of AlGaN nanowires by metalorganic chemical vapor deposition*, Applied Physics Letters 87 183108 (2005)

[Sugahara98] T. Sugahara, H. Sato, M. Hao, Y. Naoi, S. Kurai, S. Tottori, K. Ymashita, K. Nishimo, L. T. Romano and S. Sakai, *Direct evidence that dislocations are non-radiative recombination centers in GaN*, Japanese Journal of Applied Physics 37 398 (1998)

[Takeuchi97] T. Takeuchi, S. Sota, M. Katsuragawa, M. Komori, H. Takeuchi, H. Amano and Isamu Akasaki, *Quantum-Confined Stark Effect due to Piezoelectric Fields in GaInN Strained Quantum Wells*, Japanese Journal of Applied Physics 36 382 (1997)

[Tang06] H. Tang, S. Haffouz, J. A. Bardwell, *Si(111) substrates as highly effective pseudomasks for selective growth of GaN material and devices by ammonia-molecular-beam epitaxy*, Applied Physics Letters 88 172110 (2006)

[Tchernycheva07] M. Tchernycheva, C. Sartel, G. Cirlin, L. Travers, G. Patriarche, J.–C. Harmand, Le Si Dang, J. Renard, B. Gayral, L. Nevou and F. Julien, *Growth of GaN free-standing nanowires by plasma-assisted molecular beam epitaxy: structural and optical characterization*, Nanotechnology 18 385306 (2007)

[Tham06] D. Tham, C. Y. Nam and J. E. Fisher, *Defects in GaN nanowires*, Advanced Functional Materials 16 1197 (2006)

[Thelander05] C. Thelander, H. A. Nilsson, L. E. Jensen and L. Samuelson, *Nanowire Single-Electron Memory*, Nano Letters 5(4) 635 (2005)

[Thelander06]. C. Thelander, P. Agarwal, S. Brongersma, J. Eymery, L. F. Feiner, A. Forchel, M. Scheffler, W. Riess, B.J. Ohlsson, U. Gösele, L. Samuelson, *Nanowire One-Dimensional Electronics*, MaterialsToday 9 28 (2006)

[Tripathy99] S. Tripathy, R. K. Soni, H. Asahi, K. Iwata, R. Kuroiwa, K. Asami and S. Gonda, *Optical properties of GaN layers grown on C-, A-, R-, and M-plane sapphire substrates by gas source molecular beam epitaxy*, Journal of Applied Physics 85 8386 (1999)

[Uedono07] A. Uedono, K. Ito, T. Narumi, M. Sometani, K. Yamabe, Y. Miyagawa, T. Murata, K. Honda, N. Hattori, M. Matsuura, K. Asai, T. Ohdaira and R. Suzuki, *Annealing properties of open volumes in strained SiN films studied by monoenergetic positron beams*, Journal of Applied Physics 102 064513 (2007)

[Van Nostrand06] J. E. Van Nostrand, K.L. Averett, R. Cortez, J. Boeckl, C. E. Stutz, N. A. Sanford, A. V. Davydov and J. D. Albrecht, *Molecular beam epitaxial growth of high-quality GaN nanocolumns*, Journal of Crystal Growth 287 500 (2006)

[VanDam06] J. A. Van Dam, Y. V. Nazarov, E. P. A. M. Bakkers, S. De Franceschi and L. P. Kouwenhoven, *Supercurrent reversal in quantum dots*, Nature 442 667 (2006)

[VanDerPauw58] L. J. van der Pauw, *A method of measuring the resistivity and Hall coefficient on lamellae of arbitrary shape*, Philips Technical Review 20 220 (1958)

[VanDeWalle98] C. G. Van de Walle, C. Stampfl and J. Neugebauer, *Theory of doping and defects in III-V nitrides*, Journal of Crystal Growth 189 505 (1998)

[vanVechten92] J. A. van Vechten, J. D. Zook, R. D. Hornig and B. Goldenberg, *Defeating Compensation in Wide Gap Semiconductors by Growing in H that is Removed by Low Temperature De-Ionizing Radiation*, Japanese Journal of Applied Physics 31 3662 (1992)

[Varshni67] Y. P. Varshni, Temperature *dependence of the energy gap in semiconductors*, Physica 34 149 (1967)

[Vegard21] L. Vegard, Die *Konstitution der Mischkristalle und die Raumfüllung der Atome*, Zeitschrift für Physik, 5 17 (1921)

[Vennegues99] P. Vennégues and B. Beaumont, *Transmission electron microscopy study of the nitridation of the (0001) sapphire surface*, Applied Physics Letters 75 4115 (1999)

[Viswanath98] A. K. Viswanath, E.-J. Shin, J. I. Lee, S. Yu, D. Kim, B. Kim, Y. Choi and C.-H. Hong, *Magnesium acceptor levels in GaN studied by photoluminescence*, Journal of Applied Physics 83 (1998)

[Vurgaftman01] I. Vurgaftman, J. R. Meyer and L. R. Ram-Mohan, *Band parameters for III-V compound semiconductors and their alloys*, Journal of Applied Physics 89 5815 (2001)

[Vurgaftman03] I. Vurgaftman and J. R. Meyer, *Band parameters for nitrogen-containing semiconductors*, Journal of Applied Physics 94 3675 (2003)

[Wagner64] R. S. Wagner and W. C. Ellis, *Vapor-Liquid-Solid mechanism of single crystal growth*, Applied Physics Letters 4(5) 89 (1964)

[Walukievicz04] W. Walukievicz, S. X. Li, J. Wu, K. M. Yu, J. W. Ager, E. E. Haller, H. Lu and W. J. Schaff, *Optical properties and electronic structure of InN and In-rich group III-nitride alloys*, Journal of Crystal Growth 269 119 (2004)

[Wang98] K. Wang and R. R. Reeber, *Thermal expansion of GaN and AlN*, MRS Symposium Proceedings 482 863 (1998)

[Wang04a] X. Wang and A. Yoshikawa, *Molecular beam epitaxy growth of GaN, AlN and InN*, Progress in Crystal Growth and Characterization of Materials 48 42 (2004)

[Wang04b] J. Wang, J. Cao, B. Fang, P. Lu, S. Deng and H. Wang**,** *Synthesis and characterization of multipod, flower-like, and shuttle-like ZnO frameworks in ionic liquids*, Material Letters 59 1405 (2004)

[Wang06] G. T. Wang, A. Alec Talin, D. J. Werder, J. R. Creighton, E. Lai, R. J. Anderson and I. Arslan, *Highly aligned, template-free growth and characterization of vertical GaN nanowires on sapphire by metal-organic chemical vapour deposition*, Nanotechnology 17(23) 5773 (2006)

[Wang08] B.-B. Wang, J.-J. Xie, Q. Yuan and Y.-P. Zhao, *Growth mechanism and joint structure of ZnO tetrapods*, Journal of Physics D: Applied Physics 41 102005 (2008)

[Webb07] T. Webb, *Multi-wafer inerferometer*, AIXTRON LTD (2007)

[Wu96] X. H. Wu, L. M. Brown, D. Kapolnek, S. Keller, B. Keller, S. P. DenBaars, J. S. Speck, *Defect structure of metal-organic chemical vapor deposition-grown epitaxial (0001) GaN/Al_2O_3*, Journal of Applied Physics 80 3228 (1996)

[Wu03] J. Wu, W. Walukiewicz, K. M. Yu, J. W. Ager, S. X. Li, E. E. Haller, H. Lu and W. J. Schaff, *Universal bandgap bowing in group-III nitride alloys*, Solid State Communications 127 411 (2003)

[Xu05] C. X. Xu and X. W. Sun, *Multipod zinc oxide nanowhiskers*, Journal of Crystal Growth 277 330 (2005)

[Yang98] T. Yang, S. Goto, M. Kawata, K. Uchida, A. Niwa and J.Gotoh, *Optical Properties of GaN Thin Films on Sapphire Substrates Characterized by Variable-Angle Spectroscopic Ellipsometry*, Japanese Journal of Applied Physics 37 1105 (1998)

[Yang99a] C.-C. Yang, M.-C. Wu, C.-A. Chang and G.-C. Chi, *Effectiveness of multiple-pair buffer layer to improve the GaN layers grown by metalorganic chemical vapor deposition*, Journal of Applied Physics 85 8427 (1999)

[Yang99b] C. C. Yang, M. C. Wu and G. C. Chi, *Improvement of GaN layer quality by using the bulk-GaN buffer structure grown by metalorganic chemical vapor deposition*, Journal of Applied Physics 86 6120 (1999)

[Yazdi09] G. R. Yazdi, P. O. A. Persson, D. Gogova, R. Fornari, L. Hultman, M. Syvajarvi and R. Yakimova, *Aligned AlN nanowires by self-organized vapor–solid growth*, Nanotechnology 20 495304 (2009)

[Yeh92] C.-Y. Yeh, Z. W. Lu, S. Froyen, and A. Zunger*, Zinc-blende–,wurtzite polytypism in semiconductors*, Physical Review B 46 10086 (1992)

[Yoshida75] S. Yoshida, S. Misawa, and A. Itoh, *Epitaxial growth of aluminium nitride films on sapphire by reactive evaporation*, Applied Physics Letter 26 461 (1975)
[Yoshimoto91] N. Yoshimoto, T. Matsuoka, T. Sasaki and A. Katsui, *Photoluminescence of lnGaN films grown at high temperature by metalorganic vapor phase epitaxy*, Applied Physics Letters 59 2251 (1991)

[Zanin09] S. Zanin, *Nano-contacts technology and electrical characterization on ZnO and GaN nanowires*, internship report, CNRS Institut Néel Grenoble, Julien Pernot's group (2009)

[Zheng05] G. Zheng, F. Patolsky, Y. Cui, W. U. Wang and C. M. Lieber, *Multiplexed electrical detection of cancer markers with nanowire sensor arrays*, Nature Biotechnology 23, 1294 (2005)

[Zheng08] K. Zheng, C.X. Xu, G.P. Zhu, X. Li, J.P. Liu, Y. Yang, X.W. Sun, *Formation of tetrapod and multipod ZnO whiskers*, Physica E 40 (2008) 2677

[Zubia99] D. Zubia and S. D. Hersee, *Nanoheteroepitaxy: The application of nanostructuring and substrate compliance to the heteroepitaxy of mismatched semiconductor materials*, Journal of Applied Physics, 85 6492 (1999)

[Zubia00] D. Zubia, S. H. Zaidi, S. R. J. Brueck and S. D. Hersee, *Nanoheteroepitaxial growth of GaN on Si by organometallic vapor phase epitaxy*, Applied Physics Letters 76 858 (2000)